ADDIS ABABA UNIVERSITY
SCHOOL OF GRADUATE STUDIES
SCHOOL OF EARTH SCIENCES

CHARACTERISTICS AND GENESIS OF ENKAFELA MANGANESE DEPOSIT, DALLOL AREA, NORTHERN AFAR DEPRESSION

BY

ABATE ASSEN MELAKU

ADVISOR: WORASH GETANEH (PhD)
CO-ADVISOR: BALEMWAL ATNAFU (PhD)

A thesis submitted to the School of Graduate Studies of Addis Ababa University in partial fulfillment of the requirements for the degree of Master of Science in Resource Geology (Mineral Deposit)

May 30, 2018
Addis Ababa, Ethiopia

ADDIS ABABA UNIVERSITY
SCHOOL OF GRADUATE STUDIES
SCHOOL OF EARTH SCIENCES

CHARACTERISTICS AND GENESIS OF ENKAFELA MANGANESE DEPOSIT, DALLOL AREA, NORTHERN AFAR DEPRESSION

BY

ABATE ASSEN MELAKU

ADVISOR: WORASH GETANEH (PhD)
CO-ADVISOR: BALEMWAL ATNAFU (PhD)

A thesis submitted to the School of Graduate Studies of Addis Ababa University in partial fulfillment of the requirements for the degree of Master of Science in Resource Geology (Mineral Deposit)

May 30, 2018
Addis Ababa, Ethiopia

ADDIS ABABA UNIVERSITY
SCHOOL OF GRADUATE STUDIES
SCHOOL OF EARTH SCIENCES

CHARACTERISTICS AND GENESIS OF ENKAFELA MANGANESE DEPOSIT, DALLOL AREA, NORTHERN AFAR DEPRESSION

BY
ABATE ASSEN MELAKU

Approved by the Examining Committee

1.	_____	_____	_____
	Head, School of Earth Sciences	Signature	Date
2.	_____	_____	_____
	Advisor	Signature	Date
3.	_____	_____	_____
	Co-advisor	Signature	Date
4.	_____	_____	_____
	Examiner	Signature	Date
5.	_____	_____	_____
	Examiner	Signature	Date

Declaration of Originality

I hereby declare that the thesis is my original master's degree work under the supervision of Dr. Worash Getaneh and Dr. Balemwal Atnafu, School of Earth Sciences, Addis Ababa University during the year 2018. I further declare that this work has not been presented or submitted to any other university or institution for the award of any degree or diploma. All sources and materials used for the thesis have been duly acknowledged.

Abate Assen Melaku _____ _____

Signature Date

This is to certify that the above declaration made by the candidate is correct to the best of my knowledge.

Dr. Worash Getaneh (Advisor) _____ _____

Signature Date

Dr. Balemwal Atnafu (Co-advisor) _____ _____

Signature Date

Abstract

The Enkafela manganese deposit is situated in the Afar Depression, northern Ethiopia, about 20km west of Dallol at the border with the western escarpment. The geology of the Enkafela area is characterized by marine formations of reef limestone, oolitic limestone, gypsum, conglomerates and basalt. The ore body is stratabound and lies between the reef limestone and basalt. The ore stratum is characterized by two distinctive manganese layers. The bottom is massive while the top layer is powdery/friable. The main purpose of this study is to understand the geochemical characteristics and genesis (origin) of the manganese mineralization. Geological, mineralogical and geochemical data are integrated to characterize the genesis of the manganese deposit. Based on XRD mineralogical analysis, Pyrolusite, Chalcophanite and Biernessite minerals are identified as the main ore minerals in the deposit. The geochemical analysis result indicate enriched MnO (av. 70.25wt %), Ba (>10,000ppm), Sr (>10,000 ppm) and depleted Fe_2O_3 (av. 0.37wt %) and transition metals. The total REE content of the massive manganese is 172.9ppm while the powdery manganese contains total REE of 7.84ppm. The massive manganese show higher REE content than the powdery manganese. Chondrite normalized REE plot show LREE enrichment for both manganese layers. The massive manganese layer shows enrichment in Ce and no anomaly in Eu. However, the powdery manganese shows depletion in Ce and Eu. The geochemical and mineralogical studies indicate that Enkafela manganese mineralization does not originate from a pure hydrothermal source or pure hydrogenic source. The massive manganese shows mixed sources, whereas the powdery manganese shows a hydrothermal source. The Ni-Co-Zn discriminating ternary diagram indicates the powdery manganese (top layer) has a hydrothermal origin and the massive manganese (bottom layer) has mixed origin (both hydrothermal and hydrogenic). Alternatively, the Fe-(Ni + Cu + Co)*10-Mn and Fe-Si*2-Mn discriminating diagrams indicate hydrothermal activity played the major role in the formation of both the powdery and massive manganese layers. Generally, the geochemical studies show the dominance of hydrothermal activity in the formation of the Enkafela manganese deposit, though seawater contribution is undeniable in the massive manganese deposit. The two manganese layers are similar genetically and formed successively from the same source.

Key words: Birnesssite, Chalcophanite, Enkafela, Pyrolusite, Manganese, genesis, hydrothermal

Acknowledgment

At the end of this thesis, I would like to take some time to thank all the organizations and people whom without them this thesis would never have been possible. First and for most, I am so grateful to Addis Ababa University School of Earth Sciences for providing me an opportunity to study my master‘s degree and funding the research project.

I would like to express my special appreciations and thanks to my advisor Dr. Worash Getaneh who made this work possible. He has thought me the methodology to carry out a research. It is a great privilege and honor to work and study under his guidance. I have also been benefited from his constructive suggestions, invaluable comments and tireless support.

I would also like to express my deepest gratitude to my co-advisor and Head of School of Earth Science, Dr. Balemual Atnafu for his vital comments and providing me vehicle and financial support during field work.

I would like to render my warmest thanks to Ermias Filfilu for his presence, support, guidance and valuable suggestions during field work and providing his invaluable time. I am extremely grateful to Mr. Samuel Getachew who is always cooperative and take helping others as a hobby. I have benefited a lot from his comments and suggestions. The illustrated sketches are also made with his help.

The XRD laboratory analysis is done in Italy, university of Naples Federico II, DiSTAR (Dipartimento di Scienze della Terra, dell’Ambiente e delle Risorse) department. I would like to express my sincere thanks to Prof. Piergiulio Cappelletti, Dr. Francesco Putzolu and Mr. Yemane Kelemewok for their collaboration and support for the analysis. I would also like to thank ALS SERVICES PLC, for their timely submission of the geochemical analysis and for providing a discount for the analysis. I would like to thank Mr. Ali Berhale for his respectable hospitality and cooperation during fieldwork.

This thesis has also benefited comments and suggestions made by my staff members and friends specially, Mr. Million Alemayehu, Mr. Bahru Zinaye, Mr. Amdemichel Zafu, Mr. Gemechu Bedassa, Ms. Selam Tadesse, Mr. Takele Mengstie, Mr. Tenaw Mengstie and Ms. Tsedenya Aregu. I take this opportunity to thank them. Special thanks are due to Ms. Alemtsehay Seife and Yafet G/Wold for their priceless support and help.

Finally, I am extremely grateful to my parents for all their love, encouragement, and prayers.

Table of Contents

List of Figures

List of Tables

List of Acronyms

AD	Afar Depression
ANS	Arabian Nubian Shield
EARS	East Africa Rift System
GPS	Global Positioning System
HREE	Heavy Rare Earth elements
ICP-AES	Inductively Coupled plasma Atomic Emission Spectroscopy
ICP-MS	Inductively Coupled Plasma Mass Spectroscopy
JORC	Joint Ore Reserves Committee
LOI	Loss of Ignition
LREE	Light Rare Earth Elements
MER	Main Ethiopian Rift
m. s. l.	Mean sea level
NASC	North American Shale Composite
PASS	Post Archean Australian Shale
PPL	Plane Polarized Light
REE	Rare Earth Elements
XPL	Cross Polarized Light
XRD	X-ray Diffraction
XRF	X-ray Fluorescence

CHAPTER ONE

INTRODUCTION

1.1. Background

The study area is situated in the Afar depression (AD), northern Ethiopia, which represents the lowest place in the country, about 120m below sea level (Carniel et al., 2010) and covers an area of 200,000 km^2 (Bosworth et al., 2005). The AD is one of the most impressive places in east Africa, which attracts the attention of various scientists. The general tectonic structure and the geological history of the area made it one of the most interesting places in the world for different investigations in different approaches of Geosciences. On the contrary the general weather condition (very hostile) creates difficulties for many researchers.

The Afar Depression is part of the great East Africa Rift System (EARS) found at the junction of the two propagating oceanic ridges (Gulf of Aden and Red sea) and the Main Ethiopian Rift (MER) which is transitional from continental rifting to oceanic spreading (Barrat et al., 1998; Bosworth et al., 2005; Barisin et al., 2009). It is also the only place in the world where continental plate, Arabia-Africa, is presently breaking apart such that a new ocean is currently being formed (courtillot et al., 1999; Dobre et al., 2007). Previous works (e.g., Mckenzie and Morgan, 1969) suggested that AD represents the only emerged triple junction in the world. According to Hoffman et al. (1998), rifting of Africa and Arabia during the past ~30Myr produced the ~300km wide Afar depression (AD). Geological, petrological and geochemical studies reveal AD displays volcano-tectonic features characteristics of the mid oceanic rift system (Varet, 2006).

In addition to its unique geological character, the Afar depression, especially the Dallol area, becomes a target area for its potential of hosting different economically valuable mineral deposits. The evaporites (mainly Rock salt and sylvite) and geothermal energy resources are the main areas of economic interest so far. Afar is identified as one of the exceptional richest place in its geothermal energy potential comparable with Iceland on our planet (Varet, 2006; 2010; Varet et al., 2012). On the basis of geological and geodynamical criteria, many parts of Afar have a huge potential of geothermal energy and Varet (2006) describes the area as "future Gulf region for geothermal energy".

Although it is not detail, both governmental and non-governmental exploration groups were active in searching the various mineral resources of the area. Currently, there are three

companies working on potash exploration projects in the depression, these are Israel chemical Ltd. (took over from Allana –Canada), Yara International and CERCAM (https://www.export.gov/article?id=Ethiopia-Mining-Industry).

The Afar Depression is also known for a potential of metallic minerals like Au, Cu, Mn and Fe (e.g. Solomon Tadesse et al., 2003). Accordingly, this research attempts to study the manganese deposit of Enkafela Area which is among the possible occurrences of metallic mineral deposits in Afar. Except its discovery and limited trials of mining in the 1970's detail information is not known about its geology, geochemistry and genesis of the mineralization.

1.2.Geographic Setting of the Study Area

1.2.1. Location and Accessibility

The research area is found in the Afar regional state, zone 2, Dallol wereda. It is bounded by 628000m E to 636000m E and 1557400m N to 1566400m N covering a total area of 64

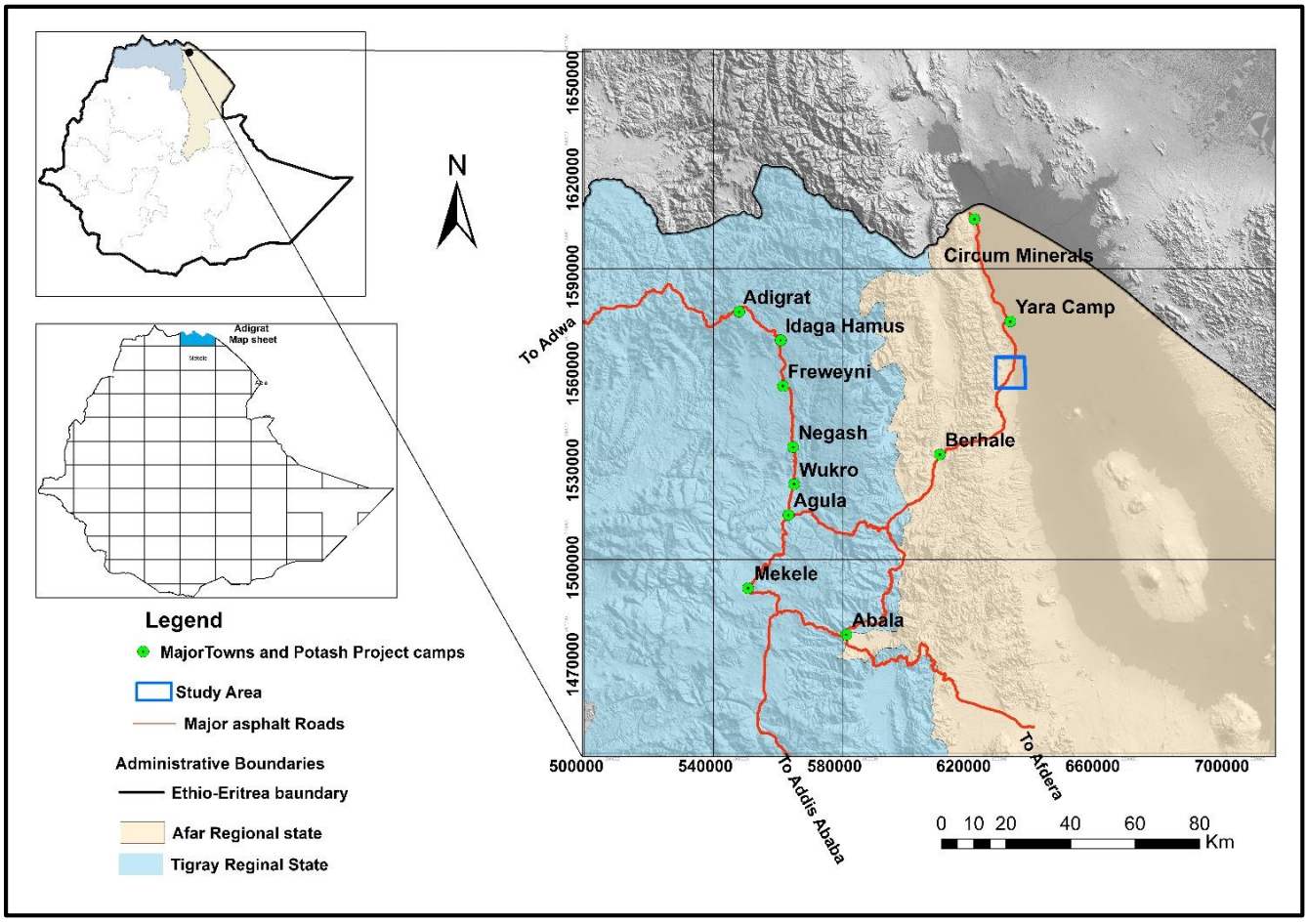

Figure 1.1: Location of the study area

km^2 (fig. 1.1). According to the Ethiopian mapping agency topographic mapping configuration, it is found in the Adigrat map sheet (ND 37-7).

Enkafela is 950km far from Addis Ababa and 170 km far from Mekele. It is accessible via asphalt road from Addis Ababa-Mekele- Berhale to Dallol. The study area is located 15-18km North-West of Hamadela village. The intermittent river gorges and gullies, which ranges 2-3km, are used as a direct access to the study area from the asphalt road.

1.2.2. Physiography and Drainage

The study area is located in the northern part of the Afar Depression close to the Ethiopian plateau and the depression runs SSE parallel to the red sea coast. The physiographically low-lying Afar depression resembles roughly a triangular shape and covers an Area of ~200,000 km^2 (Bosworth et al., 2005; Beyene & Abdelsalam, 2005). It is flanked in the west and southeast by the Ethiopian and Somali plateaus, and on the east by the Danakil and Ali-Sabieh (Aisha) blocks. There is a fundamental elevation contrast between the rift bounding Ethiopian plateau that stands well above ~3000m above sea level and the Afar Depression, which drops to ~120 meters (at Lake Assale) below sea level (Holwerda & Hutchinson, 1968; Bonatti et al., 1971; Barberi et al., 1973;CNR-SNRS, Afar team; 1973; Tesfaye et al., 2003; Bosworth et al., 2005). The Ethiopian escarpment extends north into Eritrea and closes the Afar Depression against the Danakil Alps at the Gulf of Zula (Alebachew Beyene & Abdelsalam, 2005). The Danakil Alps, which separates Afar from Red Sea, reach an elevation of about 1,300m above msl in its northern portion and more than 2,000m above m.s.l. to the south (Bosworth et al., 2005;).

The Danakil Depression is 185km long and up to 70km wide, wider to the south (Warren, 2015). It gets progressively narrower towards the northern zone and reaches to its deepest part at Dallol (Beyene & Abdelsalam, 2005; Warren, 2015). The deepest part of the northern depression, which is around 10km from the study area, is a flat lying area known as the Dallol salt flat or salt plain. It is about 40km long and 10km wide. It is covered by halite dominated evaporite formations (Franzsen et al., 2015; Warren, 2015).

The Afar Depression is a closed drainage basin in which the Eastern bounding highland areas prevent the hydrographic (surface) recharge to the depression from the red sea. Likewise, there is no river which flows across the depression to the neighboring countries/ seas like the other big rivers of the country. All the rivers are exclusively small scale

intermittent rivers or gullies which flow from the western Ethiopian highlands, perpendicular to the rift escarpment, to the Afar Depression during rainy seasons.

During rainy season the runoff from the highland areas is powerful so that it easily erodes the low lands of the depression and creates deeper and wider dry river systems. This makes most of the places in the depression suitable and accessible for field work since driving and walking through them is simple. On the other hand, erosion and alluvial transport from the highland areas have resulted in the development of significant alluvial fans along the rim of the salt plain. The alluvial fans play a significant role in reaching the underground water. Lake Assale is the only water body found in the study area covering the salt plain. It most probably gets the recharge from the highland areas.

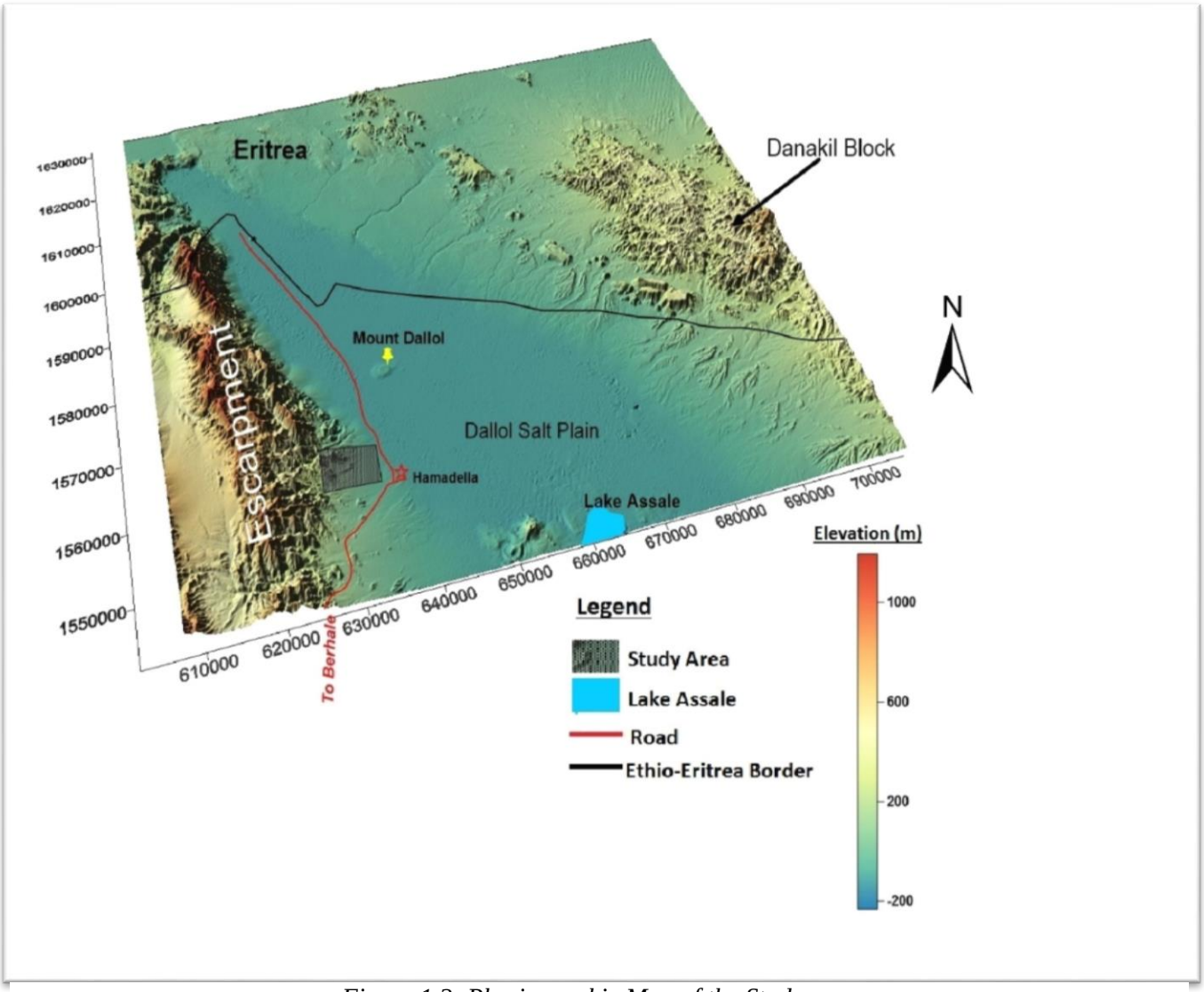

Figure 1.2: Physiographic Map of the Study area

1.2.3. Climate and Vegetation

The Afar Depression is one of the hottest places in the world fully characterized by its very hostile, awfully inhospitable climate. Dallol exhibits an extreme version of a hot desert climate typical of the Danakil desert. The region holds the official record for highest average, year-round, monthly temperatures (Pedgley, 1967; Carniel et al., 2010; Wenner, 2015,) where an average annual temperature of 34.6 °C (94.3 °F) was recorded between the years 1960 and 1966 (table 1.1). According to the data obtained from Pedgley (1967) the annual average high temperature is 41 °C (105 °F) and the hottest month has an average high of 46.7 °C (116.1 °F) (table.1.1 and fig 1.3). Accordingly, the area records highest average temperature from May to August. While, the lowest average temperature measured from December to February.

Month	Jan	Feb	Mar	Apr	May	Jun	Jul	Aug	Sep	Oct	Nov	Dec	Year
Average High ºC	36.1	36.1	38.9	40.6	44.4	46.7	45.6	45.5	42.8	41.7	39.4	36.7	41.17
Average high ºF	97	97	102	105	112	116	114	113	109	107	102.9	98	106.1
Daily mean ºC	30.5	30.5	32.5	33.9	36.4	38.6	38.7	37.6	37.3	35.6	33.2	30.8	34.62
Daily mean ºF	86.5	86.9	90.5	93	97.5	101.5	101.7	99.7	99.1	96.1	91.8	87.4	94.31
Average low ºC	24.6	24.6	26	27.1	28.5	30.4	31.8	31	31.6	29.6	27.1	25.7	28.17
Average low ºC	76.3	76.3	78.8	80.8	83.3	86.8	89.2	88	88.8	85.3	80.	78.3	82.72

Table1.1: historical climate data for Dallol (1960-1966) (derived from Pedgley, 1967).

In addition to being extremely hot year-round, the climate of the lowlands of the Danakil Depression is also extremely dry and hyper-arid in terms of annual average rainy days. It has only a few day's record measurable precipitation (table 1.2). The rainfall is very low in Dallol, reaches an average of 50mm per year (varet, 2010). Humidity is also the typical characteristics of Dallol. High humidity exhibits during the summer season.

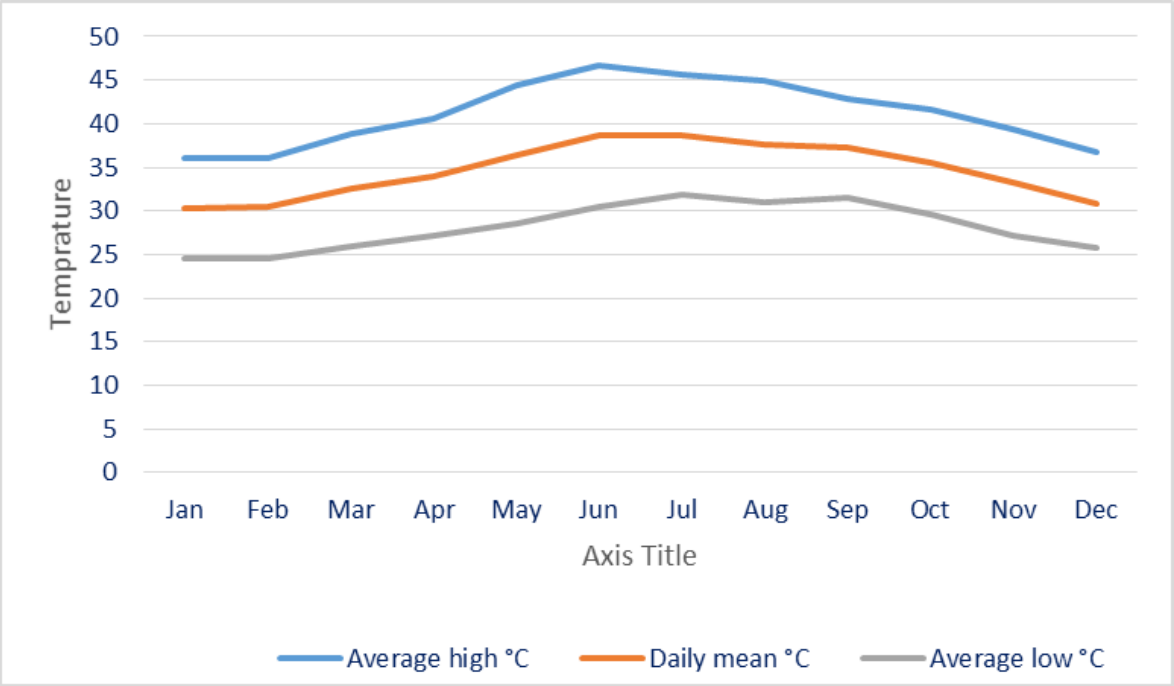

Figure 1.3: A line chart showing the climate data for Dallol (1960-1966) (derived from Pedgley, 1967).

Due to hot temperature and low rainfall, vegetation is unexpected in Dallol depression. During rainy season following the limited rainfall, small grasses and shrubs grow more specifically to the foot of the western highland areas. Since the flat, low land is covered by salt formation, it is unfavorable for any vegetation.

Months	Jan	Feb	Mar	Apr	May	Jun	Jul	Aug	Sep	Oct	Nov	Dec
High (°C)	27.8	28.3	30	32.2	34.4	35.0	36.1	35.5	35	33.3	30.5	28.3
Low (°C)	21.1	20.5	22.2	24	25.5	27.2	28.3	28.3	27.2	25.5	23.3	21.7
Average (°C)	24.45	24.2	26.1	28.1	30	31.1	32.2	31.9	31.1	29.4	26.9	25
Precipitation (mm)	0	0	0.762	1.27	1.778	0	1.27	2.286	2.032	0.762	0	0

Table 1.2: Temperature data of Dallol for 2017. https://www.accuweather.com/en/et/dalol/126842/january-weather/126842, visited on 28.01.28.

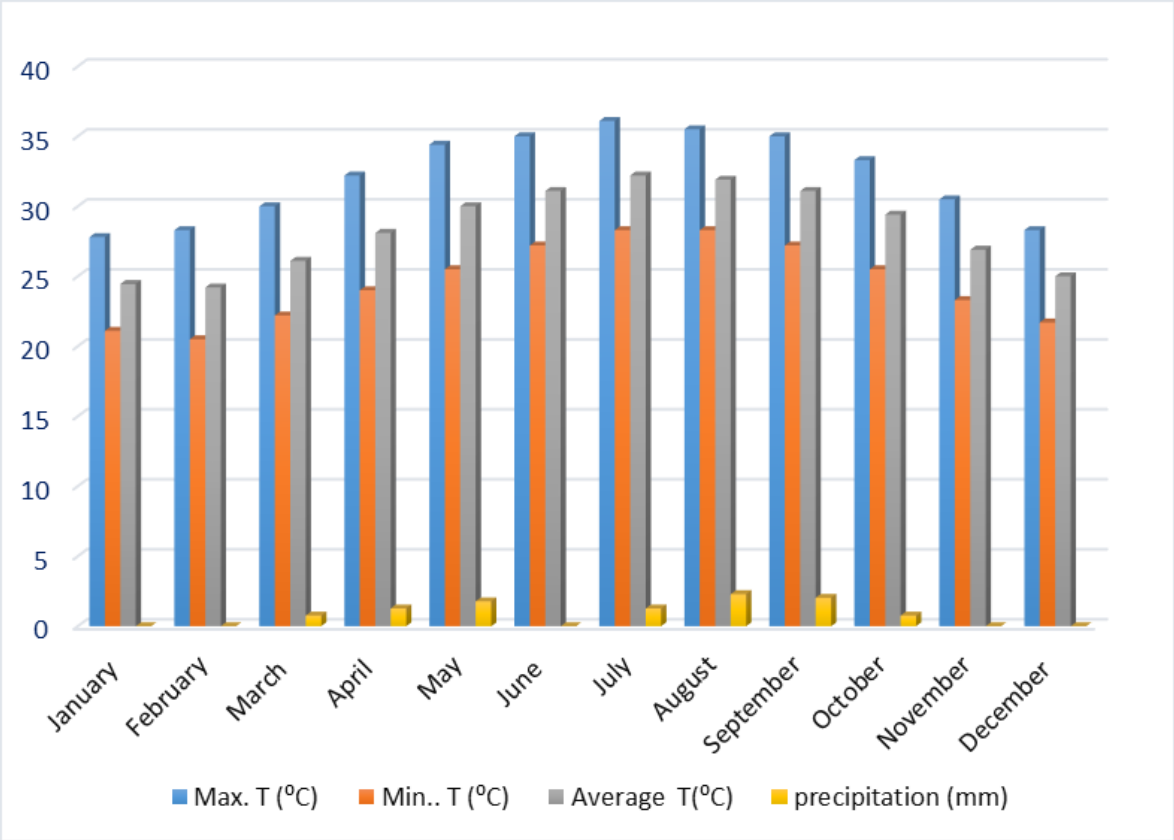

Figure 1.4: A clustered column chart showing the climatic condition of Dallol for the year 2017, https://www.accuweather.com/en/et/dalol/126842/january-weather/126842, visited on 28.01.28.

1.2.4. Population and Settlement

Because of the harsh and unfriendly condition, the Afar Depression is sparsely populated and only temporarily inhabited. The community builds small settlements sporadically and leads a pastoralist life. The Afar pastoral community is leading a communal life (using natural resources communally); and they are also mobile in search of water and grazing. On the contrary, the people living in Hamadela village, which is about 10 km from the study area, participate in the tourism industry and work as a tour guide.

According to the 2007 census by the Central Statistical Agency (CSA), the total population of the Afar National Regional State is 1,390,273 of which 83, 930 is in the Dallol Woreda. From this 46,973 of them are males and 36,957 are females. Afarigna is the predominant language spoken by almost all of the population. Islam is the main religion practiced in the region.

1.3. Problem Statement

The Afar depression has been explored for a variety of mineral resources for many years. Although it is an ongoing activity, halite and potash deposits were the primary targets of several exploration practices. Currently exploration is conducted by different private companies from the preliminary to a detailed exploration program. In addition to the evaporite deposits, the area is also characterized by the occurrences of manganese deposit around Enkafela locality on which the present study will focus.

According to Bonatti et al. (1972), the deposit is found associated with marine formations. Even if the occurrence of the manganese deposit has been known for several years, any scientific study that can characterize the deposit in detail was not available so far. The one and the only study on the Enkafela is that of Bonatti et al. (1972). The origin, geological environment, mineralogical and geochemical studies to elucidate its petrogenesis has not been well studied in detail. On the other hand the stratigraphical relationship of the ore mineral with the associated formations is not still well defined and interpreted with respect to the geologic environment. It is known that the geochemistry of Mn and Fe is similar and is expected that the two elements move and deposit together (Worash Getaneh and Solomon Tadesse, 2015). However, the deposit forms its own distinctive layer (Bonatti et al. 1972). This research will thus try to conduct detailed investigations on the nature of the mineralization and define the genesis of the deposit.

1.4.Objectives

1.4.1. General Objectives

The main objective of this study is to understand the geochemical characteristics and genesis (origin) of the manganese mineralization.

1.4.2. Specific Objectives

The specific objectives of the research are to:

- Produce a geological map of the study area
- Characterize the geochemistry of the ore and the host rock
- Determine the mineralogical assemblage of the deposit and interpret the depositional environment of mineralization
- Estimate the total resource amount of manganese deposit based on the field data

1.5.Methodology

Different investigation methods are applied in order to meet the specified objectives of the research. The methods used are outlined according to the general frame work of pre-field work, field work and post fieldwork activities. During pre-field work, any data relevant to the research were assessed and collected. Additional information regarding the methodology that would be applied, about accessibility and extent of the area etc., is obtained through discussions with advisors and other people. Both primary and secondary data are incorporated to encounter the target as per the stated research problem. The field work is dedicated to mapping, primary data collection, field observation and study. The analysis, synthesis, interpretation and presentation of the data collected, is conducted during post-field work.

During the early stages, literature review is done. The literatures that are closely related to the current study are selected in order to adopt the methodologies which would be better for this study. Literatures are also assessed to understand the general geology, geological and tectonic history, geological settings and structures of the study area. Accordingly, various ideas, information etc. obtained from a number of published and unpublished literatures are presented as a literature review or cited in the thesis. Moreover, major geological structures, rivers and different lithologies are differentiated using satellite images and from Google Earth images.

During the different phases, several kinds of tools are used, containing geological maps of varying scale, standard field sampling and measuring tools and ArcGIS 10.3, Google Earth, Global Mapper, surfur 10, Grapher 8, Petrograph beta, Match!3, Adobe Illustrator and excel software packages.

1.5.1. Field Work and Geological Mapping

The field work activity was conducted from December 20, 2017 to January 1, 2018. Field work is the only means of primary data collection while secondary data are derived from previous sources. The main target of this field investigation is to know the distribution of the manganese deposit, to take representative samples for further mineralogical and chemical analysis and to know its relation with the surrounding lithologies. Besides, the distribution of lithologies and structures (both vertically and horizontally) and collection of

representative samples for further analysis is as well the objectives of fieldwork. The fieldwork is conducted through systematically identified traverses.

The traverses are identified through streams and gullies where the maximum and variable lithological, structural and topographical variations are suspected and across the strike of the local rock units. Field notes regarding the lithological units and structures observed are documented and observation points are recorded using GPS control points (GCP). Along with this, all the information taken and observed on the ground is transferred to the base map. This helps to produce a geological map of the study area. Lithological section logs are performed along river cut and gully exposures. This time, thickness of lithologies is measured using measuring tape.

1.5.2. Analytical Methods and Data Analysis

The collected representative samples are sent to a laboratory for the appropriate test required to characterize the manganese deposit and the rocks found in the study area. The laboratory analysis plays a vital role to characterize the deposit and discriminate its genesis. The most important laboratory analyses applied consist of Geochemical, mineralogical and petrography.

A) Geochemical Analysis

Representative samples of manganese bearing samples and associated country rocks were collected during field work. A total of 10 samples, 4 manganese bearing samples and 6 rock samples are identified in this analysis. As a preliminary stage sample preparation, removal of the weathered surface and breaking into the desired size is done for the raw samples collected from the field. Then the broken sample is sent to a laboratory called ALS SERVICES PLC. In the laboratory, standard sample preparation is followed for all samples. First the samples are crushed finely to 70% less than 2mm, and then splitting of the sample using a riffle splitter off 250g is done. Finally, pulverize a split to better than 85% passing 75 microns (μm).

The prepared samples are then sent to ALS Geochemistry laboratory found in Ireland for quantification of major and trace element concentration. The elemental composition of each rock samples was determined using Inductively Coupled Plasma Atomic Emission Spectroscopy (ICP-AES), Inductively Coupled Plasma Mass Spectroscopy (ICP-MS) and X-Ray fluorescence (XRF). These analytical methods are selected based on their detection

limit, accuracy and precision standards. The laboratory uses standard certified reference materials for quality control and detection limit assurance. AMISO356, AMSIO304, ICP-4, GRE-3, OREAS-121, SY-4 are the standards used by the laboratory. In addition to this, blank material is also used for the purpose of detection limit control. In order to manipulate the geochemical result, the data should be integrated using different software packages. In this case, Microsoft excel 2013, Petrogragph version 2beta and Grapher 8 software packages are used. The outputs obtained from the software's are in the form of graphs and diagrams which are used to study and understand the geochemical behavior of the deposit and the host rock.

B) Mineralogical Analysis

Mineralogical analysis is implemented to recognize the mineralogical composition and to understand the content of these minerals present in the manganese samples as well as in the surrounding rocks. Consequently, XRD (X-ray Diffraction) is used to identify the minerals found in the samples both qualitatively and quantitatively. Five representative samples are selected for this purpose. These samples are sent to Italy, university of Naples for analysis and sample preparation were conducted there**.** The samples were powdered in an agate mortar. The XRPD analyses were carried out on a Seifert GE ID3003 diffractometer (DiSTAR), with Cu-Ka radiation, Ni-filtered at 40 kV and 30 mA, 3-70° 2θ range, step scan 0.05°, time 5 s/step, and using a low-background sample holder. A silicon wafer was employed to check the instrumental setting, whereas the RayfleX (GE) software package was used for the data processing.

C) Petrographic Analysis

Thin sections are prepared for selected samples. Six samples are selected for thin section preparation, based on the lithological variability, importance and the uncertainties to identify them during field work. This helps to identify the minerals found in the rock and understand any alteration phenomenon.

The thin section preparation is done in Geological Survey of Ethiopia. Microscopic examination is conducted at Addis Ababa University School of Earth Sciences petrography laboratory.

1.6.Research outcome

The Enkafela manganese deposit has not been studied in detail regarding the genesis, mineralogical and geochemical characteristics of the deposit. Therefore, this research work is conducted to come up with a result that can fill the existing scientific study gap.

The main outcomes of the research will be:

- An interpretation, based on the geochemical analysis, of the genetic process of the manganese mineralization whether it is a hydrogenetic, hydrothermal, diagenetic process or other mixed process?
- Fill the existing gap of detail information about the mineralization
- Well-organized and integrated detailed geological map at a scale of 1:25000 will be produced with their clear descriptions of lithological units (rock types) and geological structures, and
- An estimation of the total amount of the resource present.

1.7.Thesis Overview

The thesis is structured in to seven chapters. Chapter one gives a general information about the study area, the objectives of the study and methods followed in the research. Chapter two is a review of previous works related with the characteristics, genesis, mineralogy and geological and tectonic setting of manganese deposits in general. Chapter three deals with the regional geology and tectonic setting. Chapter four gives detail description about the lithology of the study area. In chapter five mineralogical and geochemical data is presented and interpreted. Discussion on the genesis of the Enkafela manganese deposit is presented and the genetic model of the deposit is illustrated in chapter six. Finally, the main conclusion and recommendation for the future study is presented in chapter seven.

CHAPTER TWO

LITERATURE REVIEW

2.1. Introduction

Manganese is the 12th most abundant element in the earth's crust and makes up about 0.1% of the earth's crust (Zhang and Cheng, 2007). It is a silvery white, brittle naturally occurring metallic element that is found in many types of rocks. Manganese is also the third abundant transition metal (Johnson et al, 2016), belonging to the group of siderophiles elements (a geochemical class after V.M. Goldschmidt). Having a tendency to react with oxygen, it never occurs in the metallic native state. Manganese is reactive when pure, and as a powder, it will burn in oxygen. It reacts with water (it rusts like iron) and dissolves in dilute acids. It has a density of 7.2-7.46 g/cm^3 and a melting temperature of 1244^{0}c (Kuleshov and Maynard, 2017).

Manganese has a wide range of application in the modern industry and consumed in large amount in all industrialized countries. In this regard, the metallurgical industry has accounted for the most of the world manganese consumption (Cannon et al., 2017; Kuleshov and Maynard, 2017). Manganese is mainly used in steel production by the virtue of its sulfur-fixing (Desulfurizing), deoxidizing, and alloying properties. Almost 90 to 95% (corathers, 2006; Fan and Yang, 1999) of manganese goes in to steel production as an alloying element. Refining of iron ore to metallic iron before the steel making process, is also done using manganese as a raw material.

According to the data obtained from Geology.com/usgs/manganese/,visited on 05.02.2018, the amount of manganese used per ton of steel is rather small, ranging from 6 to 9 kilograms. About 30% of that is used for refinement of the iron ore, and the remaining 70% is used as an alloy in final steel product. Cannon et al. (2017) argued that steel production is impossible without manganese since no known other substitutes for manganese has been identified in the overall conversion of iron ore to steel. The other most important areas of manganese application is in the production of alloys of non-ferrous metals like copper, aluminum and nickel. The main importance of manganese in alloys is that it enhances and keeps corrosion resistance, decreases brittleness and gives strength.

Manganese has also played a vital role in non-metallurgical applications. It is used for dry cell battery production, fertilizer, animal feed, painting, ceramics and manganese chemicals in chemical industries (Harben et al., 1998; Kogel et al., 2006).

2.2.Geochemistry and Mineralogy of manganese deposits

Naturally, manganese is found in divalent (Mn^{2+}), trivalent (Mn^{3+}) and quadrivalent (Mn^{4+}) valance states. The lower valance forms are highly soluble (mobile) and reactive, while the higher valance forms are insoluble (immobile) and both chemically and physically resistant (Kogel et al., 2006). On the other hand, manganese resembles iron geochemically (Kogel et al., 2006; Kuleshov and Maynard, 2017) and deposition of the two elements together might be expected (Yu et al., 2016; Worash Getaneh and Solomon Tadesse, 2015). Most of the time the two elements show a common association in different rocks, especially in igneous rocks, where the ratio of Mn/Fe often lies between the limits of 1/100 and 1/10 (Krauskopf, 1957). Manganese is also found in iron minerals by substituting iron and most of the time it is in the form of Mn^{2+} (Post, 1999).

Despite the fact that the two elements are found associatively together in all kinds of rocks, the separation of the two elements and the formation of their specific deposit is unescapable. The mysterious point here is the mechanism of iron and manganese separation. Therefore, the separation of the two elements and the deposition of manganese deposits seek a special ore formation process. Accordingly, it is the geochemical behavior of manganese, which finally determines the deposition of manganese ore deposits separated from the iron ore deposits. In solutions, manganese is transportable in reducing environment and it undergoes precipitation and deposition in oxidizing environment (Worash Getaneh and Solomon Tadesse, 2015). This implies that manganese should be oxidized in the form of Mn^{3+} and Mn^{4+} (Calvert and Pedersen, 1996; Tribovillard et al., 2006) in order to concentrate manganese.

On the contrary, iron forms sulfides early in reducing environments while the manganese is still in solution until it reach to an oxidizing environment (Maynard, 2010; Worash Getaneh and Solomon Tadesse, 2015). Kogel et al. (2006) and Krauskopf (1957), claimed that in oxidizing environment iron and manganese react in the same way, however iron oxidizes to its insoluble (ferric) state at much lower oxygen concentration than manganese does to its insoluble (manganic) state. This insolubility difference also plays a vigorous role in the separation of the two components in the natural system.

Generally, the separation of manganese from iron and formation of its deposits largely depends on the redox condition of the depositional environments. In this regard, the sedimentary processes and volcanogenic hydrothermal solution activities are the most prominent conditions for this special ore formation process. The divalent form of manganese (Mn^{2+}), could be considerably sourced from either weathering of terrigenous surface rocks or hydrothermal volcanogenic fluids (Post, 1999; Johnson et al, 2016). During weathering, with reference to iron, manganese may be preferentially leached due to its larger ionic size, lower ionic potential and enzymatic microbial reduction in the source area. Alternatively, if the source of both Fe and Mn elements is from terrigenous source, then during transportation Mn in ionic solution moves faster than Fe due to higher mobility and it may be separated to form its own deposit (Wolf, 1976). Alternatively, Fe may be separated during deposition by precipitating at lower PH and Eh and effective separation between the two may take place (Roy, 1997) as Mn passes into the solution. It is also believed that early precipitation of iron leaves the remaining solution enriched in manganese that subsequently precipitates as the degree of oxidation increases. As evidence, Arndt and Clement (2012) documented that in Black Sea pyrite-rich mud precipitates in the reduced deeper water while the manganese oxides precipitate in the oxidized surface water.

Manganese has a large number of known minerals. The occurrence of manganese in different oxidation states benefits the deposition of manganese minerals in diverse geological and geochemical environments. According to Kuleshov and Maynard (2017), the webmail site lists 191 minerals with manganese contents of 25% or greater. However, only about 30 of the minerals are economic ores and the rest has no commercial value except their presence as a mineral. The oxides, hydroxides and the carbonates are the dominant mineral phases of manganese (Wolf, 1976; Kuleshov and Maynard, 2017). Based on genetic sources, the manganese minerals can be precipitated from sedimentary (non-volcanogenic) and volcanogenic sources (Wolf, 1976).

Oxides and Hydroxides with a higher valance of manganese		***Oxides with Lower valance of manganese***	
Mineral Name	**Formula**	**Mineral Name**	**Formula**
Pyrolusite	MnO_2	Braunite	$Mn^{2+}(Mn^{4+}Si^{4+})O_3$
Cryptomelane	Kmn_8O_{16}	Housmannite	Mn_3O_4
Nsutite	$Mn_{1-x}^{4+}Mn_x^{2+}O_{2-x}(OH)_{2x}]$ Where x=0.06 - 0.07	Jacobsite	$MnFe_2O_4$
Birnessite	$[(Na,Ca)\ Mn_7\ O_{14}.2.8H_2O$	Bixbyite	$(Mn,Fe)_2O_3$
Todorokite	$(Ca,Na)(Mn^{2+}.Mn^{4+})_7O_{14}\cdot 3H_2O$	***Carbonates***	
Chlcophanite	$[(Mn.\ Zn)\ Mn_{\ 2}\ O_{\ 3}.2\ H_{\ 2}O]$		
Psilomelane	$[Ba,H_2O)_2\ Mn_{\ 5}O_{10}]$	Rhodochrosite	$MnCO_3$
Hollandite	BaR_8O_{16}; R = Mainly Mn^{4+}, also Mn^{2+}, Fe, Co	Manganoan Calcite	$[(Ca,Mn)CO_3]$
Coronadite	$[PbR_8\ O_{16}$;R = Mn^{4+} and $Mn^{2+}]$	Kutnahorite	$[(Ca,Mn)(CO_3)_2]$
Groutite	α-MnOOH	**Silicates**	
Feiknechtite	β-MnOOH		
Manganite	γ-MnOOH	Bementite	$[(Mn,Mg,Fe)_6Si_4(O,OH)_{18}]$
		Neotocite	$[(Mn,Fe)SiO_{3.n}H_2O]$
		Rhodonite	Mn_3SiO_3
		Spessartite garnet	$(Mn_3Al_2(SiO_4)_3)$

Table 2.1: predominant minerals of manganese, summarized after Wolf, (1976), Kuleshov and Maynard, (2017) and Kogel et al. (2006).

Even, from the minerals listed in table 2.1, rhodochrosite, braunite, cryptomelane, manganite, pyrolusite, Housmannite, todorokite and psilomelane are the dominant manganese minerals in commercial deposits of the world (Mynard, 2010; Kuleshov and Maynard, 2017). Quartz, oxides and hydroxides of iron, clay minerals, zeolites, calcite and rarely phosphates and sulfide minerals are the most common gangue minerals found together with manganese minerals in the mineral assemblages of manganese rocks (Morten et al., 1980; Heshmatbehzadi and Shahabpour, 2010, Kuleshov and Maynard, 2017).

2.3. Genesis and Geological Setting of Manganese Deposits

Manganese deposits are formed from diverse origin in the geological record of mineral deposition at different geological setting. Different researchers in different literatures present various ways of classification of manganese deposits based on their origin. Generally, manganese deposits are formed by hydrothermal, sedimentary and supergene or mixed processes (Ozturk, 1997; Roy, 1997; Shah and Moon, 2007; Oksuz, 2011; Bau et al., 2014; Kuleshov and Maynard, 2017). In addition to this, manganese deposits are also classified as sedimentary (non-volcanogenic), volcanogenic and hybrid (volcanogenic-sedimentary) deposits (Wolf, 1976; Kuleshov and Maynard, 2017). The later type of classification depends on the composition of manganese bearing formations and sources of manganese. The source of manganese could be from the weathering crust or from direct volcanism. Both the non- vcanogenic and volcanogenic- sedimentary sources manganese deposits could be geosynclinal and platform type. Wolf (1976) stated that the non-volcanogenic deposit are either geosynclinal or platform type while the volcanogenic-sedimentary manganese deposits are mainly geosynclinal and rarely of platform type. The distinctive characteristics of hydrothermal, sedimentary and supergene type manganese deposits are described in the following sections.

Hydrothermal manganese deposits precipitate from low temperature hydrothermal fluids at the periphery or during the waning stage of a high temperature system (Oksuz, 2011; Kahrazehi et al., 2015; Kuhn et al., 2017). These kind of deposits could be either volcanogenic- sedimentary or volcanogenic manganese deposits (Wolf, 1976). By dimensions and reserves, these types of deposits are the smallest and in the economic regard are of low profitability (Fan and Yang, 1999). Hydrothermal manganese deposits may be stratabound or occur as irregular bodies and epithermal veins.

Hydrothermal manganese deposits are distributed in different parts of the world in a wide range of geological setting. They are formed in the marine environment near spreading centers (active plate margins), mid-plate seamounts and or in subduction-related island arc settings and have been recognized from both modern and ancient geological setting (Bonatti et al., 1976; Glasby 1988, Robertson and Varnavas, 1993; Shah and Moon, 2007). According to Roy (1997) and Nicholson (1990), stratabound hydrothermal manganese deposits can be produced in shallow continental basins through the emission of hydrothermal solutions. These authors also noted that Vein-type hydrothermal deposits are

hosted mainly in volcanics of wide-ranging compositions as well as in a variety of sedimentary rocks of different ages.

A number of hydrothermal manganese deposits formed at the active plate margin, which could be similar to the Ethiopian case, are widely distributed in the world, such as the Northern Apennine (Italy), Pindos (Greece), Othris (Greece) and Olympic Peninsula (USA) (Bonatti et al., 1976; Robertson and Varnavas, 1993 and Park, 1946 as cited in Nicholson et al., 1997). Deposits from Australian Alps, Japan, Chile, Morocco, China and Russia are also identified from similar geological setting (Roy, 1997; Kuleshov and Maynard, 2017).

The sedimentary manganese deposits are those formed as a chemical sediment through precipitation in normal pressure and temperature conditions from solutions enriched in dissolved manganese irrespective of sources (Roy, 2006). Comparing with the hydrothermal and hybrid type, the largest and world class accumulation of manganese deposits are by far formed by sedimentary process (Heshmatbehzadi and Shahabpour, 2010, Kuleshov and Maynard, 2017). These are larger in terms of size and spatial and temporal relationship (Roy, 1997). Sedimentary manganese deposits are mostly hosted in sedimentary rocks, especially in carbonate rocks and rarely associated with volcanic rocks.

Sedimentary manganese deposits are generally formed in marine (deep and shallow marine) basins during marine transgression and regression phases (cannon and Force, 1986) and in continental environments. In the shallow marine environment, these non-volcanogenic manganese deposits are formed around the rims of anoxic basins during higher sea-level rises at locales where the accumulation of clastic sediment is minimum (cannon and Force, 1986). In this case the source of manganese could be multiple (endogenous or exogenous), but the most common sources are sub-marine hydrothermal and terrestrial weathering processes (Roy, 1997).

These hydrothermally or terrestrial weathering generated metal may be transported a long distance from its original site to the depositional basin and directly precipitate or deposit in the basin aided by diagenesis. Manganese deposits of this type are found all over the world. For example, the largest ores are, the Proterozoic ore bodies of the Kalahari in South Africa (Kuleshov and Maynard, 2017), the Cretaceous ores of Groote Eylandt in Australia and the Rhodochrosite ores of the Molango district of Mexico (Arndt and Clement, 2012).

Marine Sedimentary manganese deposits usually formed by two major processes, hydrogenic and diagenic processes (Lange et al., 1992; Bau et al., 2014; Kuhn et al., 2017,).

Accordingly, hydrogenetic process refers to the slow settling of Mn colloids from the oxygenated bottom layer. In this case all the constituents are sourced from the ambient seawater as initially colloidal particles within the water column (Bau et al., 2014). On the other hand, diagenetic processes represent the precipitation of manganese from the pore water within the underlying suboxic /reducing sediment. According to Kuleshov and Maynard (2017), the source of manganese for diagenetic process is an exogenetic source: weathering crust, from the washout of the feeding land mass.

2.4. Manganese Occurrences in Ethiopia

In Ethiopia, the distribution and occurrence of manganese are rare or very minimum or poorly known. According to the promotional data compiled by geological survey of Ethiopia (2013), the Enkafela Manganese deposit, under which the present work is focused, is the only primary manganese deposit known in the country. It was mined in the late 1960's. A prospection license and lease for exploitation was given in 1955 covering an area 300 m by 350 m only, and in 1958 primitive mining started under a private license. The ore was transported by truck to the port of Mersa Fatma on the Red sea coast, and exported via Massaua to USA. The total ore reserve was estimated to be around 75, 000 tons (Getaneh, 1985 as cited in Solomon Tadesse et al., 2003). Out of this about 40,000 ton of manganese were mined from 1959 to 1963 (Solomon Tadesse et al., 2003).

Other manganese occurrences are found in Tigray at Mussley, Beliga, Handeda, Adi Berbere, Adi Chigono areas. However, the origin of these occurrences is not well defined (Solomon Tadesse et al., 2003). Some of them are at least partly of secondary origin (gossan-type?, e.g. Mussley, Adi Berbere). Manganese is also found at Melka Sedi (Kaffa) associated with laterites.

CHAPTER THREE
REGIONAL GEOLOGY

3.1.Tectonic Setting and Geological History of Afar

The Afar Depression illustrates one of the few fascinating places on earth where a rift-rift-rift triple junction of three divergent plate boundaries, the southern red sea, the Main Ethiopian Rift and western Gulf of Aden, unite at one place (Bosworth et al.,2005; Barisin et al., 2009;). On the other hand, the Red Sea, Gulf of Aden and the Main Ethiopian Rift systems, which diverge, propagate and joins at the Afar triangle, are the most important tectonic structures which separates the Arabian, Nubian and Somalian plates (Courtillot et al., 1999; Eagles et al., 2002; Bosworth et al., 2005; Chorowicz, 2005; Doubre et al., 2007; Barisin et al., 2009; Guidarelli et al., 2011). The three plates, the Africa plate, the Arabian plate and the Somali plate, are moving away from each other at different rates by forming the spreading centers (Red Sea, Gulf of Eden and MER) between them (e.g. Tesfaye et al., 2003). Accordingly, the Arabian plate is currently moving away from Africa at ~1.6 cm/yr (Chu and Gordon, 1998, Tesfaye et al., 2003) while the Somali plate is moving away from Africa at 3-6 mm/yr (Justin et al., 1994; Bilham et al., 1999; Chu and Gordon, 1999 as cited in Tesfaye et al., 2003). According to Nobile et al., (2012), the current spreading rates along Afar varies from ~7mm/yr at the northern edge to ~20mm/yr further south at the Dabbahu segment.

The triangular shaped AD is separated from the elevated areas of the Ethiopian plateau to the west, the southeast plateau (Somalia plateau) to the south, and the Danakil horst to the east by fault controlled escarpments (Makris and Ginzburg, 1987; Thurmond et al., 2006). The western escarpment is probably due to step faulting and (Barberi and Varet, 1970; Barrat et al., 1998) rather than to flexuring warping down of the Ethiopian plateau. At the southern tip of the triangle the MER joins the depression.

The tectonic and geological history of the Afar Depression has been the focus of different researchers, though much detail work is still substantial. The Afar rift system is part of the great East Africa Rift system (EARS) along-with the Main Ethiopian Rift (MER), which resides in Ethiopia, shows an ongoing continental extensional zone (Rechert et al., 2012).

Afar Depression also represents the place where new ocean is currently being formed due to the breaking apart of the continental plates (Arabia-Africa) (Doubre et al., 2007). However, breaking is not yet completed. Tesfaye et al. (2003) argued that the Afar Depression could characterize the only active rift on the earth where both early continental break up history and the present-day extensional tectonism can be observed.

The nature of the crust beneath Afar has been the subject of controversy for many years (Abbate, 1995; Barrat et al., 1998; Gupta and Scholz, 2000; Tilahun Mamo, 2004; Chorowicz, 2005). Some argue the nature of the Afar crust is oceanic (Barberi and Varet, 1977; Barrat et al., 1998), while others claim that it is a thinned continental crust and transitional from continental to oceanic crust (Makris and Ginzburg, 1987; Tilahun Mamo, 2004, Doubre et al., 2007; Atalay Ayele et al., 2009). However, the controversy is not still resolved.

The region is characterized by intense tectonic and volcanic activities (e.g. Barrat et al., 1998). The main tectonic features are vertical step-faulting and open tensional features. Faulting and volcanism within the northern Afar depression have localized to 60-km-long and 20km wide (Hamling, et al., 2009) axial volcanic ranges with aligned chains of basaltic cones, shallow seismicity and fissural flows, punctuated by stratovolcanoes, since 4 Myr ago (Wright et al., 2006; Darrah et al., 2013). These volcanically and seismically active magmatic segments are Dabbahu, Alayta, Tat ‘Ale and Erta ‘Ale. All are similar in size, morphology and structure.

A continental break-up can be caused by either the influence of heating (mantle plume uplift/active rifting) or stretching (passive rifting) or the combination of both. However, the mechanism by which continental lithosphere under Afar rift system initially breaks apart and its continued evolution to seafloor spreading are still controversial (Keir et al., 2011; Rechert et al., 2012). The main concept here is the sequence of events. In passive rifting, the sequence would be rifting-uplift-volcanism. Instead, in active rifting the sequence becomes uplift-volcanism-rifting (Alebachew Beyene and Abdelsalam, 2005 and references therein). Courtillot et al. (1999) pointed out both scenarios (active rifting and passive rifting) can be applied in the case of the Afar rift system.

According to many authors (e.g. Courtillot et al., 1999; Wright et al., 2006; Redfield et al., 2003; Doubre et al., 2007; Rowland et al., 2007; Keir et al., 2011; Amaha Atnafu et al., 2013; Darrah et al., 2013; field et al., 2013), rifting of Africa and Arabia starts 30 Myr ago. The horizontal extension on the southern Red Sea Rift within the Afar depression has been localized on magmatic segments (Hayward and Ebinger, 1996, Guidarelli et al., 2011). These magmatic segments are formed by the injection of dikes into the upper crust from underlying magma chambers (Ebinger et al., 2008). Similarly, Bonatti et al. (2015) suggested that the rifting process could have been triggered by the rise of a thermal and/or compositional mantle plume from the upper mantle below Afar. Intrusive basaltic magmatism plays a vital role in triggering the rifting process in Afar.

Bostow and Keir (2011) claimed, from their observation of dike injection, the ongoing Dabbahu Rifting episode show that principally magma intrusion, rather than faulting and ductile stretching, is the cause of extension in this section of the rift, and repeated dike intrusion episodes can reproduce the rift morphology. Generally speaking, many researchers agreed for the cause of vast volcanism in the Afro-Arabian region is related to upwelling mantle plume.

The southern Red Sea rift was initiated by ~29 Ma, and progressed to seafloor spreading by 4 Ma. The Main Ethiopian Rift, the third arm of the Afar triple junction, commenced at around 18 Ma southwestern Ethiopia, and propagated northward into the Afar depression after 11 Ma (Bastow et al., 2005; Beutel et al., 2010 and reference therein; Rechert et al., 2012). Wolfenden et al. (2004) argued that the MER is a much younger, and less evolved, rift than the Red Sea and Gulf of Aden rifts, rather than a failed rift arm. The MER terminates in the north in the Afar Depression, with the east-northeast trending Gulf of Aden and northwest trending Red Sea (e.g. Kogan et al., 2012) .It is an area of thin crust, seismically related to extension, and intense intrusive and extrusive, mostly basaltic, magmatism.

In addition to the breakup of the Africa-Arabia plates, the other complexity which creates the Afar Depression was, separation of the Danakil block, which was once part of the western Ethiopian plateau, by tensional and rotational movements (Bonatti et al., 1971; Tazieff et al., 1972; Bosworth et al., 2005). The Danakil block is an area of highly stretched continental material, experienced between 200% and 400% stretch, isolated due to the landward migration of the Red Sea rifting between Arabia and Nubia (Redfield et al., 2003).

Bosworth et al. (2005), explains the anticlockwise rotation of the Danakil block started since ~6-5 Ma and suggested a total of 23^0 rotations since the initiation of the separation between the Ethiopian plateau and the Danakil. In addition to the vertical-axis rotation, the Danakil block has also undergone a strike-slip translation toward $N20^0E$ (Collet et al., 2000; Tesfaye et al., 2003). Eagles et al. (2002) suggested that the Danakil block will isolate and stand as a micro-continent on the Arabian margin, due to the linkage of the Red Sea and Aden rifts through Afar.

3.2. Lithological Units of The Afar Depression

The geology of the Afar depression and its marginal areas and highlands, like the tectonic and magmatic history, makes it a unique place and is of great interest from diverse scientific perspective. This is because it contains the complete sequence of rocks ranging from the Neoproterozoic to the present time. The geological formations of the Afar Depression and its marginal areas and surrounding plateaus can be divided into four broad units (Figure 3.1): (1) pre-rift complexes; (2) Syn-rift igneous rocks; (3) Pliocene-Pleistocene volcanic rocks; and (4) Quaternary volcanic and sedimentary rocks (Beyene and Abdelsalam, 2005; Bosworth et al., 2005; Mazzarini, 2007).

3.2.1. Pre-Rift Complexes

The pre-rift complexes include the Neoproterozoic basements, the Mesozoic sedimentary rocks and Eocene-Miocene basalts.

The Neoproterozoic basement rocks, which are part of the Arabian-Nubian shield (ANS), is exposed on the periphery of the Afar Depression (Alebachew Beyene and Abdelsalam, 2005; Bosworth et al., 2005). These basement rocks are found to the north and northwest of AD in eastern Eritrea and Northern Ethiopia (Varet and Gasse, 1978; Vail, 1985; Berhe, 1990; Stern, 1994 as cited in Alebachew Beyene and Abdelsalam, 2005). The basement rocks are also found within the Danakil and Ali-Sabieh blocks (Varet and Gasse, 1978; Alebachew Beyene and Abdelsalam, 2005; Bosworth et al., 2005).

The influence of the pre-existing structures of the basement on the development of the MER, Red Sea and Gulf of Aden, creates a point of discussion among different researchers. Accordingly, some researchers (e.g. Alebachew Beyene and Abdelsalam, 2005 and references therein; Bosworth et al., 2005 and references therein) argued that the structural and stratigraphic evolutions of these structures have been significantly influenced by pre-existing basement structures. On the contrary, Kazmin (1971) concluded that the faulting in

the Afar region was not determined by the pre-existing structures in the sediment. Mohr (1975, as cited in Alebachew Beyene and Abdelsalam, 2005), has also argued that these rifts did not exploit pre-existing regional structural fabrics because the MER run Oblique to the nearest Neoproterozoic structural trends. According to Bosworth et al. (2005), the old regional lineament called Marda fault trending NNW-SSE, could be taken as an evidence for the influence of pre-existing basement structure. It is aligned with some Pleistocene volcanic centers and the main trend of the Red Sea.

The Neoproterozoic basement rocks are covered by the Mesozoic sedimentary rocks (Varet and Gasse, 1978). The Early Jurassic Adigrat sandstone, Late Jurassic Antalo limestone and Cretaceous upper sandstone (Debre Libanos sandstone) are the typical sedimentary rocks found on the Ethiopian plateau (Varet and gasse, 1978; Alebachew Beyene and Abdelsalam, 2005).

The Mesozoic sediments are overlain by the flood basalts of the Trap Series with a marked unconformity (Bosworth et al., 2005). On the Ethiopian plateau, the sequence have a thickness of ~2km and covers 600,000 km^2 (Mohr, 1983b; Zanetin, 1993 as cited in Bosworth et al., 2005). According to Hofmann et al. (1997), the Trap Serious volcanic rocks were erupted over a short period of time at ~30Ma (Oligocene).

3.2.2. Syn-Rift Igneous Rocks

Flood basalts of Miocene, which are exposed along the margins of the depression represent the syn-rift volcanic formations (Varet and Gasse, 1978; Alebachew Beyene and Abdelsalam, 2005). They consist of either of eruptive basalt and of either eruptive or intrusive alkaline to per-alkaline granites. The flood basalts of AD ranging ~25-15 Ma age, are deeply weathered and highly faulted during the eruption (Alebachew Beyene and Abdelsalam, 2005; Bosworth et al., 2005). These rocks occur in limited areas around the Gulf of Tajura and the Ali-Sabieh block (Varet and Gasse, 1978). The oldest volcanic rocks are assigned to the Adoli, Mabla and Dahla series (Varet and Gasse, 1978; Bosworth et al., 2005). The Mabla serious consists of rhyolite and ignimbrites with minor intercalation of basalts, erupted along the N-S trending vents (Varet and Gasse, 1978). The Dalha Serious is dominantly basaltic found inter-bedded with rare detrital sedimentary rocks and ignimbrites (Alebachew Beyene and Abdelsalam).

The alkaline to per-alkaline granitic intrusions intruded the Precambrian basement, the Jurassic sedimentary rocks (limestone) as well as the old trap serious (Varet and Gasse,

1978). These occur along the western and the eastern Afar margin and the northern Afar Depression.

3.2.3. Pliocene-Pleistocene Volcanic Rocks

Most of the Afar Depression is covered by Pliocene-Pleistocene volcanic rocks and these formations are called Afar stratoid series (Barberi et al., 1975; Varet and Gasse, 1978; Alebachew Beyene and Abdelsalam, 2005; Bosworth et al., 2005). It covers, approximately 2/3 of the Afar floor, and its thickness reaches 1500m. According to Alebachew Beyene and Abdelsalam (2005), the preservation of igneous features and tectonic activities of the depression is highly manifested in these units.

The Afar stratoid series overlie the Dalha Series unconformably suggesting a prolonged erosion period and reduced magmatic activity (Bosworth et al., 2005). The eruptive style and structuring of the Afar Stratoid series shows the transition from continental rifting to oceanic spreading (Barberi et al., 1975; Bosworth et al., 2005). Varet and Gasse (1978) based on age determinations (which lie between 4.4 and 0.4 Myr) suggested that the Stratoid formations were built during Plio-Quaternary times.

3.2.4. Quaternary Volcanic and Sedimentary Rocks

Basaltic flows, scoria cones and alkaline to per-alkaline silicic rocks are the major Quaternary volcanic rocks exposed in the Afar Depression (Varet and Gasse, 1978). Fissures and shield volcanoes are the style of eruptions and erupted in the Afar Depression over the past 1My (Bosworth et al., 2005). Active rifting continued through the Quaternary west of the Danakil horst, at Erta'Ale, Tat Ali, and Alayta and within Afar at Manda Hararo, Manda Inakir and Dama Ale (Tazieff et al., 1971; Barberi and Varet 1977 as cited in Bosworth et al., 2005; Varet and Gasse, 1978). The Quaternary volcanic rocks of northern Afar are characterized by shield volcanoes. The axial range basalts get progressively younger from the marginal zone towards the axial zones and show characteristics similar to mid-oceanic ridges (Barberi and Varet, 1977; Alebachew Beyene and Abdelsalam, 2005).

The separation of the Danakil block from the African plate creates the physiographically low laying AD. This makes the depression suitable depositional environment for sedimentary rocks. Quaternary sedimentary rocks, in addition to volcanics, are the other characteristic lithological formations of AD. Significant shallow water sedimentary rocks were deposited along Manda Harraro-Goba'adi, Manda Inkir grabens and Dobe rift basins

in the central Afar between ~12 and 1Ka (Alebachew Beyene and Abdelsalam, 2005). The Dallol depression is covered by evaporite and lacustrine sedimentary rocks of several meter thick (Varet and Gassse, 1978).

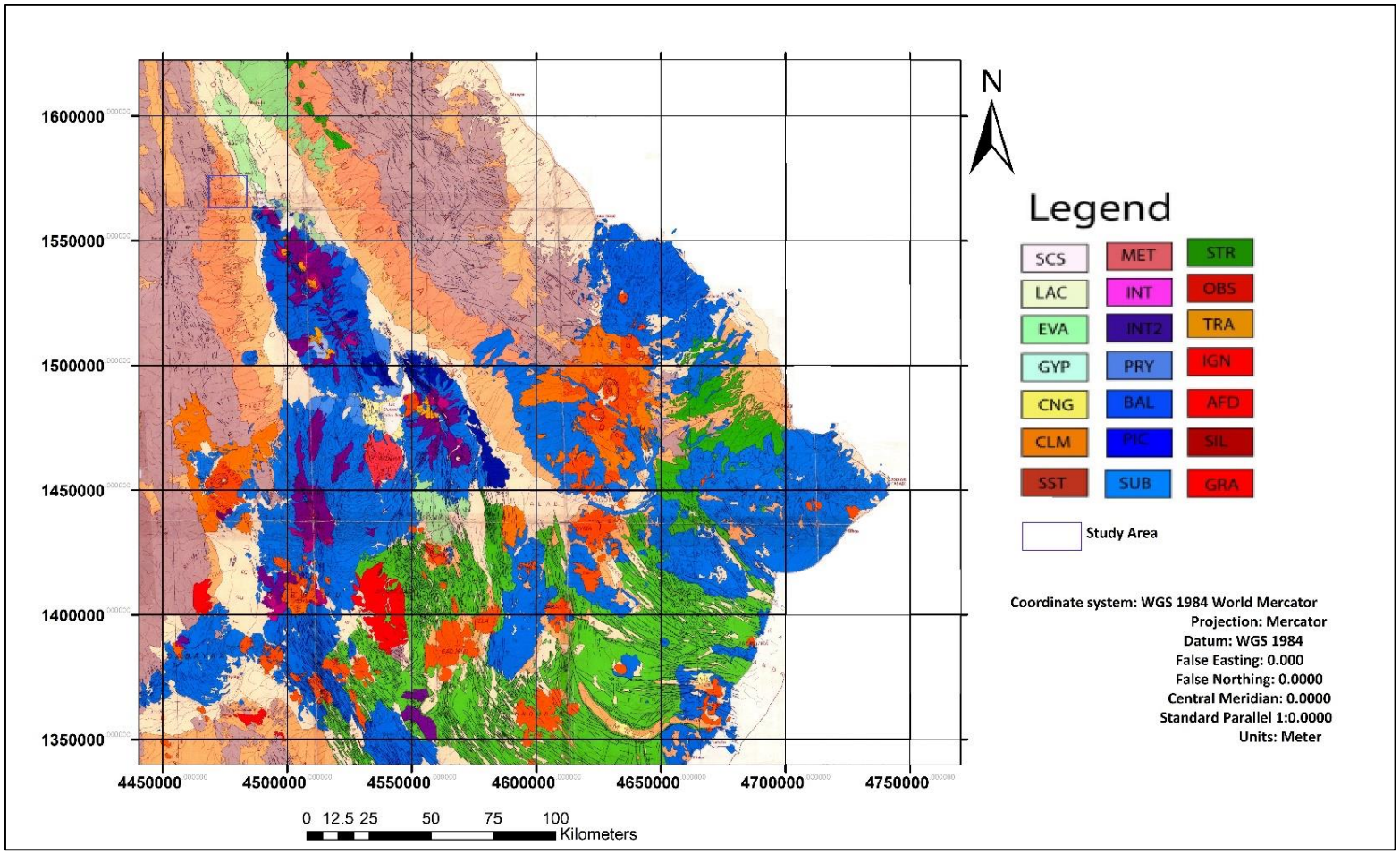

Fig. 3.1: Geological map of Danakil Depression, Northern Afar, Ethiopia (Barberi et al., 1973). Note. SCS: silts, clays and sands (mud flats); LAC: lacustrine limestone and diatomite; EVA: evaporites (mainlyhalite, potassic salts and salt domes); GYP: gypsum deposits bordering the Depression

CNG: continental conglomerate; CLM: coral limestone locally gypsum; SST: sandstones, sands, red or polychromatic shales and associated volcanites; MET: epimetamorphic basement, granites, basic intrusions, Mesozoic cover (limestone and sandstone) and tertiary plateau traps; INT: lavas of intermediate composition (trachyte); INT2: lavas of intermediate composition (hawaiites, andesine basalts, ferrobasalts) ; PYR: basic pyroclasts of subaerial origin; BAL: basic lava flows, lava fields and related spatter cones, mainly basaltic composition; PIC: picritic basaltic flows and related spatter cones; SUB: basic subaqueous (submarine and sublacustrrine) lava flows, hyaloclastitic ash rings and layers locally covered by marine deposits (coral limestone); STR: recent traps of the Depression (stratoic basaltic lavas and ignimbritic sheets, locally covering rhyolitic massifs): submarine flows with pillow-lavas (MARSA FATMA); OBS: peralkalinerhyolitic obsidians (flows and domes); TRA: alkaline oversaturated trachytes, alkaline and peralkaline rhyolites, mainly in glassy flows and domes (Erta Ale Range); IGN: ignimbrites, pumice flows and pumice layers mostly of rhyolitic composition; AFD: intermediate and silicic lavas of Afdera volcano; SIL: silicic massifs, mostly of rhyolitic composition (lava flows and domes); GRA: alkaline and peralkaline granites and associated aplites and pegmatites intruded into the old tertiary traps of the Depression (Affara Dara massif).

CHAPTER FOUR
LOCAL GEOLOGY

4.1. Introduction

The presence of a number of intermittent river cut, road cut and gully exposures and the absence of vegetation and soil cover makes the access to encounter the lithological units of the study area very simple. The lithologies are well exposed and the contacts between them are visible; it is therefore simple for mapping. On the contrary the intense nature of tectonism and deformation affects the distribution and contact relationship of some rock units. Consequently, some of the rock formations are found as patchy here and there or covered by other units. Some of these rocks are not included in the current scale of geological map (1: 25000) but their characteristics and relationship is presented in the lithological sections. Geo-referenced Google Earth image map is used as a base map for geological mapping and contacts between the rock units was collected using GPS readings. Since the area is desert and barren, the GPS reading is almost perfect and coincides with the geo-referenced Google Earth image map.

The geology of the study area is characterized by an extensive distribution of both volcanic and sedimentary rocks. The major lithological units exposed in the study area and its surroundings are;

- Basalt
- Sandstone (Red Series)
- Gypsum and reef limestone
- Conglomerate
- alluvial and lacustrine sediments

The rock units are described and mapped according to their vertical and lateral contact relationship and using information from previous works. The limestone unit isn't extensive and found as patchy covering a small area and associated with gypsum. As a result, these two units are not mapped separately. On the other hand the red serious sandstone is exposed only in river cut and gully exposures, mostly covered by the other units. Therefore, the red sandstone is not mappable in the current geological map, at a scale of 1: 25000. Instead it is well illustrated and presented in lithological section (Fig. 4.8). The areal distribution of the

rocks is presented on the geological map (Fig. 4.1) and the detail description of each unit is also presented below.

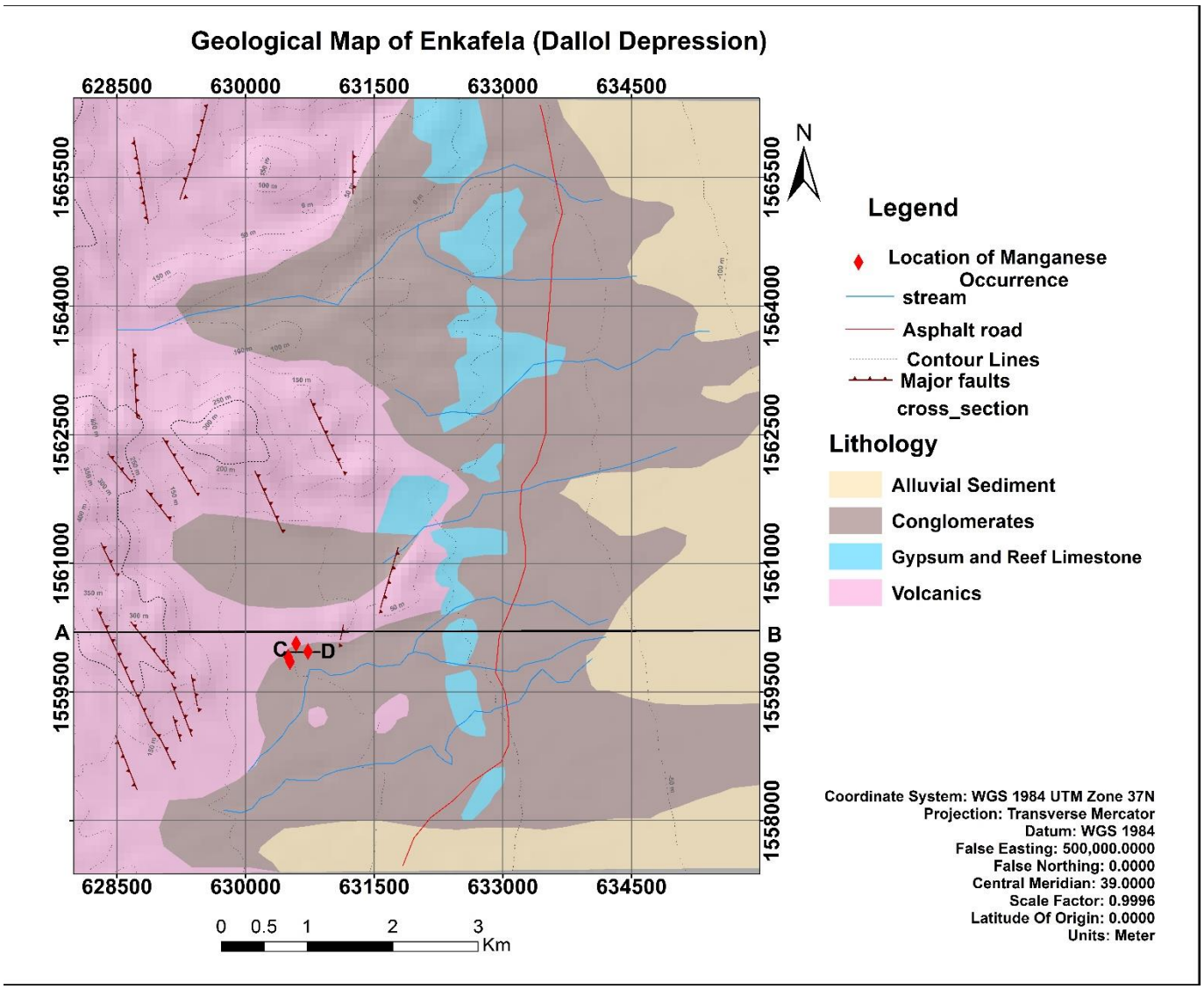

Figure 4.1(A): Geological map of the Study Area

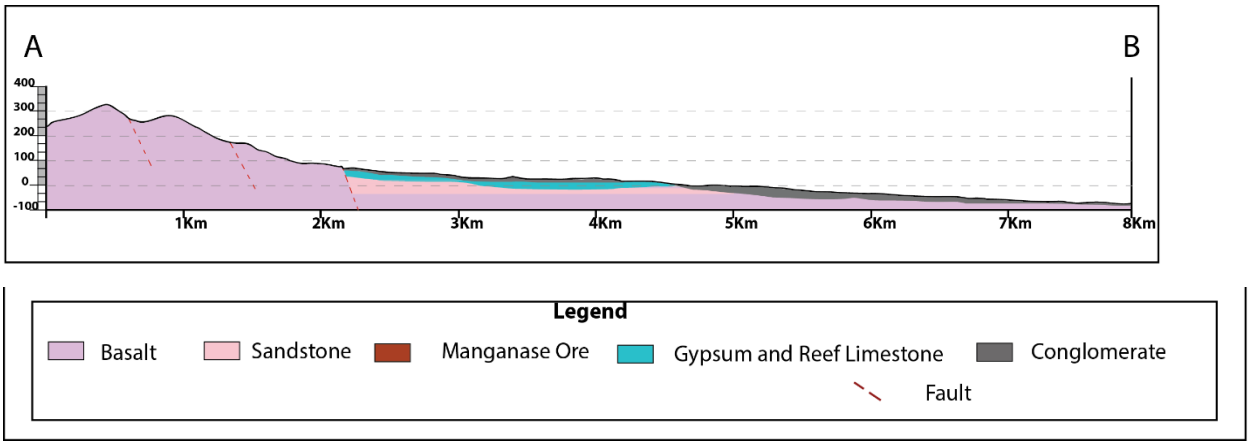

Figure 4.1(B): Geological cross section along A-B

4.2. Lithologic and Petrographic Descriptions

4.2.1. Basalt

As Part of the volcanically active Afar Depression, the study area is comprised of different volcanic rocks. Basalt is the major lithological unit found in the study area. It covers an area of about 24 km^2. The western highland part of the mapped area is totally covered by this unit. This area is part of the western escarpment. The basalt has two varieties. The first type of basalt (basalt I) covers a large area while the second unit (Basalt II) is found intercalated with the sandstone unit (the red series) (Fig. 4.3) and it is not extensive. The basalts are of two different ages. Basalt I is part of the pre-rift Oligocene (~30Ma) trap series. Basalt two is part of the syn-rift Miocene Dalha series (6-8 Ma) (Alebachew Beyene and Abdelsalam, 2005), found inter-bedded with the Red Series sandstone.

Basalt I is highly weathered, fractured and jointed (Fig. 4.2 A&B). The joints are generally trending NNW and filled by secondary minerals like quartz and iron rich materials (Fig. 4.2 A). It is exposed on the marginal escarpment forming steep cliff topography and covers the rugged mountainous terrain which is dissected by intermittent rivers. The fresh out crop basalt is dark greenish color but due to the intensive nature of weathering its color is changed to reddish.

In most cases it has aphanitic texture. However, at some places it also shows porphyritic texture and contains coarser crystals of feldspar and greenish olivine. Sometimes, where the topography is relatively flat, it is covered by a sheet of talus. The talus is comprised of a collection of broken rock fragments of different composition.

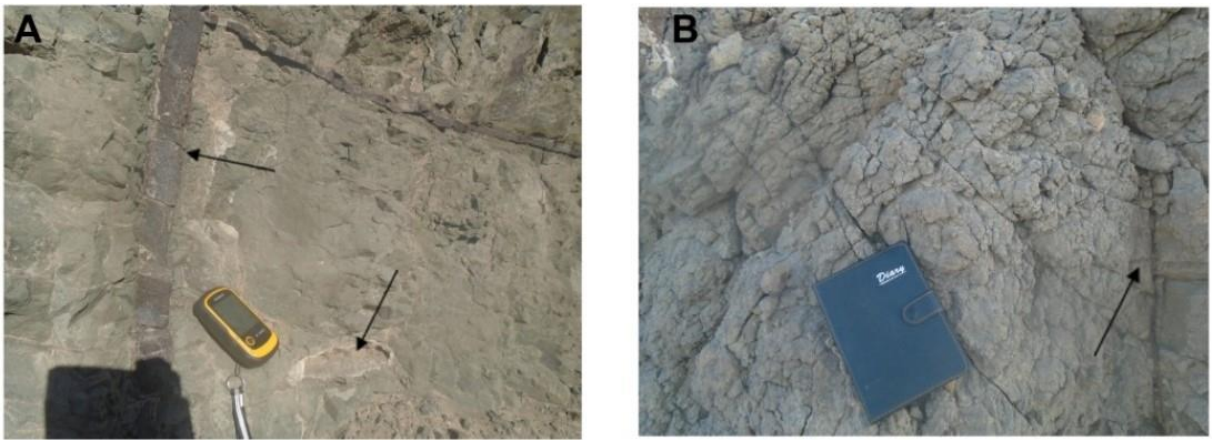

Figure 4.2: Basalt I *(A) the arrows show veins of iron rich material and cavities filled by quartz (B) Highly weathered and fractured basalt, the arrows show open fractures*

Basalt II is amygdaloidal and is found intercalated with the ferruginous sandstone (Fig. 4.3A). The exposure of this unit is found in river cut and gully exposures and shows SE-dipping layering (Fig. 4.3A) with18m total average thickness. It is greenish- gray, with white crystals within the vesicles (Fig. 4.3B) and sometimes it shows pillow structure. The amygdales are filled with zeolites, calcite and quartz (Fig. 4.3B&C). The petrographic study also confirmed the presence of these minerals filling the amygdales. The presence of calcite minerals is also checked on site using hydrochloric acid test. It shows effervescence at the grain boundary of the vesicles. In most cases the basalt is jointed and the joints are filled by secondary minerals. The joints show two joint systems. Polygonal joints are also observed at some places. The joints are continuous to the intercalated sandstone unit and similar minerals fill the joints.

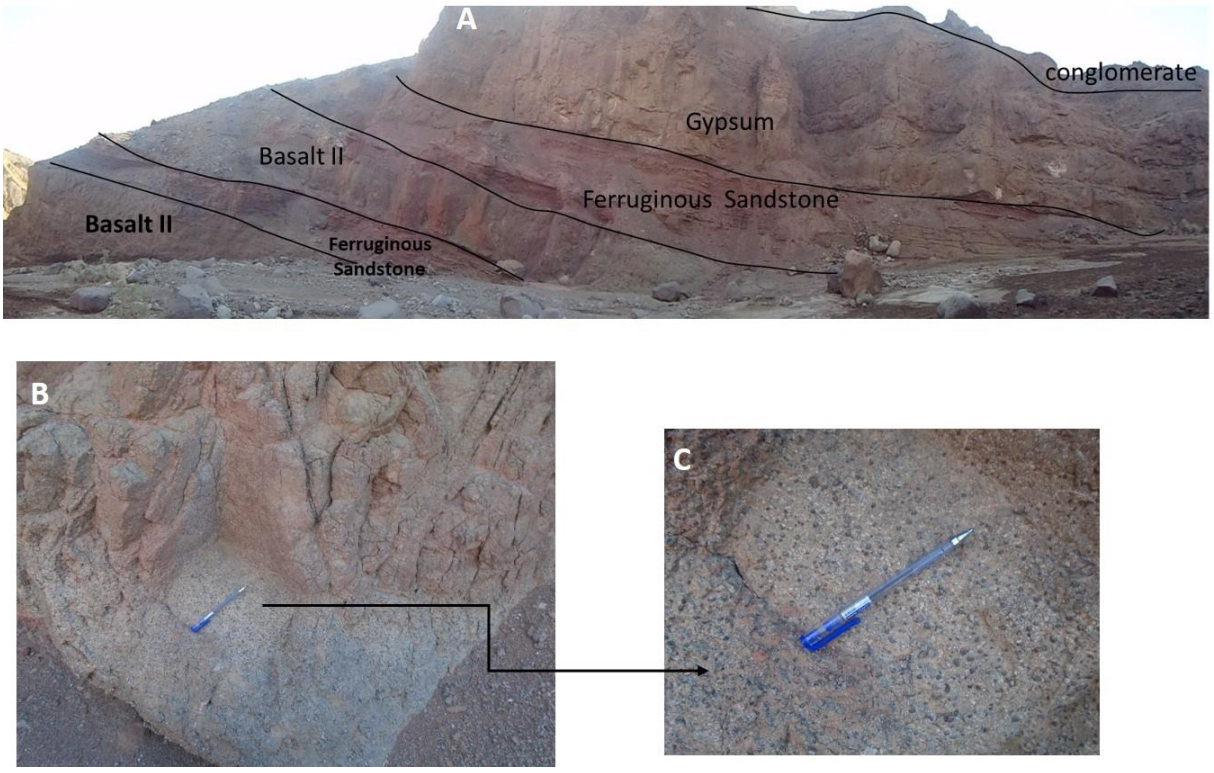

Figure 4.3 Basalt II (A) panoramic view of river cut exposure, exhibit intercalation of basalt with ferruginous sandstone, sub-horizontal SE dipping beds (B) amygdaloidal basalt exposure (C) close up look of image 'A' showing the amygdales and the filling secondary minerals

Microscopic study of this rock reveals that the rock is dominantly composed of plagioclase feldspar (40%), pyroxene mainly diopside (5%), olivine (10%), relatively dark colored and fine grained opaque minerals (20%) and the remaining 25% is represented by secondary

minerals. The common secondary minerals are zeolite, calcite and quartz. Acicular (needle like) zeolite crystals fills the amygdales of the altered basalt (Fig.4.4 A, B, E, F) while the quartz and calcite minerals precipitate through the veins of the main rock (Fig. 4.4 C&D). Zeolites are observed replacing the high temperature pyroxene and olivine minerals. This shows that the basalt experiences alteration by hydrothermal fluids.

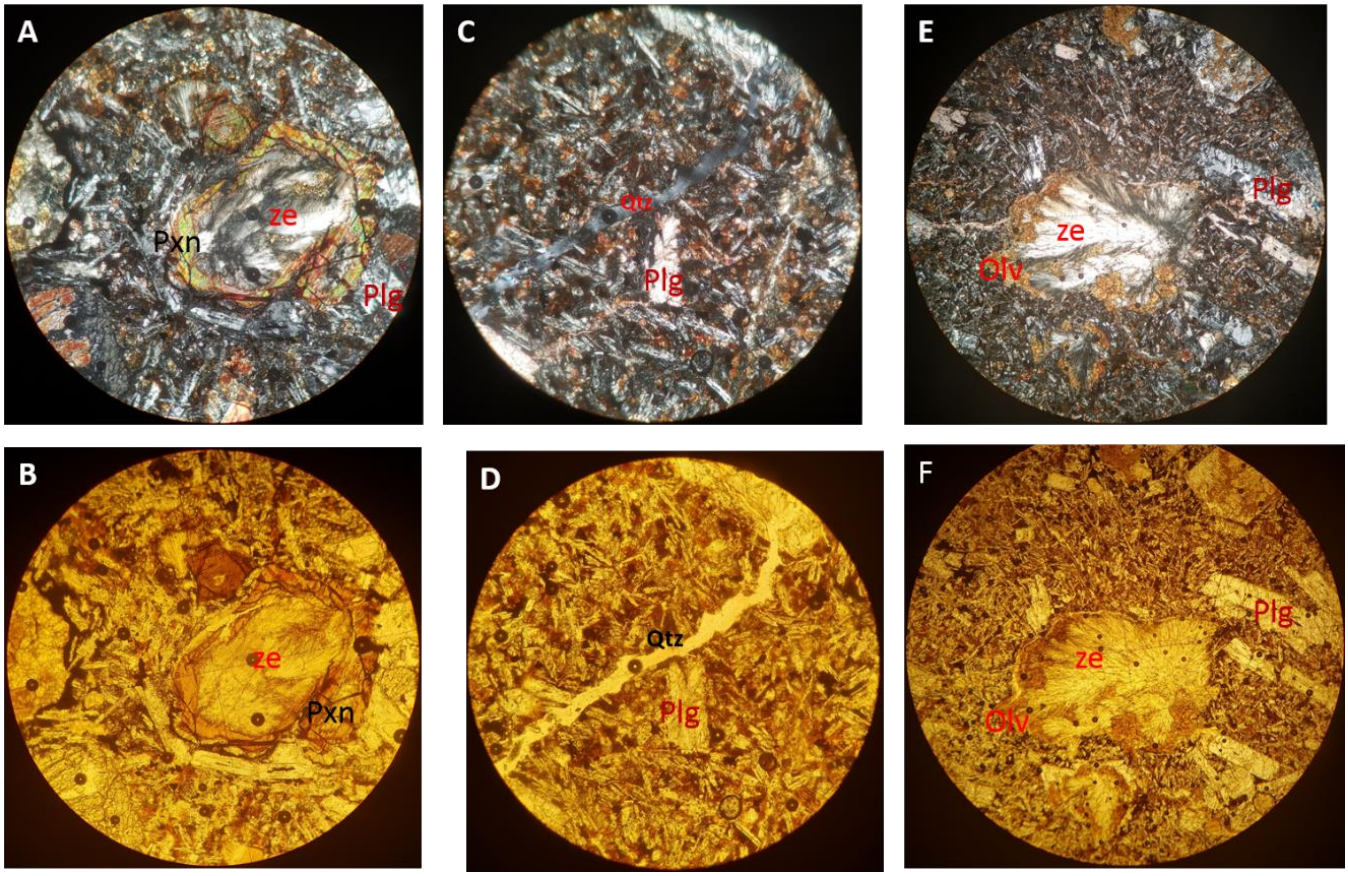

Figure 4.4: photomicrographs of thin sections of Basalt II at 10x magnification. A, C &E are under XPL and B, D &F are under PPL view. A and B shows the replacement of pyroxene by zeolite, C and D shows quartz veins, E and F shows replacement of olivine by zeolite mineral. The labels stands for Ze.-zeolite, Plg.- plagioclase feldspar, Qtz.- quartz, Pxn.- pyroxene and Olv.- olivine

4.2.2. Sandstone

The sandstone rock is found at the base of the escarpment and it is known by the name 'Red Series'. It is unmistakably dark-red or violet-red colored (Fig. 4.5B), possibly because of high content of iron oxide. This reflects the intensive weathering and removal of lateritic soils from the highland areas of the depression shoulder. The high iron content is possibly derived from the highland volcanic rocks. The outcrop is exposed in wide channeled streams and intercalated with the amygdaloidal basalt intrusion (Fig 4.5A).

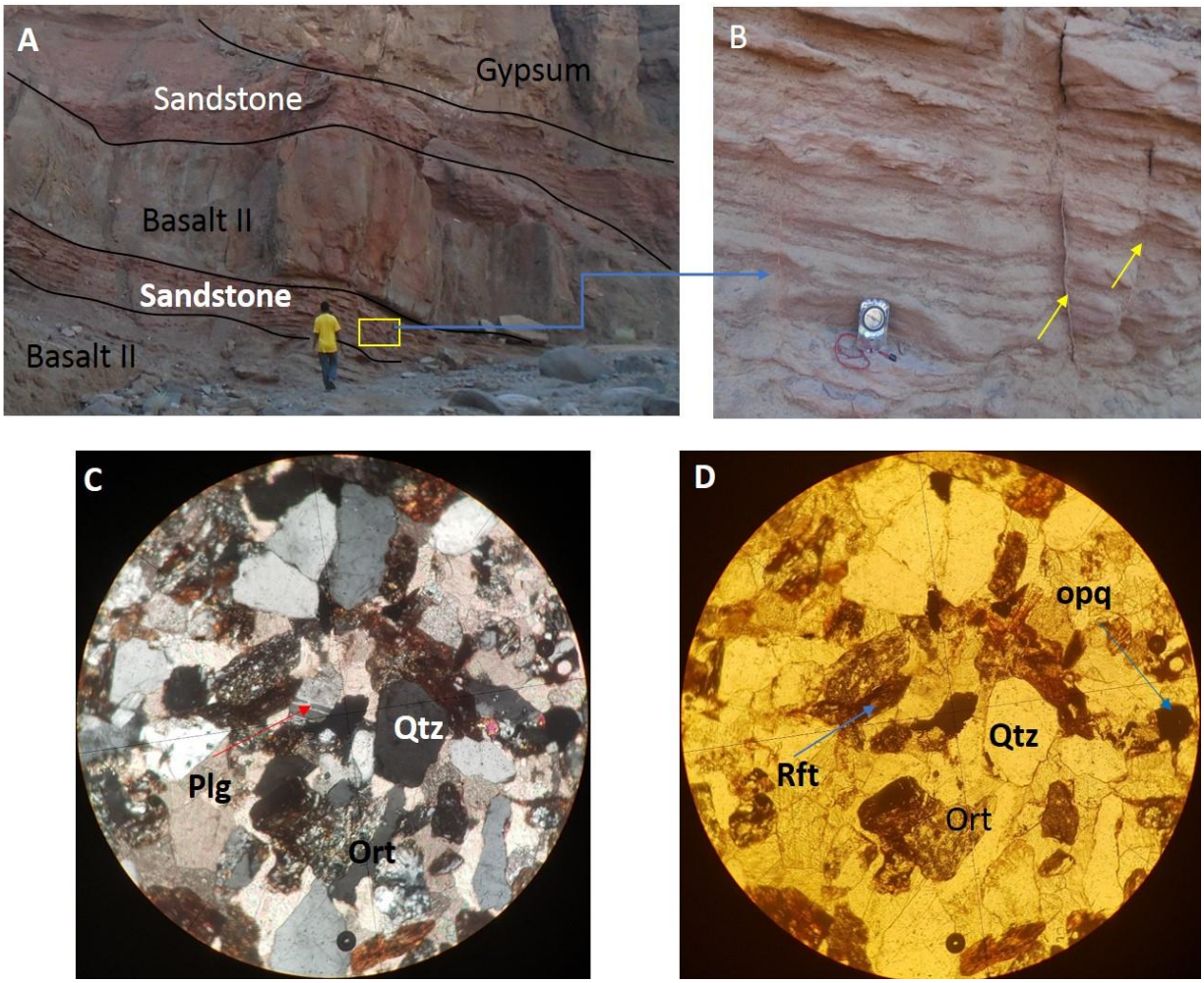

Figure 4.5 sandstone outcrops and thin section photos (A) sandstone intercalated with basalt and overlain by gypsum (B) close up look of image A, represented by the yellow rectangle (C &D) sandstone thin sections under XPL and PPL, the labels stands for Qtz-quartz, Plg- plagioclase feldspar, Rft-rock fragments and Ort-orthoclase feldspar

The sandstone is medium to coarse grained, laminated, well sorted and sometimes friable. Stream exposures indicate that the sandstone is covered by the gypsum unit and the associated reef limestone and later by conglomerates. Its bed is not continuous throughout the study area since it is highly affected by the regional tectonics. It is also affected by veins of different system. These veins are filled by quartz or calcite. These veins are continuous to the intercalated amygdaloidal basalt (Basalt II).

The exposed outcrop has a thickness ranging from 2m to 8m. However, outside the study area, the thickness of this sandstone is higher and mapable exposure is found. According to Barberi et al. (1972), this detrital formation (red series) represents the oldest sediment found in the depression. It is dated as lower-Miocene (24M. Y.) These authors also noted that the age of this series provides the upper limit for the subsidence of the Danakil rift.

Examination of thin section (Fig. 4.5C&D) reveals that the sandstone is mature, moderately sorted, grain supported and contains sub-angular to sub-rounded minerals dominantly quartz. It is mainly composed of quartz (75%), orthoclase feldspar (10%), twined plagioclase (2%), rock fragments (8%) and opaque minerals which could be iron oxide (5%). Both mono-crystalline and polycrystalline quartz are common. The orthoclase shows brown or cloudy appearance which could be due to alteration but the quartz is white and an altered.

4.2.3. Gypsum and Reef Limestone

Gypsum and the reef limestone cover a total area of 4 square kilometers. The units are exposed in the central part of the study area. As shown in the geological map (Fig. 4.1), the units are not continuous throughout the study area rather they are distributed sporadically along the NNW direction. Most of the time, the intermittent rivers incised these units. (Fig. 4.6A). Interlayering of gypsum and reef limestone is common. The gypsum unit is rarely found overlaying the reef limestone and sometimes covered by conglomerates. It is also calcareous, found intercalated with fine grained mudstone and lacustrine sediments. The gypsum is white, soft, fine grained, horizontally to sub-horizontally layered and shows lamination (Fig. 4.6B). Selenite type of gypsum is common within the layers. Primary selenite exhibits clear-white, radiating, fibrous, rarely euhedral and transparent growth crystals (Fig. 4.6C&D). Moreover, Secondary selenite is observed associated with carbonates. It fills cavities within the carbonates.

Oolitic limestone and calcarenite rocks are found separated by reef limestone. These rocks are observed at Enkafela manganese deposit (see Fig. 5.1).The true total thickness of the gypsum and reef limestone is well exposed in gully exposures and ranges from 5m to 20m. The reef carbonates are rich in shallow marine coral reefs and fossils. Red algae, gastropods, tridacna (kind of bivalve), are the common coral reef facies observed. Barberi and Varet (1970) noted that these reef deposits are related to the invasions of the Red sea into the Danakil Gulf 200,000 and 80,000 years.

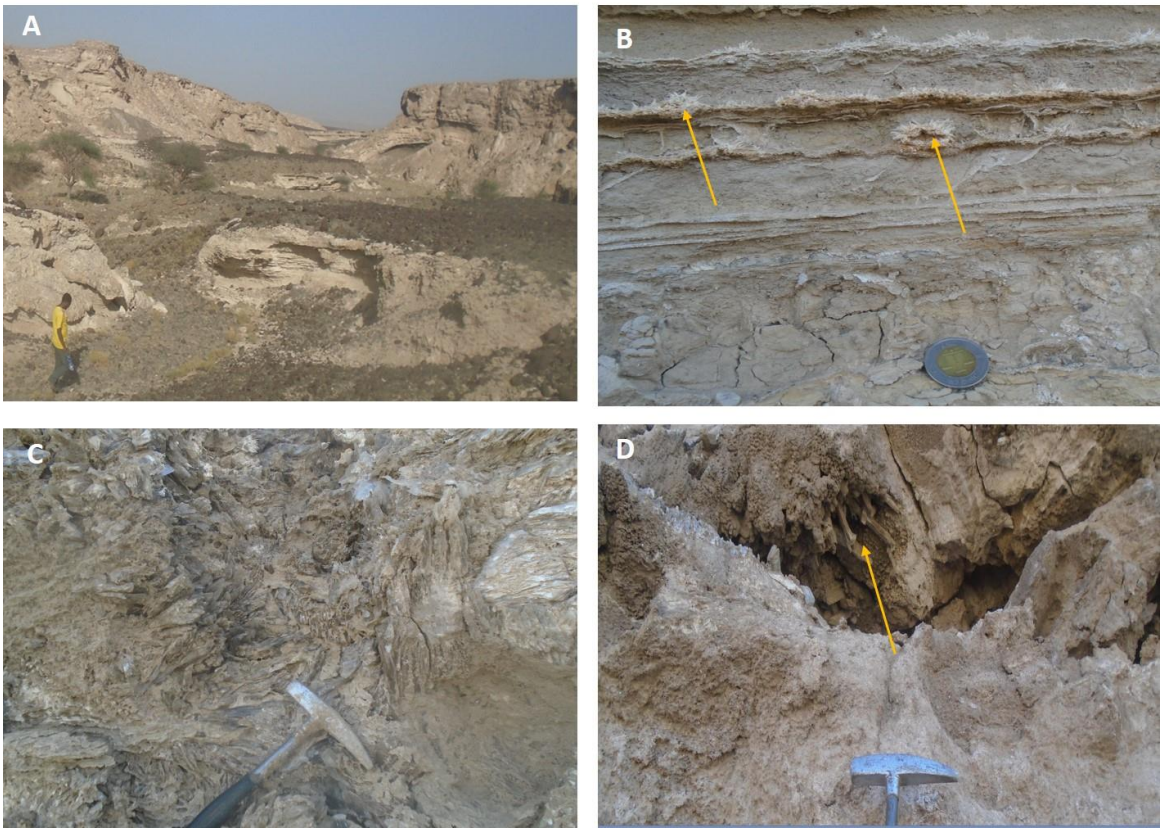

Figure 4.6: Gypsum out crops. *(A) Cliff forming gypsum incised by river (B) Euhedral prismatic crystalline selenite (C) laminated calcareous gypsum, the arrows show fibrous crystals of selenite (D) secondary selenite (indicated by arrow) filling cavities in carbonates*

4.2.4. Conglomerate

This unit is exposed in the central part of the study area covering a total area of about 31 km^2. It covers the gentle slope from the foot of the western escarpment to the lower flat area. Mostly, it is well exposed on river cuts and gullies overlying the gypsum and reef limestone unit (Fig. 4.7 A). It is found as a distinctive layer; and has a thickness ranging from 3m to 15m. The thickness varies from east to west; generally increases towards west. The conglomerate unit is composed of sub-rounded to rounded pieces of clasts with varying grain sizes ranging from granule to boulder size (Fig. 4.7 B). These clasts consist of highly durable rock fragments of various compositions which could be derived from the western highland volcanic and basement rocks. It is poorly sorted, normally graded and matrix supported. Occasionally, this unit shows good sorting and upward coarsening. The matrix is fine to coarse grained sand and even finer clasts. On occasion, fine grained gravel clasts support the pebble to boulder size clasts as a matrix. According to Boggs (2006) genetic classification of conglomerates, the conglomerate is classified as a ploymictic conglomerate as it consists of frame work grains that are of mixed composition.

4.2.5. Alluvial Sediments

These units are sediments of different composition covering the flat topography of the study area. They are often found overlying the conglomerate unit and cover around 12 km^2 of the study area. The sediments are found forming stream flow-dominated alluvial fans. The alluvial sediments are formed by the intermittent rivers which flow from the dissected western mountain caused by flash floods during rainy season. The sediment load carried by these streams finally deposited on the flat area between the western highland and the depression. The alluviums exhibit almost all types of debris ranging from boulder size to size (Fig. 4.7 C&D). The boulders are found close to the ridge; nearby the source region. The finer clasts cover lowest part of the depression. It has a 2m maximum thickness. The thickness of the deposit decreases and sediment sorting increase dawn towards the depression.

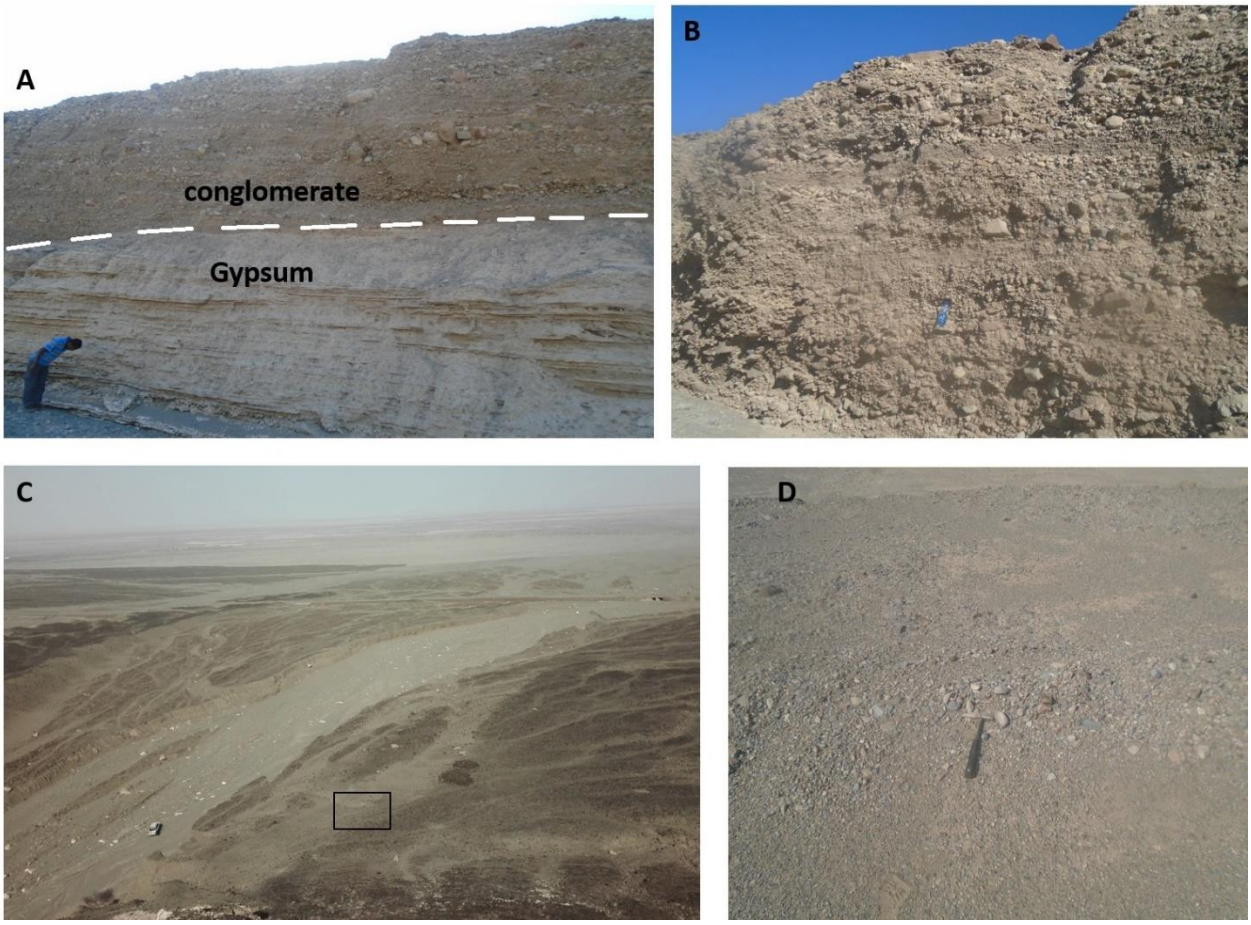

Figure 4.7: Conglomerate and alluvial sediments (A) bedded conglomerate underlain by gypsum (B)conglomerate exposure (C) panoramic view of alluvial sediment exposure (D) close up view of image A represented by the black rectangle

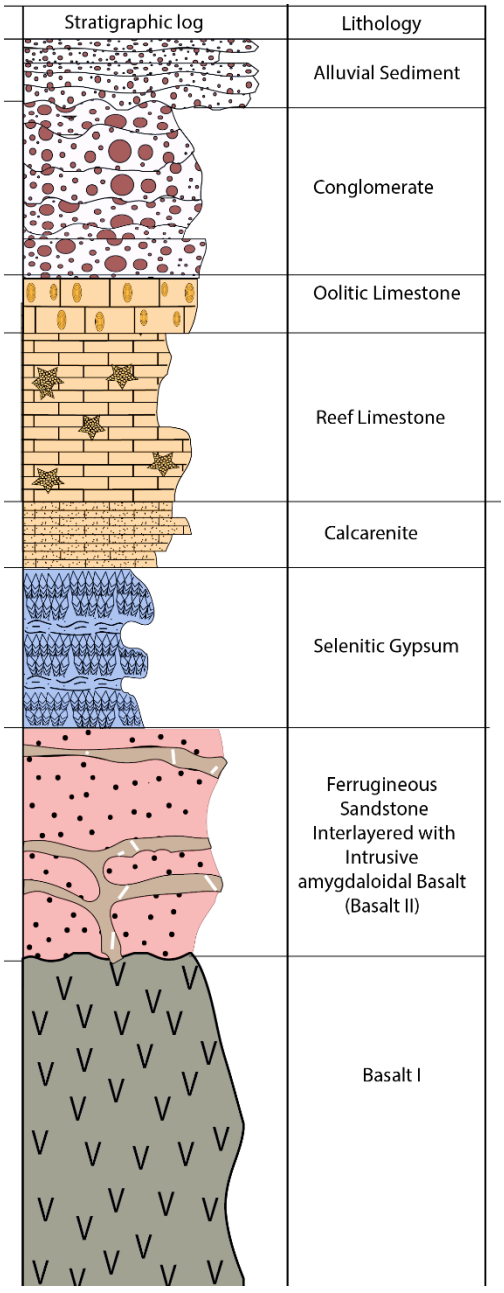

Figure 4.8: General Lithological Stratigraphy of the Study Area (not to Scale)

Geology and Geochemistry of Enkafela Manganese deposit

5.1. Introduction

In this chapter, the detail geology (including geological setting) and geochemical analysis results of Enkafela manganese deposit are presented. The investigation is supported by field observations and various analysis techniques such as geochemistry and mineralogy. The analyses are designed in order to describe the general characteristics of the deposit in terms of the nature of mineralization. Finally, it is applied to understand and define the genesis of the deposit.

5.2. Geological Settings

The Enkafela Manganese deposit is the only known primary manganese ore deposit in the country. The deposit is situated about 20km west of Dallol at the border between the salt plain and the western escarpment in the northern AD, specifically at the location of 630729 E and 1559971 N (Fig. 4.1). Prospection and small scale mining of the deposit were started in a small area in the 1960's. The ore was transported by truck to the port of Mersa Fatma on the red sea coast, and exported out of the country (Geological Survey of Ethiopia, 2013).

The geology of the Enkafela area is characterized by fossil coral reefs and marine formations composed of gypsum, alluvial sediments and conglomerates. Around the salt plain to the western margin belts of gypsum, coral reefs and conglomerates are exposed. These were deposited in the shallow sea along the former coastline. These marine formations indicate the incursion of the area by the red sea during the Pleistocene. Lalou et al. (1970) documented, by dating corals using Th^{230}/U^{234} dating method, that there were two main stages of marine invasions at 80,000 and 200,000 years ago (Bonatti et al., (1972). The study area is also characterized by sandstone called red series and volcanic rocks.

The manganese deposit under study is found interstratified within the marine formations. It is actually exposed in dry channels, the old mine site and other man-made exposures. Otherwise, it is covered by the marine formations. Consequently, understanding the aerial extension of the deposit, especially its northern extension is difficult without drilling. A typical lithological section is presented in figures 5.1 and 5.2, as observed from intermittent stream exposure North West of the old open pit. The section shows highly weathered basalt overlain by the thin manganese layer. Reef limestone, which is cemented by manganese oxide, covers the manganese ore deposit and later overlain by Oolitic limestone. A thin sheet of conglomerate consisting of unconsolidated rock fragments overlay the Oolitic limestone. On the other hand

reef limestone and calcarenite marine formations inter-fingers or wedges into the manganese ore layer. This situation marks the end point of the extension of the manganese strata in the eastern part.

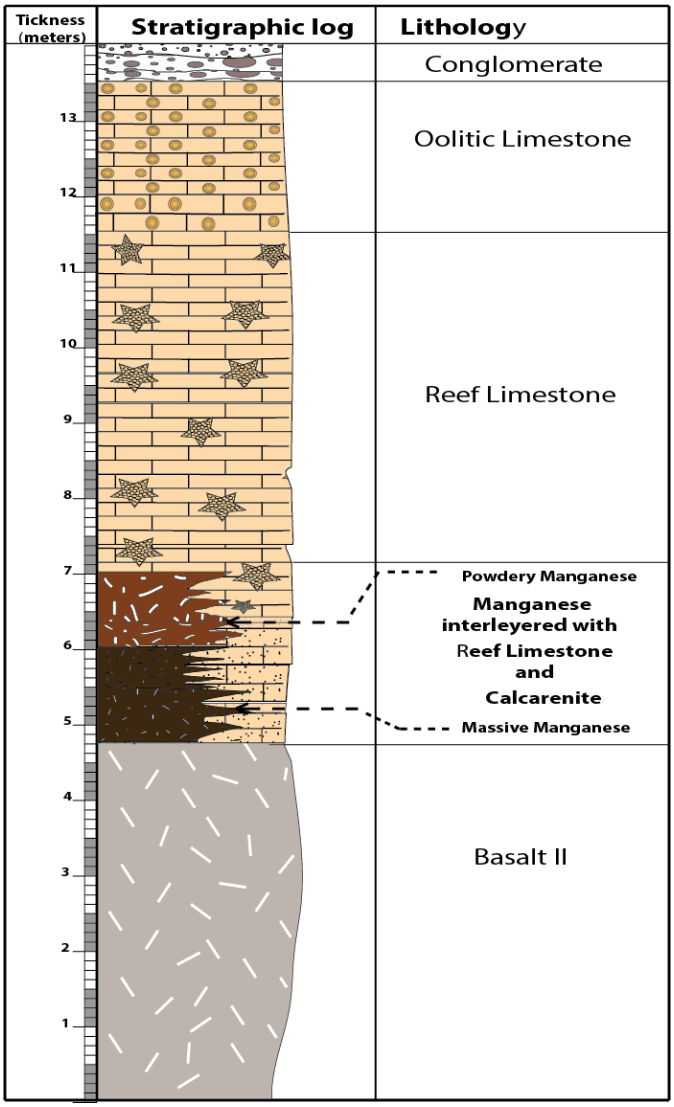

Figure 5.1: Lithological section of the Enkafela Manganese deposit

The manganese deposit is normally confined between the basalt unit and the reef limestone. The ore deposit thickness is variable, ranging from 10cm to 2.15m. Generally, the ore stratum is characterized by two distinctive manganese layers, one is massive and the other is powdery/friable (Fig. 5.2). The massive manganese is relatively thicker with maximum thickness of 1.25m and underlain by the basalt unit. It is black in color, sometimes shiny, pure, hard and compact mass and shows botryoidally radiating outer surface (Fig. 5.3 A). It is smooth on its outer surface, but it also shows very fine crystalline texture from inside when it breaks or through cavities (Fig. 5.3 B). In the southern part where the thickness is

about 1m, it is exposed alone without being overlain by the powdery manganese (Fig. 5.3 C).

The powdery manganese is relatively thinner, reaches to 0.9m in thickness. The thickness increases from south to north, and is almost absent in the southern part of the study area. It is friable, powdery which looks like soot (Fig. 5.3 D).The manganese ore is occasionally coated on the coral reefs which is overlaid it (Fig. 5.4). This shows replacement of the corals by the manganese ore due to alteration of the corals by the hydrothermal solutions. Furthermore, the shape of the corals is preserved indicating the low temperature nature of the hydrothermal fluids.

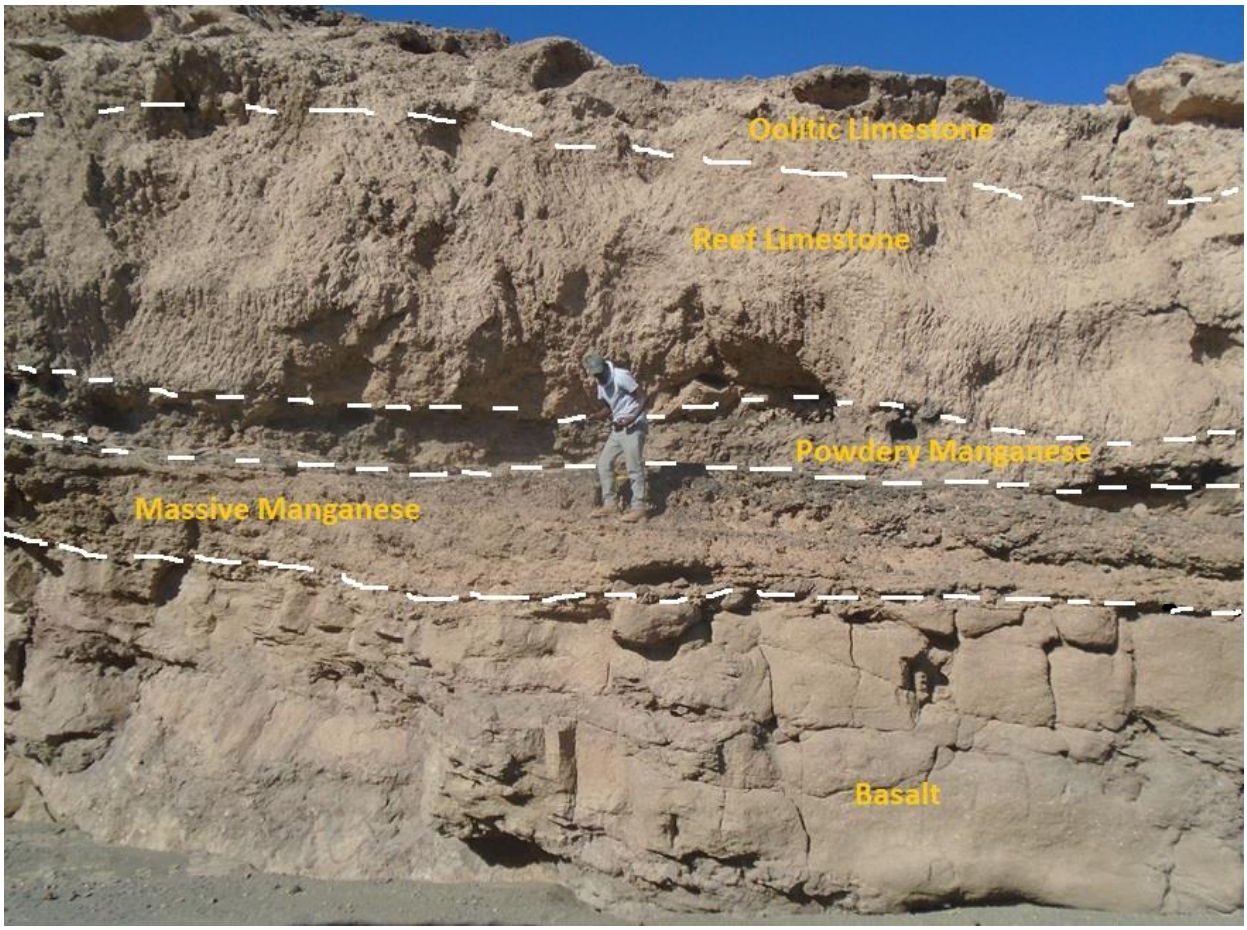

Figure 5.2: Section showing the Exposed part of Enkafela manganese deposit

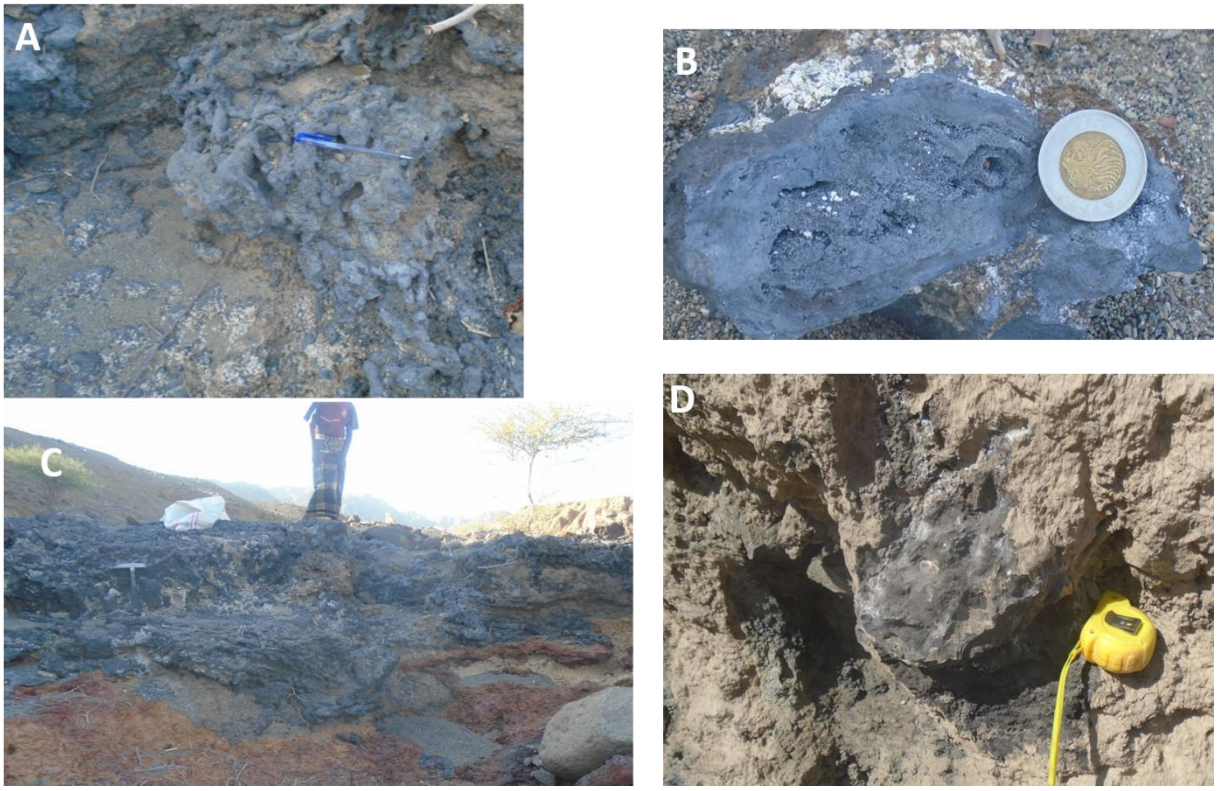

Figure 5.3: Manganese ore exposures *(A) Botryoidal massive manganese ore (B) a chunk of fine crystalline massive manganese ore (C) exposed massive manganese ore (D) sooty/powdery manganese ore*

Figure 5.4: Manganese ore replacing corals

5.3. Mineralogy

The mineralogical composition of the manganese ore and the surrounding rocks is determined using X-ray diffraction (XRD) analysis. The XRD results are presented in figure 5.5 A-E. The XRD analysis of powdery manganese sample ENK-06A (Fig. 5.5A) confirmed the presence of pyrolusite (MnO_2), chalcophanite ((Mn.Zn) $Mn_2O_3.2H_2O$) and birnessite ($(Na,Ca)Mn_7O_{14}.2.8H_2O$). Pyrolusite is detected at characteristic peaks at d=3.10Å (2θ= 28.7), 2.3Å (2θ=37.5) and 1.6Å (2θ=57). Chalcophnaite and Birnessite are detected at d=6.9Å (2θ=12.8), 4.06Å (2θ=21.8), 2.2Å (2θ= 40.4) and 7Å (12.6), 1.9Å (2θ=45.7), 1.4Å (2θ=65.7) respectively. The observed peak positions of these minerals showed that they are almost indistinguishable and weak, indicating the minerals are poorly crystalline.

The massive manganese sample ENK-06B consists of pyrolusite and chalcophanite (Fig. 5.5 B). The graph reveals sharp and intensive reflection peaks, indicating that these minerals are well crystallized. Pyrolusite, chalcophanite and birnessite are the higher valance (tetravalent) oxides of manganese ores. Birnessite and chalcophanite are common layered hydrated manganese minerals, mostly formed in the oxidized environment by telethermal hydrothermal processes (Jeffrey and Daniel, 1988; Xionghan et al., 2005; Pracejus , 2008). Calcite and barite are the major gangue minerals identified from massive manganese ore (sample ENK-08, Fig. 5.5C). Calcite is characterized by its unique high reflection peak detected at d= 3.0Å (2θ=29.4). Whereas barite is detected with very weak reflection peaks similar to pyrolusite.

XRD analysis is also conducted on samples taken from the reef limestone and basalt units, found above and below the manganese layers (Fig. 5.1). The analysis is made to know if there is any genetic relationship between the manganese layers and the surrounding rocks. The reef limestone consists of calcite and quartz (Fig. 5.7 D). Whereas the underlying basalt is composed of albite, quartz, goethite, aerinite, laumontite, mordernite and faujasite.

Aerinite, laumontite, mordernite and faujasite are zeolites, which are the results of low temperature hydrothermal alteration. This may perhaps lead us to assume that the hydrothermal process which formed the Mn have also affected the underling basalt.

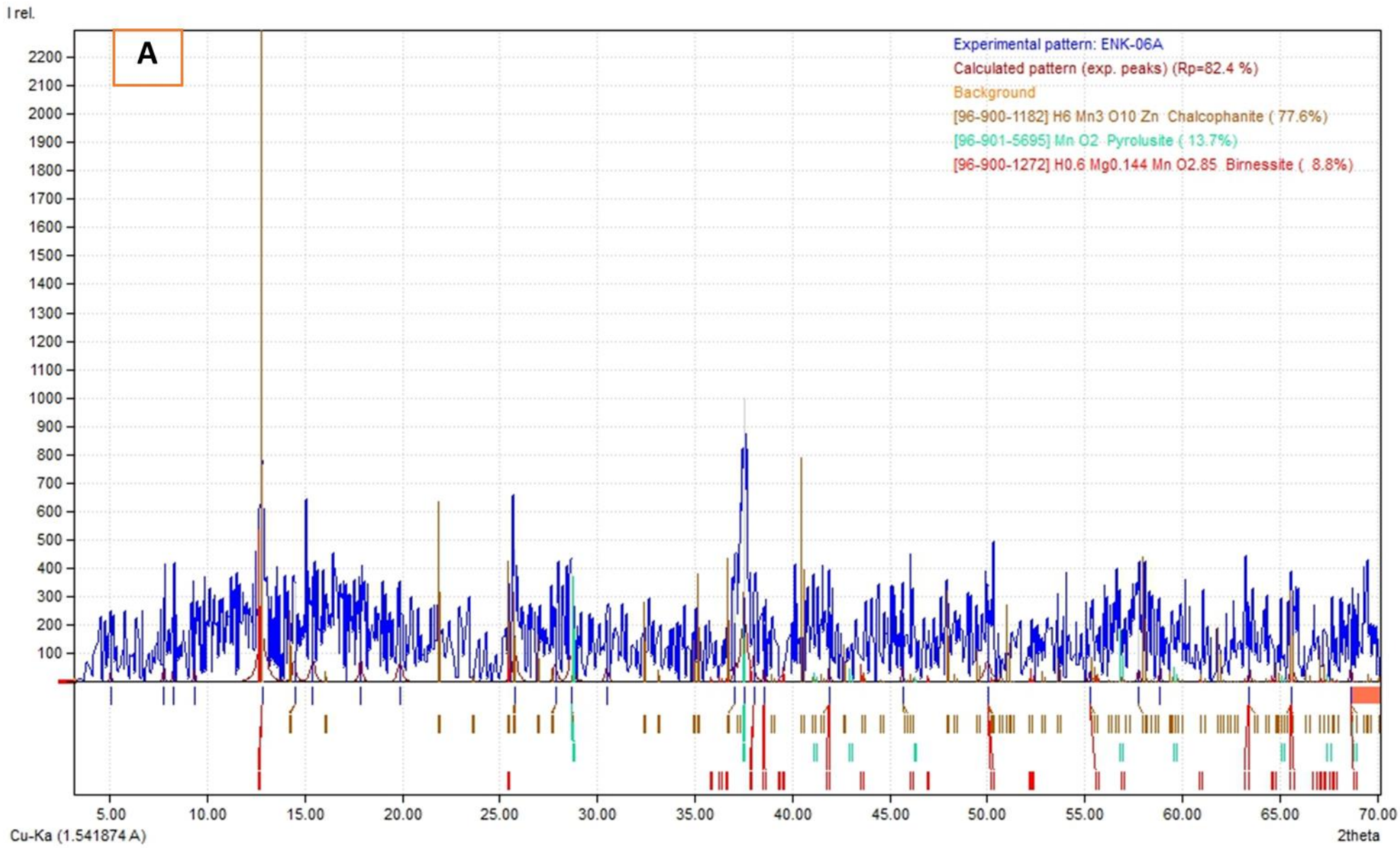
I rel.
A
Experimental pattern: ENK-06A
Calculated pattern (exp. peaks) (Rp=82.4 %)
Background
[96-900-1182] H6 Mn3 O10 Zn Chalcophanite (77.6%)
[96-901-5695] Mn O2 Pyrolusite (13.7%)
[96-900-1272] H0.6 Mg0.144 Mn O2.85 Birnessite (8.8%)
2200
2100
2000
1900
1800
1700
1600
1500
1400
1300
1200
1100
1000
900
800
700
600
500
400
300
200
100
5.00
10.00
15.00
20.00
25.00
30.00
35.00
40.00
45.00
50.00
55.00
60.00
65.00
70.00
Cu-Ka (1.541874 A)
2theta

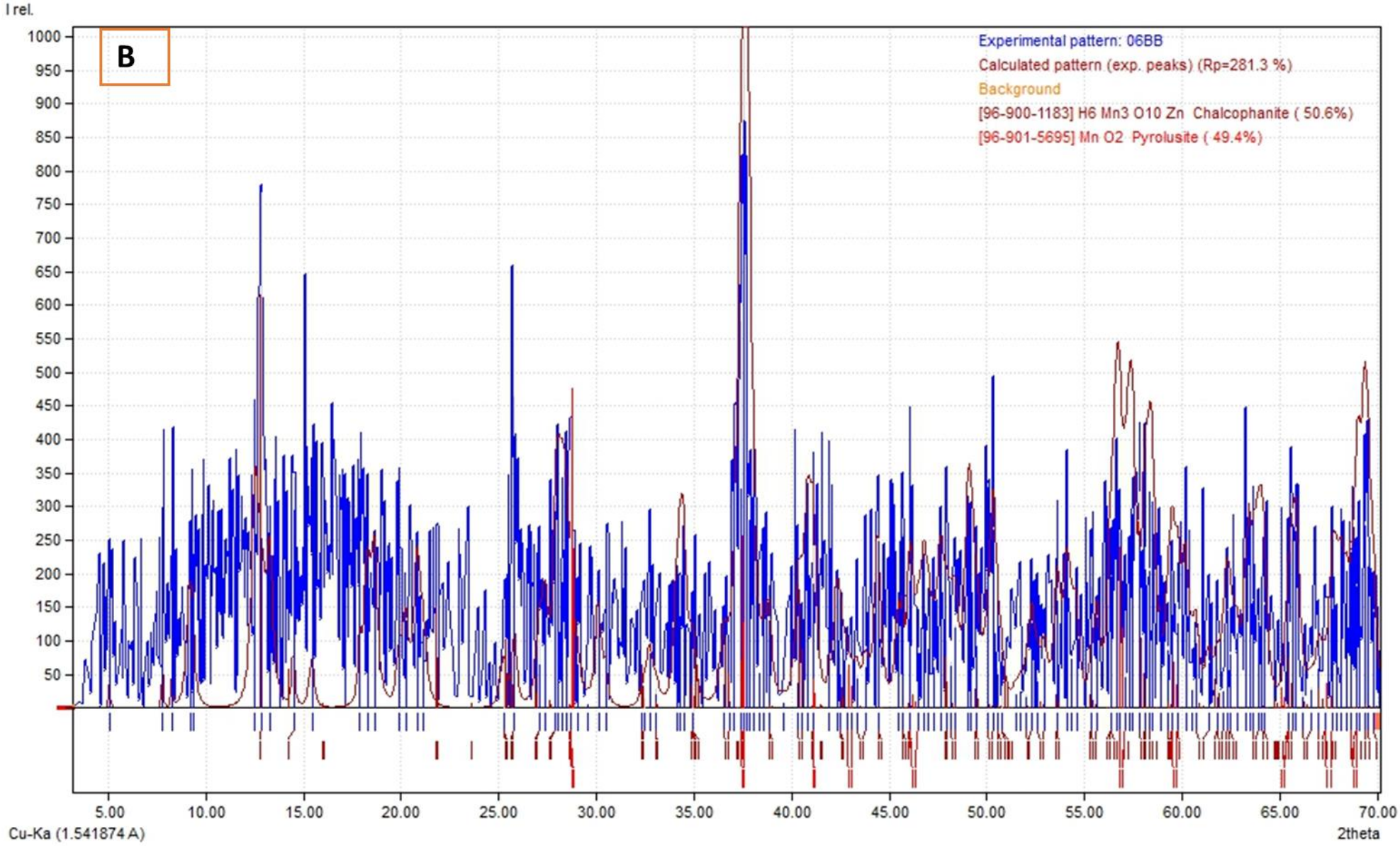
I rel.
B
Experimental pattern: 06BB
Calculated pattern (exp. peaks) (Rp=281.3 %)
Background
[96-900-1183] H6 Mn3 O10 Zn Chalcophanite (50.6%)
[96-901-5695] Mn O2 Pyrolusite (49.4%)
1000
950
900
850
800
750
700
650
600
550
500
450
400
350
300
250
200
150
100
50
5.00
10.00
15.00
20.00
25.00
30.00
35.00
40.00
45.00
50.00
55.00
60.00
65.00
70.00
Cu-Ka (1.541874 A)
2theta

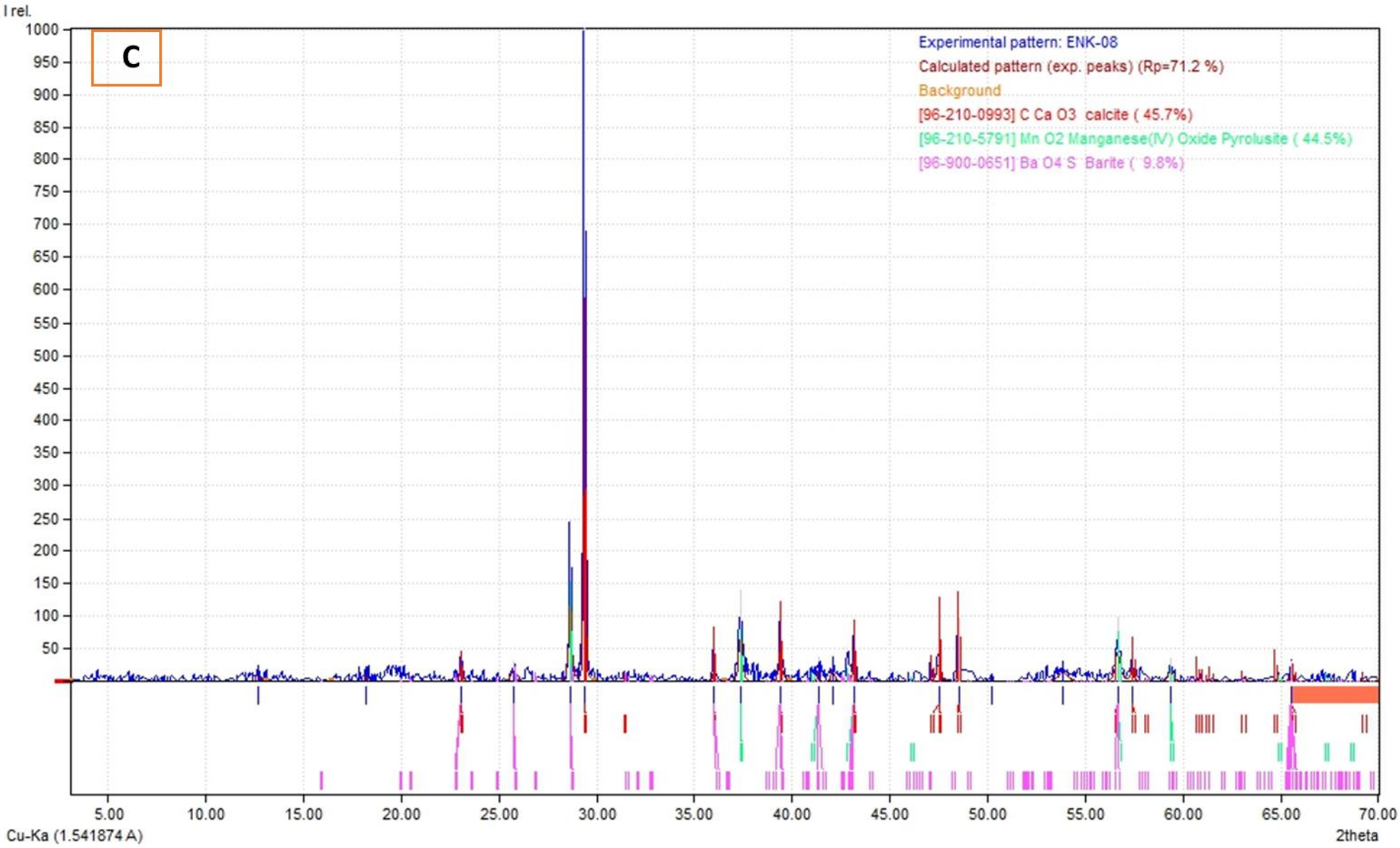
C
I rel.
Experimental pattern: ENK-08
Calculated pattern (exp. peaks) (Rp=71.2 %)
Background
[96-210-0993] C Ca O3 calcite (45.7%)
[96-210-5791] Mn O2 Manganese(IV) Oxide Pyrolusite (44.5%)
[96-900-0651] Ba O4 S Barite (9.8%)
Cu-Ka (1.541874 A)
2theta

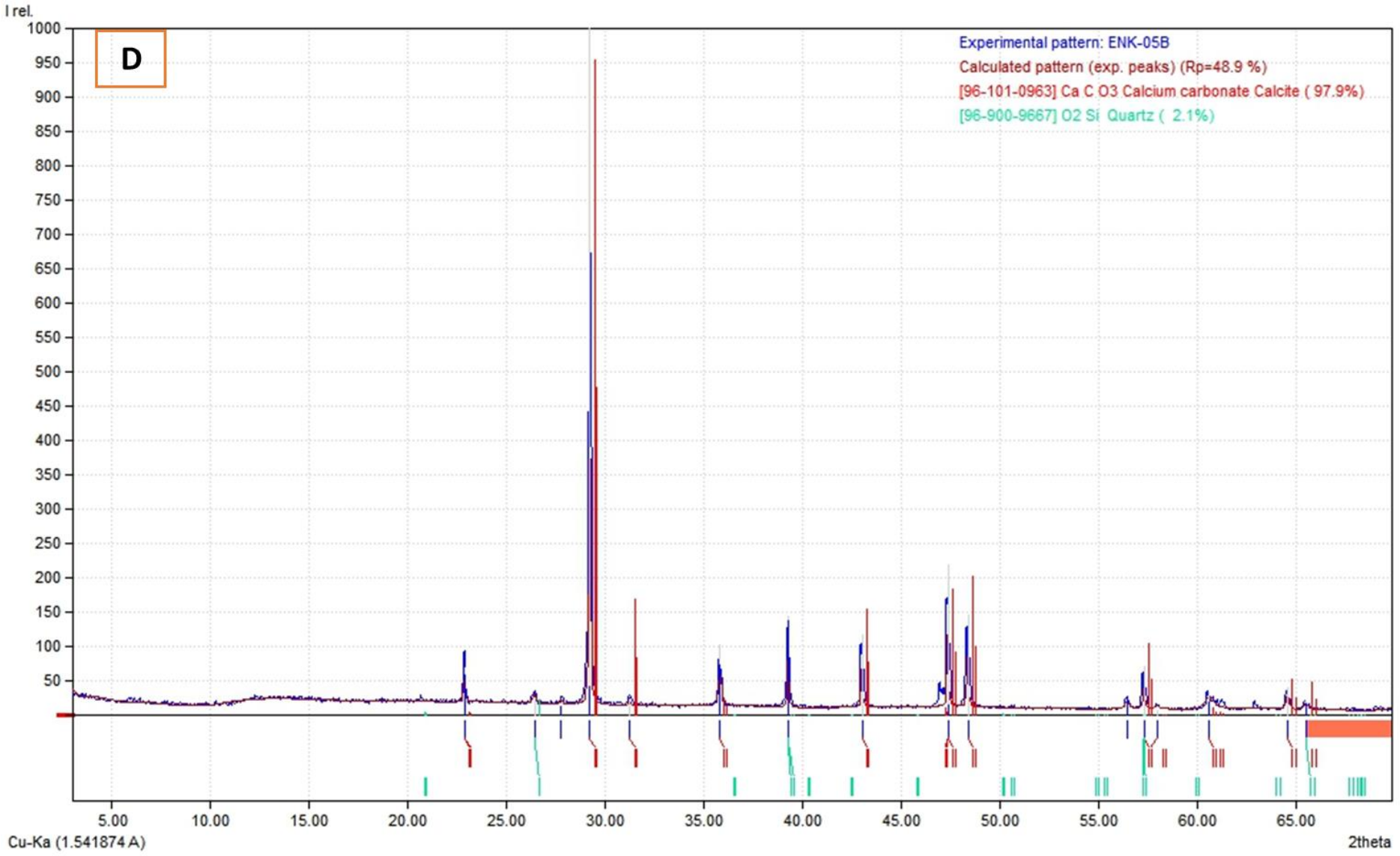
D
I rel.
Experimental pattern: ENK-05B
Calculated pattern (exp. peaks) (Rp=48.9 %)
[96-101-0963] Ca C O3 Calcium carbonate Calcite (97.9%)
[96-900-9667] O2 Si Quartz (2.1%)
Cu-Ka (1.541874 A)
2theta

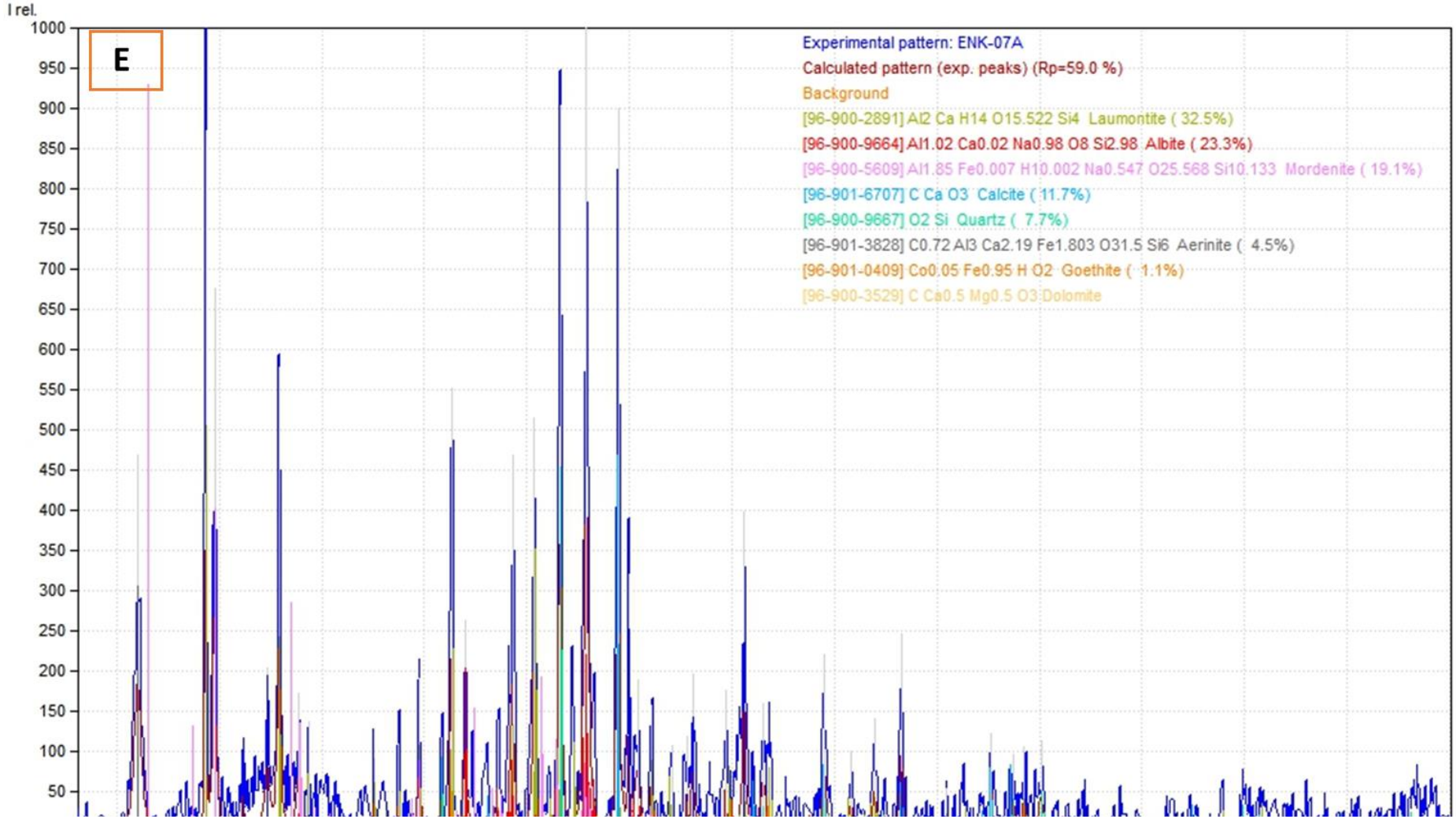

Figure 5.5: XRD patterns of selected manganese ore samples and associated rocks (A) powdery manganese (B&C) massive manganese (D) Reef limestone (E) underlying weathered basalt

5.4. Resource Estimation

The resource potential of the manganese deposit is estimated conventionally using the plan view map of the deposit (Fig 5.6), field observations and thickness measurements of the exposed deposit. As mentioned in the previous section, the thickness of the deposit is not constant. Thus, the calculation considers this variation and average thickness of the deposit is used. Additionally, the total area is further divided in to two blocks (block 1 and block 2) considering thickness variations.

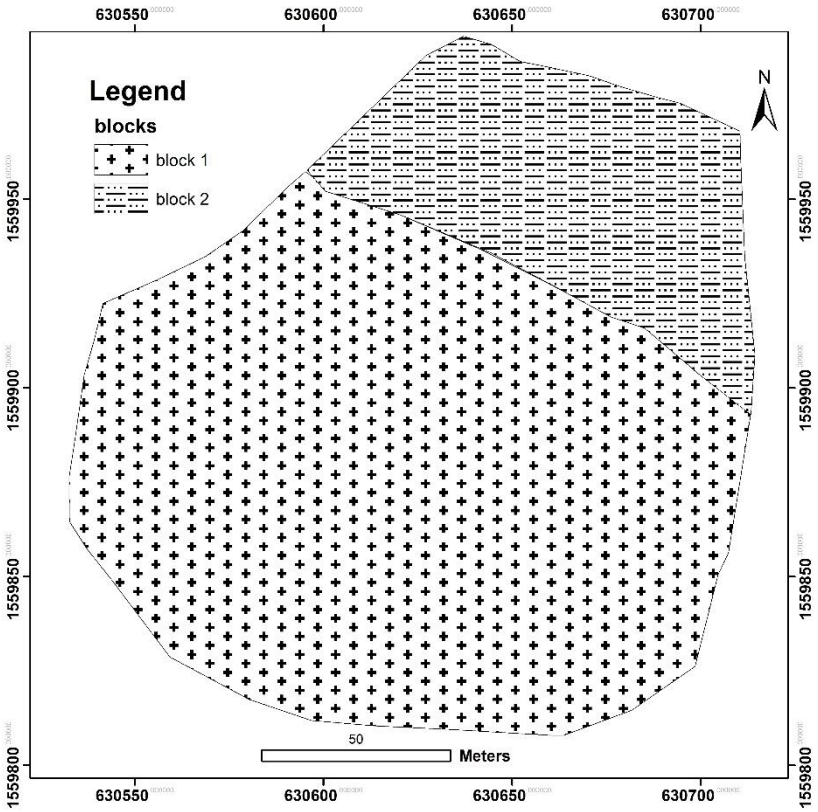

Figure 5.6: Plan view of Enkafela Manganese deposit

The resource is calculated applying the formula,

Resource = A x **h** x**ρ**

Where 'A' is area calculated from the plan view map,

'h' is average thickness and 'ρ' is bulk density.

The mineralogical composition of the deposit is determined using XRD (section 5.3). Accordingly, pyrolusite, birnessite and chlcophanite minerals are identified as a dominant phases. According to http://webmineral.com/data assessed on 21.04.2018, the bulk density of pyrolusite, Birnessite and Chlcophanite is 4.73 g/cm^3, 3 g/cm^3 and 3.91 g/cm^3 respectively. Average bulk density (3.88 g/cm^3) of the three minerals is used to calculate the resource as follows.

Blocks	Area (m^2)	Average thickness (m)	Bulk density (g/cm^3)	Estimated resource (ton)	Total estimated resource (ton)
Block 1	19459.2	0.2	3.88	15,100.3	**44,402.1**
Block 2	5900.0	1.28	3.88	29,301.8	

Table 5.1 Calculated resource of Enkafela Manganese deposit

Considering the level of geological knowledge and confidence this resource is classified under indicated mineral resource. This classification is made because the number of data points used to estimate are small and no drilling data is available to know the lateral and vertical extension of the deposit. It is estimated using only field observations and mineralogical tests. Mineral resources are transformed to ore reserves in accordance with principles such as those diagrammatically presented in figure 5.7. Assuming the quality of the ore, free from gangue minerals, and considering the modifying factors listed by the JORC Code, 2012 (Fig. 5.7) this resources could be transformed from resource level to reserve level with additional data generated from drilling.

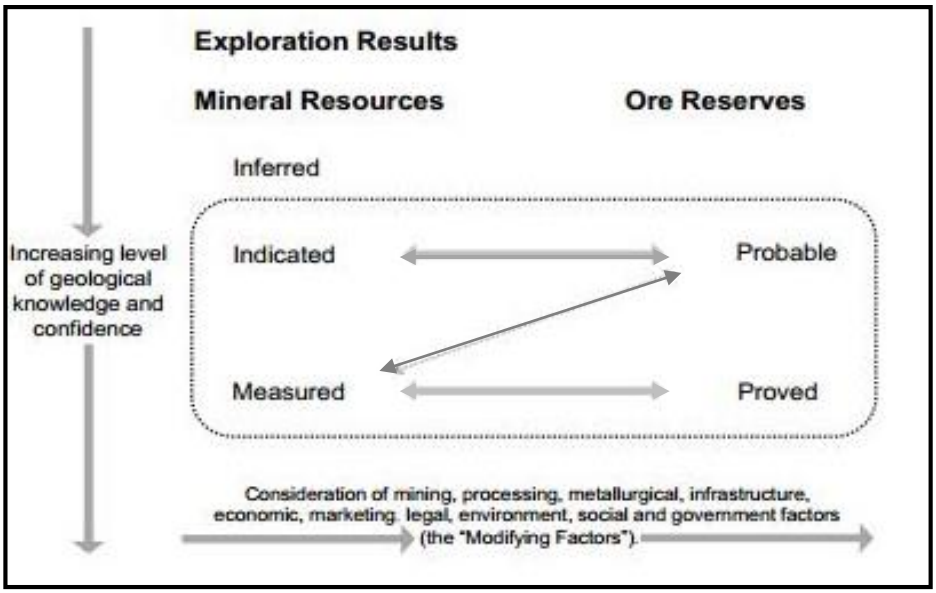

Figure 5.7: Relationship between Mineral resources and Ore reserves JORC code 2012

5.5. Geochemistry

One of the main tasks of this study is characterizing the geochemical characteristics of the manganese ore and the associated host rocks. Geochemistry is considerably the main choice used in different studies to understand, characterize and study the genesis, depositional history and depositional environment of manganese deposits. Geochemically, manganese deposits are very heterogeneous and large scale variations are observed even within the same deposit. Thus, geochemical data is used to illustrate the geochemical characteristics of the manganese deposit and the associated host rocks.

Genetically, manganese deposits are divided in to Hydrothermal, hydrogenenetic and diagenetic types. These classifications are based on the source and type of aqueous fluids from which the Mn-Fe oxides (hydroxides) precipitate. Hydrothermal deposits precipitate from hydrothermal fluids at the vicinity of hydrothermal vents at sea floor. Hydrogenetic manganese oxide precipitate from colloidal particles suspended in the ambient sea water, at the surface of solid substrates. Hydrogenetic deposits are exceptionally characterized by very slow growth rates than hydrothermal and diagenetic deposits (Josso et al., 2016). Deposits have diagenetic origin when sub-oxic metals precipitated from cold pore water during diagenesis with in the soft sediment or at the sediment-water interface.

These deposits are characterized by different composition and different geochemical behavior. The origin of mineralization and type of the deposit (e.g. hydrothermal, hydrogenous and diagenetic), is elucidated applying the geochemical behavior of the constituent major and trace elements. Samples are taken from both the massive and powdery manganese ore layers and the host rocks. The major and trace elements analysis result of the analyzed samples is given in table (5.2).

Sample Code	*ENK-03*	*ENK04A*	*ENK05A*	*ENK05B*	*ENK06A*	*ENK06A2*	*ENK09*	*ENK06B*	*ENK07A*	*ENK07B*
Wt. %	*Limestone (calcarenite)*	*Limestone (olitic)*	*Reef Limestone*	*Reef Limestone Mineralized*	*Mang. powdery*	*Mang. powdery*	*Mang. Massive*	*Mang. Massive*	*Basalt (iron rich)*	*Vein sample*
SiO2	7.66	10.00	5.27	2.83	0.70	0.51	1.68	2.09	47.1	87.9
Al2O3	2.24	2.97	1.55	0.77	0.35	0.36	0.54	0.67	17.35	3.96
Fe2O3	1.43	1.90	1.04	0.55	0.31	0.23	0.37	0.58	8.85	2.50
CaO	49.1	45.9	51.00	54.00	1.13	0.93	1.24	1.66	7.96	1.79
MgO	0.76	0.93	0.54	0.30	0.13	0.17	0.13	0.33	4.37	0.54
Na2O	0.24	0.22	0.12	0.15	0.38	0.34	0.17	0.51	2.95	0.15
K2O	0.24	0.24	0.13	0.05	1.07	1.16	0.25	0.67	0.63	0.21
Cr2O3	<0.01	<0.01	<0.01	<0.01	0.01	<0.01	<0.01	0.01	0.02	<0.01
TiO2	0.21	0.28	0.15	0.08	0.01	0.03	0.04	0.06	1.32	0.11
MnO	0.11	0.34	0.6	0.31	70.9	67.83	74.7	67.6	0.23	0.04
P2O5	0.10	0.07	0.07	0.04	0.05	0.04	0.02	0.03	0.17	0.03
SrO	0.04	0.04	0.04	0.11	2.64	-	-	1.98	0.09	0.01
BaO	0.01	0.01	0.02	0.01	9.16	8.66	2.72	9.29	0.03	0.01
LOI	38.100	36.60	39.50	41.40	11.45	10.79	12.65	12.9	9.14	4.02
Total	100.24	99.50	100.03	100.60	98.29	98.94	101.80	98.38	100.21	101.27

sample code Sample wt.(ppm)	*ENK-03 limestone (calcarenite)*	*ENK-04-A limestone (oolitic)*	*ENK-05-A reef limestone*	*ENK-05-B reef limestone mineralized*	*ENK-06-A powdery manganese*	*ENK-06-B massive manganese*	*ENK-07A Basalt*	*ENK-07- vein sample*
Ba	76.60	79.10	127.00	124.50	>10000.00	>10000.00	242.00	60.2.
Ce	7.30	7.80	6.30	2.80	1.10	98.80	15.20	4.10
Cr	20.00	20.00	20.00	20.00	10.00	10.00	110.00	10.00
Cs	3.37	3.83	0.45	0.43	1.08	2.89	1.14	0.51
Dy	1.02	1.04	0.58	0.43	0.41	6.45	3.69	0.74
Er	0.65	0.69	0.31	0.24	0.38	4.26	2.09	0.52
Eu	0.30	0.33	0.16	0.13	<0.03	1.78	0.94	0.11
Ga	2.90	3.90	3.00	1.60	98.60	108.50	15.80	2.20
Gd	0.87	1.27	0.61	0.35	0.50	5.51	3.62	0.55
Hf	0.60	0.90	0.80	0.30	<0.20	<0.20	1.90	0.60
Ho	0.24	0.26	0.14	0.09	0.11	1.56	0.77	0.16
La	3.60	3.90	3.10	1.50	2.10	17.00	6.70	1.90
Lu	0.08	0.11	0.06	0.05	0.07	0.71	0.29	0.15
Nb	2.60	3.20	2.00	0.90	0.20	0.40	6.80	1.60
Nd	4.40	5.10	3.40	1.80	1.90	21.30	10.70	2.20
Pr	0.88	0.94	0.77	0.38	0.30	4.38	2.10	0.48
Rb	10.70	11.30	4.80	1.90	11.50	12.50	13.30	6.60
Sm	0.88	1.16	0.69	0.34	0.58	5.46	2.88	0.42
Sn	<1.00	<1.00	<1.00	<1.00	<1.00	<1.00	1.00	<1.00

Sr	287.00	336.00	310.00	904.00	>10000.00	>10000.00	664.00	103.00
Ta	0.20	0.10	0.10	<0.10	<0.10	<0.10	0.40	0.10
Tb	0.15	0.19	0.10	0.05	0.08	0.97	0.59	0.10
Th	0.61	0.74	0.59	0.21	0.07	0.13	0.71	0.53
Tm	0.08	0.11	0.08	0.03	0.05	0.64	0.29	0.11
U	1.92	2.99	1.15	1.20	1.97	1.46	0.21	0.12
V	43.00	79.00	41.00	25.00	335.00	1740.00	260.00	91.00
W	<1.00	<1.00	<1.00	<1.00	<1.00	9.00	1.00	<1.00
Y	6.00	6.70	3.70	2.50	7.70	34.80	19.80	3.90
Yb	0.50	0.59	0.51	0.15	0.23	4.09	2.03	0.75
Zr	25.00	31.00	29.00	11.00	2.00	5.00	67.00	21.00
Ag	<0.50	<0.50	<0.50	<0.50	<5.00	<5.00	<0.50	<0.50
As	<5.00	<5.00	<5.00	<5.00	<50.00	<50.00	<5.00	5.00
Cd	<0.50	<0.50	<0.50	<0.50	<0.50	<0.50	<0.50	<0.50
Co	4.00	4.00	3.00	2.00	<20.00	97.00	29.00	4.00
Cu	8.00	9.00	10.00	4.00	8.00	374.00	49.00	7.00
Li	10.00	20.00	<10.00	<10.00	30.00	20.00	10.00	20.00
Mo	2.00	7.00	<1.00	<1.00	49.00	76.00	<1.00	<1.00
Ni	6.00	8.00	4.00	<1.00	15.00	14.00	36.00	8.00
Pb	3.00	<2.00	<2.00	<2.00	56.00	58.00	5.00	<2.00
Sc	4.00	5.00	2.00	1.00	<1.00	2.00	22.00	3.00
Tl	10.00	<10.00	<10.00	10.00	<100.00	<100.00	<10.00	10.00
Zn	18.00	20.00	15.00	8.00	51.00	37.00	83.00	12.00

Table 5.2 major and trace element concentration of manganese ore and the host rocks

In the following section the presentation and interpretation of the geochemical data is systematically discussed along with the graphs and diagrams produced using the geochemical data

5.5.1. Major and Trace Element Geochemistry

Major elements are elements which are found dominantly both in the ore mineral and in the host rock. Most of the time major elements are analyzed in the form of oxide and expressed in weight percent. These elements include Si, Al, Mn, Fe, Ca, Mg, Na, K and P. The chemical analysis includes loss of ignition (LOI). The oxide forms of these elements are normalized to get volatile free content before directly applied for integration, interpretation and presentation. On the contrary, trace elements, by definition, are those elements present in concentrations less than 0.1% and mostly expressed in ppm (parts per million) or ppb (parts per billion). Though, they constitute a small fraction of the whole rock or mineral of interest, their importance in providing geological and geochemical information is critical. Transition metals are the common trace elements ideal for geochemical characterization of the mineralization of manganese deposits.

Major and trace element concentrations and ratios have been extensively used to evaluate the origin of manganese deposits (Ozturk, 1997; Heshmatbehzadi and Shahabpour, 2010; Kuhn et al., 2017).

The Enkafela manganese deposit is rich in MnO (av. 70.25%), BaO (av. 9.2%) and poor in SiO_2 (av. 1.24%), Al_2O_3 (av. 0.48%), Fe2O3 (av. 0.37%), CaO (av. 1.24%), MgO (av. 0.19%), Na_2O (av. 0.35%), K_2O (av. 0.78%), TiO_2 (av. 0.035%), P_2O_5 (av. 0.035%). The ore chemistry is characterized by very high Mn and low Fe content. The average Mn and Fe concentrations in the Enkafela deposit are 62.25% and 0.36% respectively. The average Mn/Fe ratio of the deposit is 172.9. Hydrogenetic manganese deposits show Mn/Fe ratio of about 1 (Salem et al., 2016). However, the Mn/Fe ratio of hydrothermal deposit is quite different, characterized by exceptionally high Mn/Fe ratios, greater than 100 (Bolton et al., 1988). This results due to higher fractionation of Mn from Fe. The Fractionation of Mn from Fe may be resulted from the early precipitation of Fe, in the form of silicates and sulfides at depth at higher temperature and pressure, before the hydrothermal fluid reach near the point of release. In this respect, the high Mn/Fe ratio of Enkafela manganese deposit is likely the characteristics of hydrothermal deposits and agrees with submarine spreading center type of

hydrothermal deposits (Oksuz, 2011). Such high Mn/Fe ratio is reported from mid-Atlantic ridge; Mn/Fe= 211-315 (Toth, 1980 as cited in Roy, 1992). Comparable with Mn and Fe contents, concentration of Al and Ti in the ore can also be used in the assessment of the origin of manganese mineralization. Al and Ti behave similarly in ore formations and show higher concentration in sedimentary formations (Oksuz, 2011 and reference therein). Ti is immobile in hydrothermal solutions and is indicative of clastic input (Shah and Khan, 1999; Sasmaz et al 2013 as cited in Kahrezehi et al., 2015). Their concentration could tell us whether there is sedimentary contribution or not during mineralization. The average concentration of Al and Ti in Enkafela manganese deposit is low, 0.59% and 0.01% respectively. Thus, sedimentary contribution during mineralization seems minimal.

The concentration of Ba and Sr is significantly high. BaO and SrO are found as a major element with average concentrations of 9.2% and 2.3% respectively. The enrichment of Ba is associated with the presence of barite mineral. The Sr enrichment is also associated with barites. Ba could be substituted by Sr due to their similarity in ionic radii (Papavassiliou et al., 2017). Bonatti et al. (1972), from laboratory analysis, confirmed that the two minerals are found as a solid solution in the form of strontio-barite. The concentration of Ba in hydrothermal solution is higher relative to seawater due to the impact of volcanic activity (Monnin et al., 2001; Oskuz, 2011; Sasmaz et al., 2013).

The concentration of transition metals, like Ni, Zn, Co and Cu is significantly applied by different authors (Bonnatti et al., 1972; Toth, 1980; Jiancheng et al., 2006; Kahrazehi et al., 2015) to understand the source and depositional mechanism of manganese deposits. Hydrogenous manganese deposits reveal higher concentrations of these metals than hydrothermal deposits. These deposits show Ni and Cu concentrations greater than 3000ppm (Oksuz, 2011). The amount of Ni and Cu in Enkafela manganese deposit is extremely low, 14ppm and 191ppm respectively, indicating hydrothermal origin. Cobalt and Ni have similar behavior. Co/Ni ratios can be used to differentiate hydrothermal and hydrogenous deposits (Toth, 1980; Jiancheng et al., 2006; Kahrazehi et al., 2015). Co/Ni <1 points to a sedimentary origin while Co/Ni >1 shows a deep marine environment, especially hot water sea bed sedimentation. The Co/Ni values in Enkafela manganese deposit range from 1.3 to 6.8 (average= 3.8). This ratio is indicative of hot deep marine origin. In addition the ratio of Co:Zn is also used to discriminate the source of metals. Hydrothermal deposits show Co/Zn ratio of 0.15, while hydrogeneous deposit types show Co/Zn ratio of 2.5

(Kahrazehi et al., 2015). Co/Zn ratio of Enkafela manganese deposit is 0.39 for powdery manganese and 2.62 for a massive manganese deposit. Though, the Co/Ni ratios indicate a hydrothermal source for manganese mineralization, Co/Zn ratios indicate that metals are also contributed from the sedimentary environment. It also specifies that the massive and powdery manganese layers could be either originated from different sources or formed at different phases. Especially, the massive manganese layer shows mixed type (both hydrothermal and hydrogenous).

Different authors have proposed major and trace element discrimination diagrams in order to distinguish manganese ores of various origins. Ni-Co-Zn (Choi and Hariya, 1992) and Fe-Si*2-Mn (Toth, 1980) ternary diagrams are used to distinguish hydrogenous, diagenetic and sub-marine hydrothermal Mn deposits.

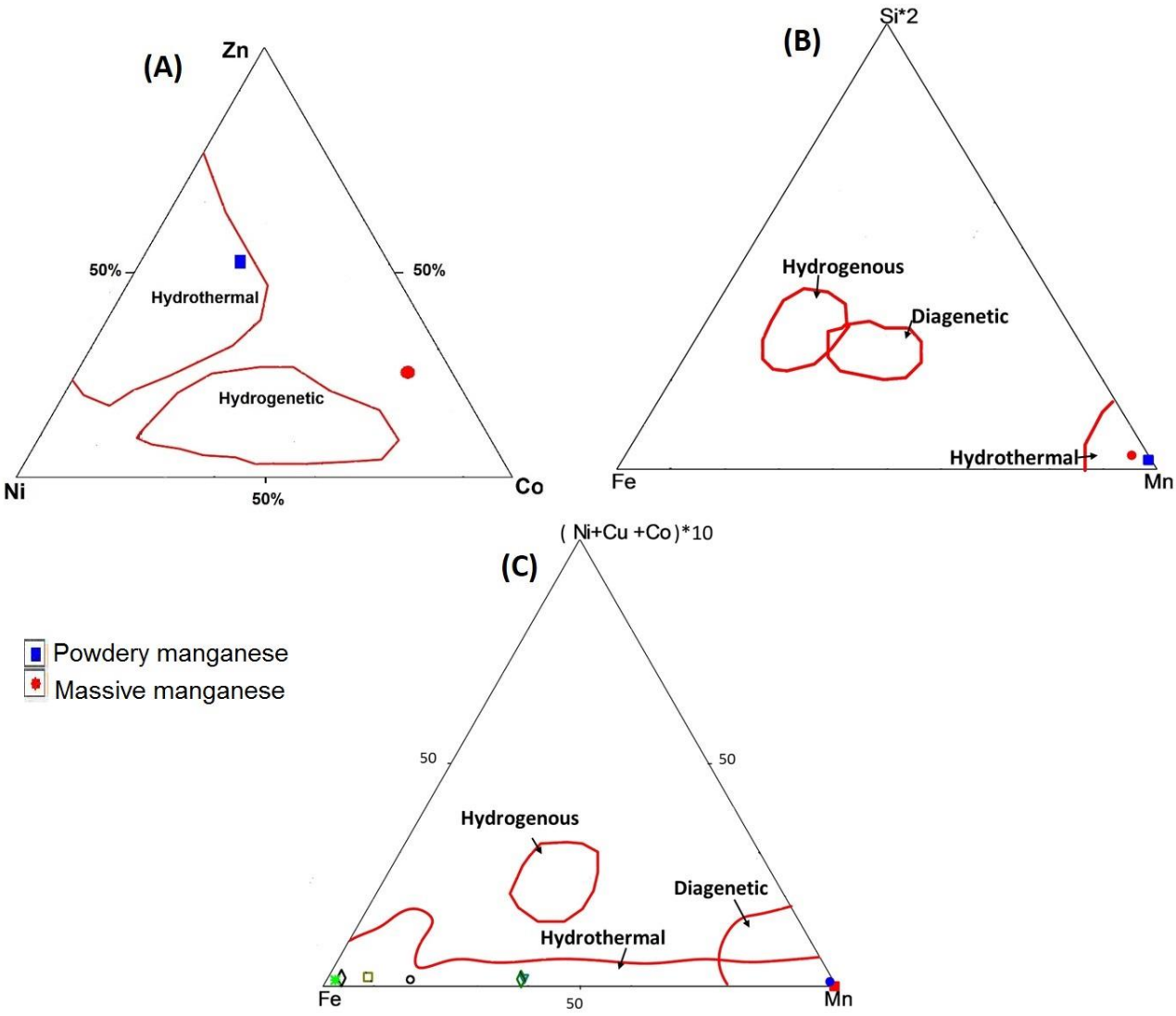

*Figure 5.8 Discrimination ternary diagrams of Enkafla manganese deposit (A) Ni-Zn-Co discriminating diagram (Choi and Hariya, 1992) (B) Fe-Si*2-Mn discriminating diagram (Toth, 1980) (C) Fe- (Ni+Cu+Co)*10-Mn discriminating diagram (Bonatti et al., 1972)*

In Ni-Co-Zn ternary diagram (Fig. 5.8 A) the two samples fall in different region. The powdery manganese is plotted in the hydrothermal region while the massive manganese is plotted out of both the hydrothermal and hydrogenous region. On the other hand, in the Fe-Si*2-Mn ternary diagram (Fig. 5.8 B) both samples are plotted in hydrothermal region. In Fe-(Ni+Cu+Co)*10-Mn, ternary diagram of Bonatti et al. (1972), all samples, including the host rocks samples, are plotted in the hydrothermal region (Fig. 5.8C). Although, the Fe-Si*2-Mn and Fe-(Ni+Cu+Co)*10-Mn diagrams indicate both manganese layers have hydrothermal source, the Ni-Co-Zn ternary diagram support the concept that the two manganese layers are different originally. The powdery manganese deposit shows pure hydrothermal origin, but the massive manganese deposit shows a mixed source, both hydrothermal and hydrogenous.

5.5.2. REE Geochemistry

REE are the most significant trace elements. The abundance of REE and their normalized patterns frequently reveal depositional processes and environment of formations (Usui and Someya, 1997). REE have similar chemical properties (Tostevin et al., 2016) and behave coherently, resulting in smooth, predictable distribution patterns when normalized to Chondrites or NASC.

Normalization is commonly done to remove the natural variations in absolute concentrations of REE or to eliminate questionable data sets (Bau et al., 2014) and allows a comparison with the REE composition of the upper crust in which shale is a proxy.

Sample	La	Ce	Pr	Nd	Sm	Eu	Gd	Tb	
ENK 06-A	2.10	1.10	0.30	1.90	0.58	0.03	0.50	0.08	
(Powdery	Dy	Ho	Er	Tm	Yb	Lu	LREE/HREE	∑REE	Ce*
manganese)	0.41	0.11	0.38	0.05	0.23	0.07	3.28	7.84	-0.616
ENK 06-B	La	Ce	Pr	Nd	Sm	Eu	Gd	Tb	
(Massive	17.00	98.80	4.38	21.30	5.46	1.78	5.51	0.97	
manganese)	Dy	Ho	Er	Tm	Yb	Lu	LREE/HREE	∑REE	Ce*
	6.45	1.56	4.26	0.64	4.09	0.71	6.14	172.9	0.394

Table 5.3: Rare earth element concentrations of Enkafela manganese deposit (ppm)

The ∑REE content in the manganese deposit 172.91 ppm for the massive manganese and 7.84 ppm for powdery manganese. The results are extremely contrasting. Therefore, like the NI-Co-Zn ternary diagram (Fig. 5.8 A), this could convey that the two manganese layers are unlike.

Shah and Moon (2007) documented that lower concentrations of REE is characteristics of hydrothermal manganese deposits. This is because in hydrogenetic deposits REEs are scavenged from seawater by the settling manganese oxides. Moreover, the ratio of ∑LREE and ∑HREE could give information about the hydrogenous and the hydrothermal nature of mineralization (Oksuz, 2011).

These ratios are calculated as;

∑LREE=La+Ce+Pr+Nd+Sm+Eu, and ∑HREE=Gd+Tb+Dy+Ho+Er+Tm+Yb+Lu.

The ∑LEE/∑HREE ratio of the Enkafela manganese deposit is 3.28-6.14 averaging 4.71 that indicates the enrichment of the LREE during the deposition of the manganese deposit (table 5.3). The enrichment of LREE relates to the mobility of REE elements in hydrothermal systems. LREE are more mobile than HREE in hydrothermal solution and easily transported until they reach to the point of deposition, while the HREE remain close to the point of fluid input. Mishra et al. (2007) noted that enrichment in LREE could point toward mineralization through hydrothermal processes. Hydrogenetic deposits show HREE enrichment over LREE. In seawater REE are partitioned into the suspended fractions. Either they are adsorbed by manganese oxides suspended in the water body or they form complexes with complexing ligands dominantly with CO_3^{2-}. The complexes stability increases with increasing atomic number, i.e., the HREE are more strongly partitioned into the complexed fractions than LREE. Finally, when optimum condition is reached, the REE separate themselves from the complex and deposited at the bottom of the sea with manganese. The La_N/Yb_N ratio of hydrothermal solutions is above unity (Pierret et al., 2010). The La_N/Yb_N ratio of the Enkafela deposit is 1.4-2.0, averaging 1.7, which gives evidence as hydrothermal solutions are responsible for the manganese mineralization. According to Bau et al. (2014), the ratio of Y_{PASS}/Ho_{PASS} (PASS normalized) is used to discriminate the different genetic types of manganese. The Y_{PASS}/Ho_{PASS} ratio is used to know the separation of the geochemical twins Y and Ho, which produces Y_{PASS}/Ho_{PASS} anomalies, because of its very similar ionic radius to Ho^{3+}. This decoupling result from preferential scavenging of Ho relative to Y on metal oxide surfaces due to lower stabilities of Y surface-complexes (Bau et al., 2014).

Hydrothermal deposits characterized by Y anomaly, Y/Ho>1 and hydrogenetic and diagenetic deposits show negative anomaly, Y/Ho<1. The Y/Ho ratio of the Enkafela manganese deposit shows both enrichment and depletion in Y. The massive manganese layer shows Y/Ho=0.8 while the powdery manganese shows Y/Ho=2.5. The values indicate that the powdery manganese layer is pure hydrothermal whereas the massive manganese layer shows hydrogenetic behavior.

Cerium occurs in +3 and +4 valances while Eu occurs in +2 and +3 valances. This makes the two elements redox sensitive, and apparently the most important REEs for indicating the redox condition of the depositional environment and to predict the fluid source (Kahrazehi et al., 2015). The Ce anomaly is calculated using the formula of Elderfield and Greaves (1981); $Ce^{*} = \log (3 (Ce_{sample}/ Ce_{shale}) / (2 (La_{sample}/La_{shale}) + (Nd_{sample}/Nd_{shale}))$, where NASC is used for normalizing Ce, La and Nd values.

Accordingly, the Ce anomaly value is 0.394 and -0.616 for massive manganese and powdery manganese layers respectively (table 5.3). The powdery manganese deposit show depletion in Ce while the massive manganese deposit show enrichment in Ce. Based on the result we can envisage that the two manganese deposits are not similar originally. The Ce anomaly obtained from the formula gives information about the origin of mineralization. The growth rate of hydrothermal deposits is faster than hydrogenetic deposits. Ce has slow oxidation kinetics (Josso et al., 2016). Ce will be enriched (positive anomaly) in hydrogenetic deposits whereas the rapid growth rate of hydrothermal deposits can prevent the formation of Ce anomaly due to slow oxidation kinetics. The negative Ce anomaly (for powdery manganese) clearly supports hydrothermal origin, whereas the positive anomaly (for massive manganese) indicates the contribution of the sea water for the massive manganese deposit.

The REE content of the two manganese layers is plotted in figure 5.9, normalized to Chondrite as given by Boyton (1984). The REE pattern of the two manganese layers has displayed contrasting pattern. The chondrite normalized pattern of the massive manganese ore displays enrichment in Ce and relatively smooth or flat pattern in the other REEs. The positive Ce anomaly is typical of hydrogenetic manganese deposits (Flohr and Huebner, 1992; Shah and Moon, 2007; Josso et al., 2016). Flohr and Huebner (1992) suggested that positive Ce anomaly for hydrothermal deposits could indicate a contribution from fine volcanic-derived detritus which are exposed to the action of seawater.

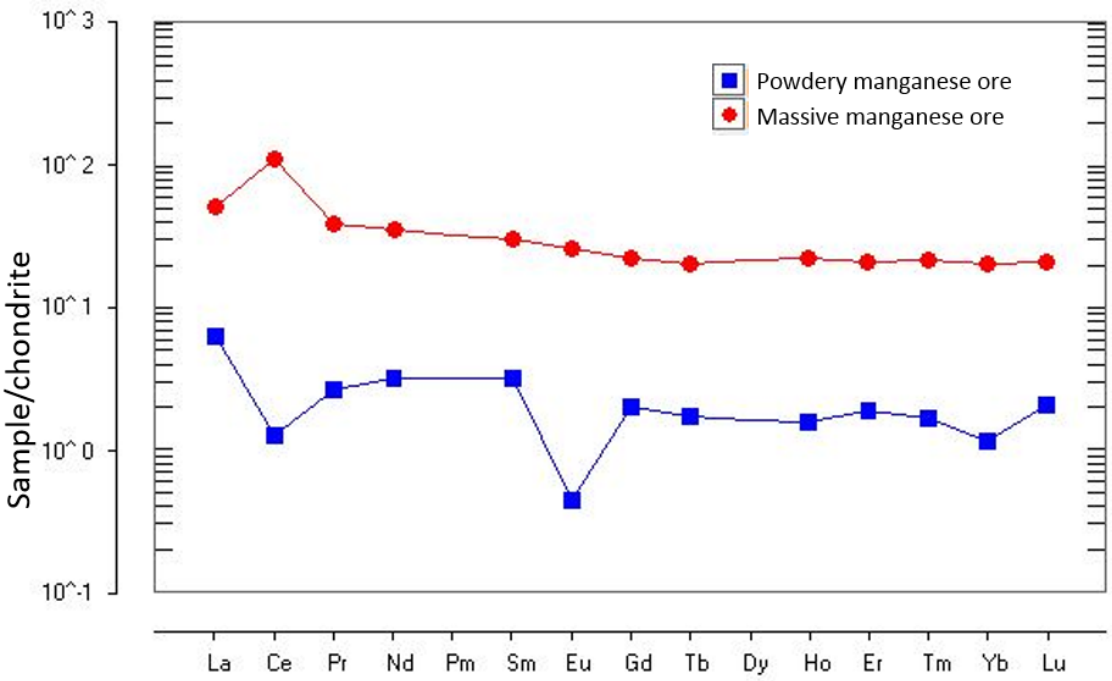

Figure 5.9: REE variation diagram of Enkafela manganese ore, *Chondrite normalizing values are determined from Boyton (1984).*

On the contrary the powdery manganese ore displays depletion in Ce, and Eu. The negative Ce anomaly indicates loss of Ce in to sea water (Papavassiliou et al., 2017). Depletion of Ce is characteristics of low temperature hydrothermal deposits in mid-oceanic and island arc spreading centers (Carlo and McMurty, 1992; Hodkinson et al., 1994 as cited in Kahrazehi et al., 2015).

The negative Eu anomaly might be explained from different perspectives. Under reducing conditions hydrothermal solutions are expected to be enriched in Eu since Eu^{2+} is highly mobile than the other REE^{3+}. In addition, Eu is recognized by the substitution of Ca in plagioclase. The negative Eu anomaly could indicate the absence of leaching of plagioclase by the hydrothermal solution.

Alternatively, negative Eu anomaly could be due to precipitation of Eu rich minerals such as barite or anhydrite from the fluids before the manganese oxide is formed. Based on thermodynamic study, Glasby et al., (1997) proposed that Eu^{2+} is enriched in fluids with temperature >250°c whereas Eu^{+3} is dominant at lower temperature. The presence of negative Eu anomaly in the Enkafela manganese ore samples may show the formation of the deposit at temperature <250°c. The influence of lithogenic sediments is also significant in Eu anomaly. The negative anomaly could also indicate contamination from sediments, especially sediments rich in carbonates.

5.5.3. Host rocks Geochemistry

As mentioned in section 5.1 the manganese deposit is hosted in limestone rocks and underlain by basaltic rock. The major and trace element content of these rocks is given in table 5.2. In this section, the geochemical characteristics of these rocks will be discussed. At the same time we can figure out any geochemical relation and implication to the origin of the manganese deposit. Since the number of samples is small, it is difficult to attempt any statistical treatment of data and know the relation made between elements or understand about the depositional environment and the condition from their relation.

Generally, the reef limestone shows high CaO value, average 80wt%. The average concentrations of SiO_2, MnO and Fe_2O_3 are 10wt%, 0.5wt% and 1.2wt% respectively. Comparing to the manganese ores, the Fe content is relatively higher in the limestone, with an average concentration of 0.86wt %, while the manganese ores contain 0.31wt%. The highest content of Ba is found in the manganese ores (>10,000ppm). However, the limestone has an average Ba content of 102ppm. High Ba content is interpreted as indicative of a hydrothermal origin.

The Chondrite normalized (after Boyton, 1984) REE patterns of the limestone samples is more or less flat and it shows a slight enrichment in LREEs and slight depletion in HREEs (fig 5.9). Any significant Ce anomaly is not observed in all samples. Positive and negative Eu anomaly is observed in the reef limestone. Positive Eu anomaly is detected in the manganese coated reef limestone. Positive Eu anomaly in limestone is either due to the influence of the hydrothermal solution or the inclusion of detrital feldspar during diagenesis of the limestone (Abedini and Calagari, 2015). In this case, the effect of plagioclase is minimum or absent since the XRD mineralogical analysis reveals the absence of plagioclase.

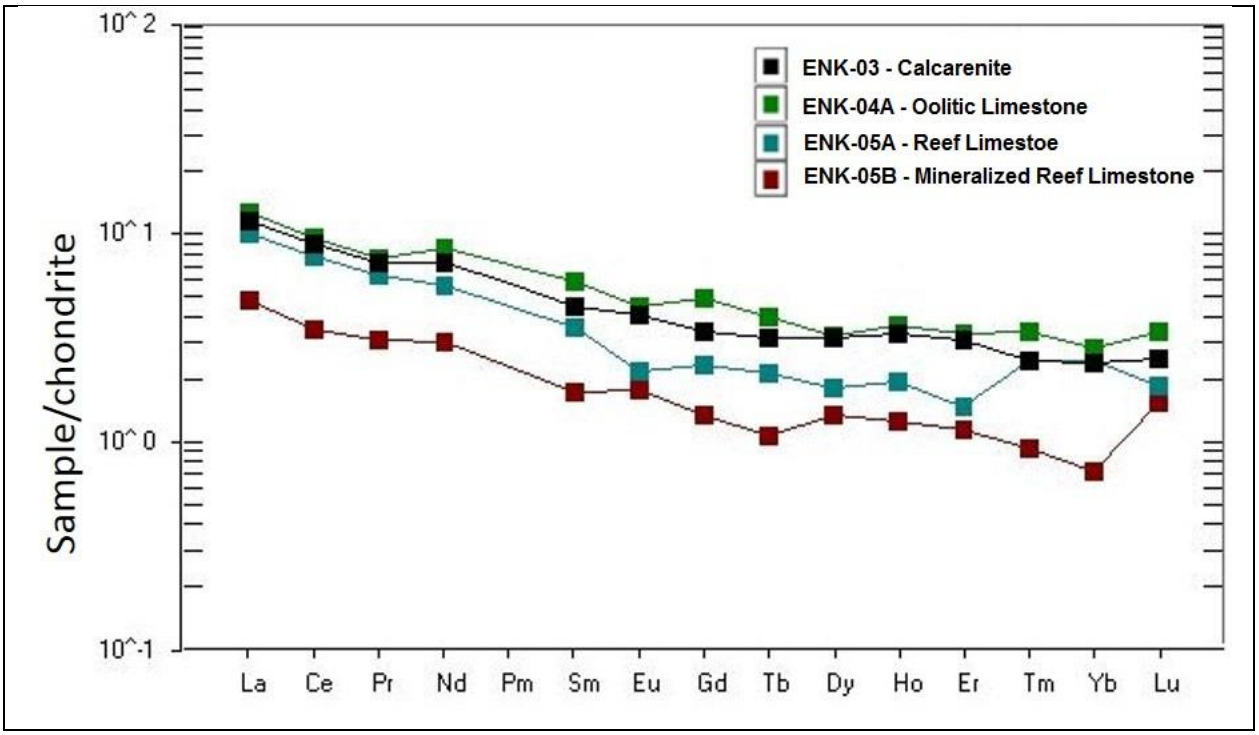

Figure 5.10: Chondrite-Normalized REE patterns for limestone, after Boyton (1984)

The REE pattern of the limestone is comparable with the manganese layers and exhibited non-seawater like REE pattern. Seawater exhibits progressive enrichment of heavy REE relative to light REE and depletion in Ce (Piper and Bau, 2013). The average ∑LREE/∑HREE of the reef limestone is 5.5 indicating LREE enrichment. Light REE enrichment in limestone is resulted from two sources. The first is contamination of seawater from detrital materials and the second one is deposition of carbonates under hot fluids (Liu et al., 2017). The massive manganese exhibits ∑LREE/∑HREE of 6.14 almost close to the reef limestone. However, the powdery manganese has ∑LREE/∑HREE of 3.28 relatively lower than the reef limestone and the massive manganese. This indicates that the influence of detrital material in the powdery manganese is lower than the massive manganese.

A volcanic rock is found under the manganese layer. In the Total Alkali silica (TAS after Le Bas et al., 1986) classification of volcanic rocks, the analyzed sample falls in the Sub-alkaline region (basalt). It contains 51wt% SiO_2 and 3.9wt% Na2O + K_2O. It is rich in Fe_2O_3 (9.7wt %) and Al_2O_3 (19wt %). The XRD mineralogical analysis also revealed the presence of goethite and zeolite minerals, which are rich in Al. Primitive mantle normalized multi-element variation diagrams is plotted (fig 5.10) based on MacDonough and Sun (1995). Accordingly, the sample is characterized by positive Ba, K, Pb and Sr anomalies. These enrichments could be explained by plagioclase accumulation. Another possible explanation is proposed by Daoud et al. (2010) that considers the effect of surface processes in the hot desert environment. Surface processes are able to create Ba and Sr anomalies due to the development of secondary minerals like calcite and zeolites. This may be in agreement with the thin section and mineralogical analyses (fig 5.7E). Moreover, chondrite normalized REE elements (after Boyton, 1984) is plotted (fig 5.11) for both the basalt (ENK-7A) and for the sample taken from the vein (ENK-7B) in the basalt. The graph shows a slight enrichment in LREE relative to HREE for the basalt. On the other hand the REE pattern of the vein sample is characterized by significant negative Eu anomaly.

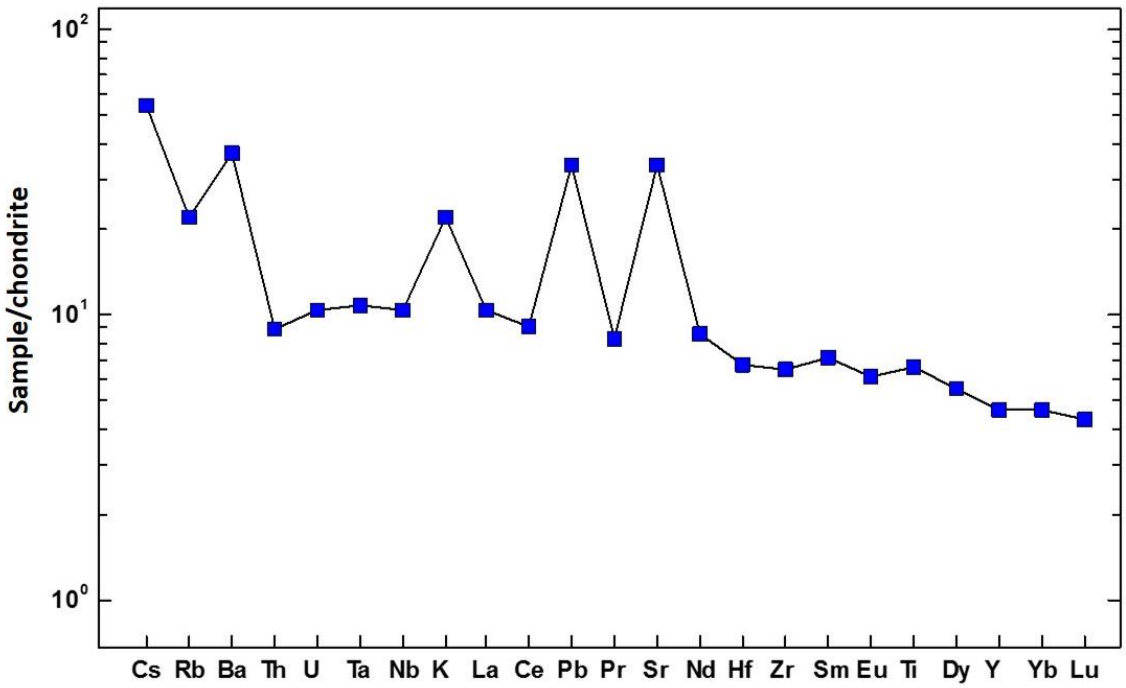

Figure 5.11: Primitive mantle normalized multi-element variation diagrams (MacDonough and Sun (1995)

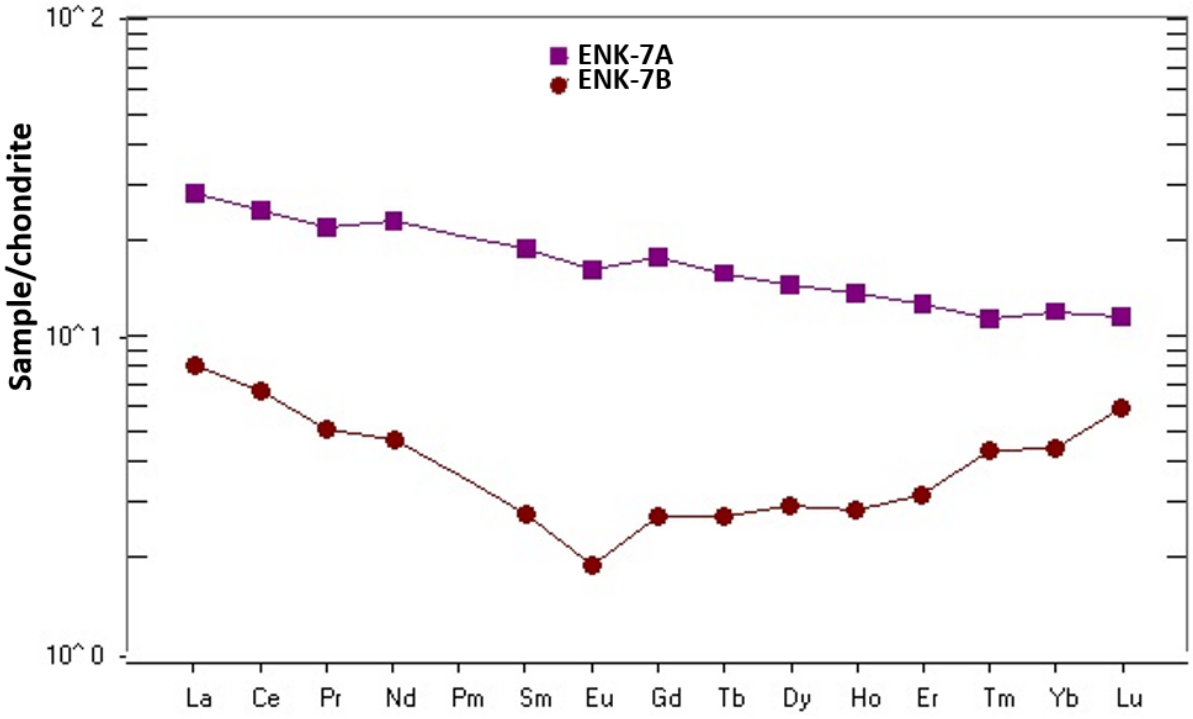

Figure 5.12: Chondrite-normalized REE patterns for basalt, after Boyton (1984)

CHAPTER SIX

Discussion

6.1. Genesis of Enkafela Manganese Deposit

It is known that manganese deposits have diverse origin. They can be formed by hydrothermal, hydrogenetic or diagenetic processes. Hydrothermal manganese ores are deposited directly from hydrothermal solutions. They are formed in marine environment near spreading centers, mid-plate seamounts and/or in subduction-related island arc settings and have been recognized from both modern and ancient geological settings (Roy, 1997; Shah and moon, 2007; Kahrazehi e al., 2015). Hydrogenous deposits are formed from slow precipitation of seawater (Roy, 1997; Salem et al., 2016). Digenetic deposits are precipitated from pore water within altered sediments (Roy, 1997; Salem et al., 2016).

In the preceding sections, based on the geochemical data, the two manganese layers (the massive and powdery manganese layers) exhibit slightly variable geochemical behavior. Although, the hydrothermal nature apparently predominates over the powdery manganese, the massive manganese shows mixed hydrothermal and hydrogenetic property. The seawater influence on the massive manganese is first revealed in its REE pattern (Fig. 5.9). It shows enrichment in Ce which is typical of hydrogenetic manganese deposits. The total REE of the massive manganese is higher than the powdery manganese. The Ni-Co-Zn (Choi and Hariya, 1992) ternary diagram also displays the mixed behavior of the massive manganese as it falls out of both hydrothermal and hydrogenetic region (Fig. 5.8A). The concentration of Co and Cu show variation significantly between the two layers. The massive manganese has Co and Cu concentrations of 97 ppm and 374ppm respectively. However, the powdery manganese contains 20ppm and 8ppm. Higher Co and Cu should have precipitated with the manganese ore only if the hydrothermal fluid were mixed with seawater. Therefore, it is possible to consider that a different hydrothermal phase have been participated in the manganese deposition.

Based on the available data, we can assume that the deposition of the manganese oxides took place into two major phases. Likewise, two principal fluid phases participated in the formation of the two distinctive manganese layers, hydrothermal fluid and seawater. Initially, manganese were precipitating from seawater before the advent of the hydrothermal fluids. Later, the ascent of magmatically derived hydrothermal fluids and mixing with seawater and the early precipitated manganese causes the deposition of the massive

manganese layer. The hydrothermal fluid didn't totally destroy the seawater contribution for the mineralization. It also illustrates the low temperature nature of the hydrothermal fluids. This time, in addition to the hydrothermal fluid some constituents were contributed from seawater. However, the proportional contribution of the two fluids need further study and clarification. In the second phase, the arrival of the hydrothermal fluid has played the role for the deposition of the powdery manganese deposit. The hydrothermal activity dominantly obliterated the effect of the seawater during deposition. The ternary diagrams (Fig. 5.8) and the REE pattern (Fig. 5.9) signify the minimum contribution of seawater for the later hydrothermal phase. In the ternary diagrams the sample falls in the hydrothermal region and the REE pattern shows depletion in Ce. This depletion show that seawater was more oxidizing favoring manganese deposition in higher oxidation state (Mn^{4+}). The coating of the manganese ore on the overlying coral reefs is resulted from this phase.

In order to support this concept, it is ideal to add some comments about the volcanic and exhalative activity in the Afar Depression. Understanding the volcanic history of the area significantly help us to know whether a different phases of hydrothermal activity have existed or not during the deposition of the manganese layers.

The Afar Depression is known for its extreme tectonic activity and volcanism. Magmatism is almost continuous from at least Lower Miocene to recent in the Danakil Depression (Barberi et al 1972). The CNR-CNRS Afar team (1973) documented that the volcanics of the axial zone (Earta Ale, Tati Ali and Alyta) are quite young ranging from 1.2my up to present. The volcanic activity has been and is practically intensive, several eruptions are recorded even recently. A number of volcanic products have been emitted from these young axial ranges even in the last 10,000 years (Barberi et al., 1972). This is quite younger than the marine formations of the depression. Balemual Atnafu et al. (2015) documented that Dallol area was flooded and covered by the Red Sea during some time in the past few hundreds of thousands of years. The fossil coral reefs and marine formations found at the edges of the Danakil Depression, covering volcanic rocks below, marked the invasion of the region by the Red Sea. The manganese deposit under study is found within one of these marine formations. Thus, the approximate age of the deposit is expected to be simultaneous (Pleistocene) with the marine formations (Bonnati et al., 1972). These authors also noted that volcanism derived exhalative-hydrothermal activity is extremely intense in the Afar Depression. Thus, the immense hydrothermal activity on the Afar depression affected the volcanic formations and the marine sedimentary formations. As an example, the XRD

analysis result (see Fig. 5.5E) of the basalt unit found below the massive manganese, shows the presence of zeolite minerals like Aerinite, laumontite, mordernite and faujasite. These minerals have usually resulted from the action of hydrothermal activity (Papavassiliou et al., 2017). Moreover, hot springs (e.g., hot springs at the Dallol salt plain), hot grounds and fumaroles are commonly found over the depression (Varet et al., 2012; Darrah et al., 2013) which witnesses the volcanic and hydrothermal activity in Afar is a continuous activity since Miocene. The presence of these surface manifestations is the result of still an ongoing volcanic activity in the Depression.

Therefore, considering all these continuous volcanic and exhalative hydrothermal activities, we can assume that intensive hydrothermal activity could have also been flourished during the Pleistocene. This is the time when the depression was under marine situation. Though, there is no evidence that indicates the number of times that the hydrothermal activity happened at the time of manganese deposition, it is reasonable to assume as different hydrothermal phases could have happened. Most importantly the pure hydrothermal nature of the second phase indicates the progressive rise in the intensity of hydrothermal activity in the study area.

The other important evidence used to consider the different phases of hydrothermal activity in the deposition of the two different manganese layers is mineralogy. As described in the mineralogy section (section 5.3) birnessite is only detected in the powdery manganese. Alternatively the massive manganese contains calcite while the powdery manganese doesn't show any calcite content. Pyrolusite, Chalcophanite and barite are commonly found in both layers. Pyrolusite, chalcophanite and birnessite are the most common minerals in hydrothermal manganese deposits (Xionghan et al., 2005; Pracejus, 2008; Kuleshov and Maynard, 2017). Similarly, calcite could also be found as a gangue mineral in hydrothermal manganese deposit (Salem et al., 2016). It is an open question to distinctively identify minerals of hydrothermal origin and seawater origin. However, the two manganese layers should have had similar mineralogical composition if they were deposited at the same time and in the same condition. It is possible to assume that the calcite found in the massive manganese originated from seawater. It may also indicate the stability of calcite in the first hydrothermal phase. Simultaneously, it magnifies the temperature of the first hydrothermal phase being low. The absence of calcite in the powdery manganese might indicate the temperature of the second hydrothermal phase. It could be hot enough in order to affect the calcite present in seawater. Consequently, precipitation of calcite with the manganese

minerals could be unlikely. Therefore, it is again undeniable to assume the two manganese layers in a separate phase.

In summarizing about the source of Mn, it can be stated that volcanic derived hydrothermal activity has provided the major components of the ore deposits. Certainly, on the basis of the preceding discussion, seawater has also played some part in the case of the massive manganese ore. The simplified and schematic genetic model that could illustrate the formation of Enkafela manganese deposit is presented in figure 6.1. Upward circulation of hydrothermal fluids through fractures in the underlying basalt, are likely the main agents of mineralization. The rising thermal fluid is expected to be rich in Mn, Fe and other trace metals. Substantial manganese is therefore introduced into seawater by hydrothermal fluids in the bottom seawater. Upon rising the hydrothermal fluid might leached the underlying volcanic rocks and could be more enriched in manganese until it reaches to the bottom water. In the first phase Mn, trace metals and REE are also supplied from seawater.

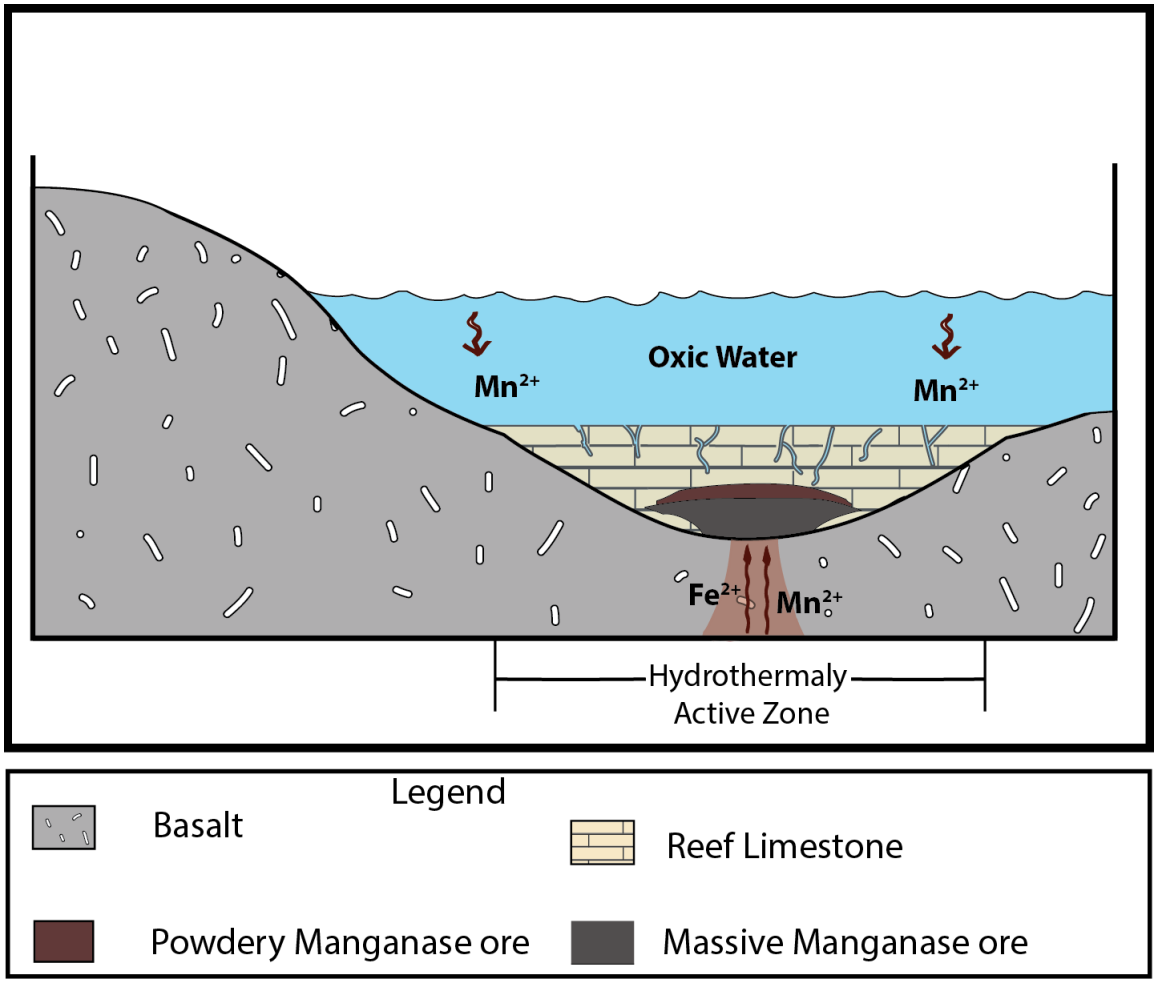

Figure 6.1: Simplified schematic diagram of the mineralizing process in Enkafela manganese

The most important question here is the separation of Mn from Fe to precipitate in a separate phase. The two elements are almost similar geochemically and a special condition should exist to separate the two elements (Kuleshov and Maynard, 2017). Fractionation is the most ideal mechanism to concentrate the two elements separately. Such fractionation may occur during the ascent of hydrothermal solution. Mn-Fe fractionation results due to pre-precipitation of iron in the form of sulfides before the manganese reached to the seawater, as proposed by Bonatti (1975). In the lower zone, in less oxygenated solutions, Fe^{2+} and other metals like Cu leave the system, while manganese is preferentially kept and transported in solution in the form of Mn^{2+}. For example, the concentration of iron in the underlying basalt is relatively higher than manganese, 6.8wt% Fe and 0.2wt% Mn. This could be resulted from pre-precipitation of iron in lower zones. When the hydrothermal solution enters to seawater, Mn^{2+} will be oxidized to Mn^{4+} by oxygenated seawater, probably according to the following reaction, after Bonatti et al. (1972):

$$2Mn^{2+} + 2H_2O + O_2 \rightleftharpoons 2MnO_2 + 4H^+ \text{ (acid)}$$

This reaction finally leads to the formation of the manganese layers. Similarly, in the first phase, Mn^{2+} and trace metals like Co^{2+}, Cu^{2+} and REE^{3+} suspended in water and/or precipitated early from seawater finally precipitate with manganese of hydrothermal origin upon mixing with the hydrothermal fluid.

The acid produced due to the above reaction may also be the cause for the absence of calcite in the hydrothermal manganese layer (the powdery manganese). The acid easily reacts with calcite and avoids precipitation with manganese. However, in the massive manganese seawater could buffer the acid produced by the reaction.

CHAPTER SEVEN

Conclusion and Recommendation

7.1. Conclusion

In this study much attention is given to the assessment of data obtained from field work, mineralogy, major element, trace element and REE geochemistry in order to understand the main mechanism for the formation of the Enkafela manganese deposit. Based on the result obtained the following conclusions are stated.

1. The geological mapping and stratigraphic section logging reveal that the manganese ore is hosted in the reef limestone and two distinctive layers of manganese ore are identified. The bottom layer shows a massive nature while the top layer is powdery.
2. Based on the following reason it is believed that successive phases of hydrothermal activity have participated in the formation of the two manganese layers. Seawater contribution has also observed in the deposit.

a. In Ni-Co-Zn discriminating ternary diagram, the powdery manganese (top layer) falls in the hydrothermal region while the massive manganese (bottom layer) falls in the mixed region (both hydrothermal and hydrogenic).

b. The REE elements distribution pattern has displayed contrasting pattern for the two manganese layers. The massive manganese shows enrichment in Ce which is typical characteristics of sea water. However the powdery manganese shows depletion in Ce. It shows seawater was more oxidizing favoring manganese deposition as Mn^{4+}.

c. The ∑REE content in the two manganese layers are also significantly contrasting. The ∑REE content is 172.9 and 7.84 in the massive manganese and powdery manganese respectively.

d. It can be concluded that both hydrogenic and hydrothermal conditions existed during the formation of the massive manganese. The constituents are originated from both the uprising hydrothermal fluid and seawater. On the contrary, it is only hydrothermal activity which causes the deposition of the powdery manganese with still be the same sources of metal (hydrothermal solutions and seawater).

3. The Fe-(Ni + Cu + Co)*10-Mn and Fe-Si*2-Mn discriminating diagrams show the dominance of hydrothermal activity in the formation of the Enkafela manganese deposit. Both powdery and massive manganese samples fall in the hydrothermal region. Likewise, the Mn/Fe ratio being high supports the dominating of

hydrothermal activity over hydrogenetic precipitation. Fractionation of Mn from Fe is characteristics of hydrothermal deposits.

4. The source of Mn is assumed to be dominantly the underlying volcanic rocks which are leached by volcanically derived thermal fluids during the ascent through fractures.
5. Following a plan method (Area, deposit thickness and bulk density) the resource estimation is conducted. Accordingly, 44,402 tons of manganese ore is estimated under indicated mineral resource category.

7.2. Recommendation

a. The number of samples used in this study could be considerably smaller to elucidate the genesis of Enkafela manganese deposit. Therefore, analyzing more samples will be necessary, especially to apprehend the different phases of hydrothermal activity clearly.
b. Isotopic study like U and Th could give more detail information about the proportional contribution of seawater and volcanic derived hydrothermal activity. It could also indicate the different hydrothermal phases of mineralization.
c. The resource estimation method followed for this study is conventional. It considers average thickness and area only exposed on the surface. The lateral extension of the deposit is not known in detail. Thus, further exploratory workings like drilling should be conducted to better visualize the deposit in three dimensions and scaling up to a reserve level.
d. The active tectonic and volcanic activity of Afar Depression could be an ideal place for hydrothermal manganese deposits. Previous studies and the local people (personal communication) have mentioned the presence of manganese in the other side of Dallol. Thus, further detail study is needed to find similar manganese deposit in the depression

REFERENCES

Abbate, E., Passerini, P. and Zan, L. (1995). Strike-slip faults in a rift area: A transect in the Afar Triangle, East Africa. *Tectonophysics*, **241**: 67-97.

Abedini, A. and Calagari, A. A. (2015). Rare earth element geochemistry of the Upper Permian limestone: the Kanigorgeh mining district, NW Iran, *Turkish J. Earth Sci*. **24**:365-382.

Ameha Atnafu, Tesfaye Kidane, Rowland, J. and Bachtadse, V. (2013). Counterclockwise block rotation linked to the southward propagation and overlap of sub-aerial Red Sea segments, Afar Depression: insight from Paleomagnetism, *Tectonophysics*, **593**:111-120.

Alebachew Beyene and Abdelsalam, M. G. (2005). Tectonics of the Afar Depression: review and synthesis. *J. Afr. Earth Sci*. **41**: 41-59.

Arndt, N. and Clement, G. (2012). Metals and society: an introduction to Economic geology, *pringer*, 175pp.

Atalay Ayele, Keir, D., Ebinger, C., Wright, T. M., Stuart, G. W., Buck, W. R., Jacques, E., Ogubazghi, G. and Sholan, J. (2009). September 2005 mega-dike emplacement in the Manda-Harraro nascent oceanic rift (Afar Depression). *Geophys. Res. Lett.* **36**: L20306.

Balemwal Atnafu, Tesfaye Kidane, Foubert, A., Vogel, D. J., Schaegis, J. C. and Henriet, J. P. (2015). Ocean history from Afar. News Article in Earth & Space Science News, Editors: Richman, B. T., Cohen, C. M. S., Gordon, W. S., Stein, C. A., Fuentes, J. D. and Halpern, D. Eos. 96 (2): 12-14.

Barberi, F. and Varet, J. (1970). The Erta Ale volcanic range (Danakil Depression, northern far, Ethiopia), *Bull. Volcano*, **34**: 848-917.

Barberi, F., Borsi, S., Ferrarea, G., Marinelli, G., Santcroce, R., Tazief, H. and Varet, J. (1972). Evolution of the Danakil Depression (Afar Ethiopia) in light of radiometric age determination, *Journal of Geology*, **80**-720–729.

Barberi, F., Marinelli, G., Santacroce, R., Tazieff, H., Varet, J., Chedeville, E., Faure, H. and Giglia, G. (1973). Geology of Northern Afar (Ethiopia). *Rev. Geogr. Phys. Géol. Dyn*. **15**: 443-489.

Barberi, F., Ferrara, G., Santacroce, R., and Varet, J. (1975). Structural evolution of the Afar triple junction, Afar Depression of Ethiopia, Stuttgart, *Germany, Schweizerbart, Scientific Report*, **14**:38–54.

Barberi, F. and Varet, J. (1977). Volcanism of Afar: small scale plate tectonics implications. *Geol. Soc. Am*. Bull. **88**: 1251-1266.

Barisin, I., Leprince, S., Parson, B. and Wright, T. (2009). Surface displacements in the September 2005 Afar rifting event from satellite image matching: asymmetric uplift and faulting. *Geophys. Res. Lett*. **36**: L07301.

Barrat, J. A., Fourcade, S., Jahn, B. M., Cheminée, J. L. and Capdevile, R. (1998). Isotope (Sr,Nd, Pb, O) and trace element geochemistry of volcanics from Erta ‘Ale range (Ethiopia). *J. Volcano. Geotherm. Res*. **80**: 85-100.

Bastow I.D., and Keir D. (2011). The protracted development of the continent–ocean transition in Afar, published online, *Nature Geoscience*, 4: 4pp.

Bau, M., Schmidt K., Koschinsky, A., Hein, J., Kuhn, J., and Usui, A. (2014). Discriminating between different genetic types of marine ferro-manganese crusts and nodules based on rare earth elements and yttrium, *Chemical Geology*. **381:** 1-9.

Berhe, S.M. (1990). Ophiolites in northeast and east Africa: implication for Proterozoic rustal growth. *Journal Geological Society London*, **147**: 41–57.

Beutel, E., Wijk, J. V., Ebinger C., Keir, D. and Agostini, A. (2010). Formation and stability of magmatic segments in the Main Ethiopian and Afar rifts, *Earth and Planetary Science Letters*, **293**: 225–235.

Bilham, R., Bendick, R., Larson, K., Mohr, P., Braun, J., Tesfaye, S., and Asfaw, L. (1999). Secular and tidal strain across the Main Ethiopian Rift, *Geophysical Research Letters*, **26**:278–2792.

Boggs, S. (2006). Principles of sedimentology and stratigraphy. Pearson Prentice Hall, New Jersey, 662pp.

Bolton, B. R., Both, R., Exon, N.F., Hamilton, T. F., Ostwald, J. and Smith, J. D. (1988).

Geochemistry and mineralogy of seafloor hydrothermal and hydrogenetic mn oxide deposits from the manus basin and Bismarck Archipelago region of the southwest Pacific Ocean, *Marine Geology*, **85**:65-87.

Bonatti, E., Emiliani, C., Ostlund, G. and Rydell, H. (1971). Final Desiccation of the Afar Rift, Ethiopia. *Science*, **172**: 468-469.

Bonatti, E, Fisher, DE, Joensuu, O, Rydell, H. S., Beyth, M. (1972). Iron manganese-barium deposit from the Northern Afar rift (Ethiopia). *Econ Geol*. **67**:717–730.

Bonatti, E., Kraemer, T., Rydel, H. (1972). Classification and genesis of submarine iron-manganese deposits. In: Horn DR, editors. Ferromanganese Deposits on the Ocean Floor, Washington, D.C. Natl Sci Found.149–66pp.

Bonatti, E. (1975). Metallogenesis at oceanic spreading centers, *Ann. Rev.Earth Plan. Sei*. **3**:401-431.

Bonatti, E., Zerbi, M., Kay, R., and Rydell, H. S. (1976). Metalliferous deposits from the Apennine ophiolites: Mesozoic equivalents of modern deposits from oceanic spreading center, *Geological Society of America Bulletin*, **87:** 83:94.

Bonatti, E., Cipriani, A. and Lupi, L. (2015). The Red Sea: Birth of an ocean. Springer Earth System Sciences. Editors: Rasul, N. M. A. and Stewart, I. C. F. *The Formation, Morphology, Oceanography and Environment of a Young Ocean Basin*. **19**: 29-44.

Bosworth, W., Huchson, P. and McClay, K. (2005). The Red Sea and Gulf of Aden basins, *J. Afr. Earth Sci*., **43**: 334-378.

Boynton, W. (1984). Cosmo chemistry of the rare earth elements. Elsevier.

Calvert, S. E. and Pedersen, T. F. (1996). Sedimentary geochemistry of manganese; implications for the environment of formation of manganiferous black shales, *Econ. Geol*. **91**: 36–47.

Cannon, W.F., Kimball, B.E., and Corathers, L.A. (2017). Manganese, chap. L of Schulz, K.J., DeYoung, J.H., Jr., Seal, R.R., II, and Bradley, D.C., eds., Critical mineral resources of the United States-Economic and environmental geology and Prospects for future supply: U.S. Geological Survey Professional Paper, **1802**: L1-L28.

Carlo, D. E. and McMurtry, G. (1992). Rare earth element geochemistry of ferromanganese crusts from the Hawaiilan Archi-pelago, central Pasifc, *Chem Geol*. **95(3–4)**:235–250.

Choi, J H, Hariya Y. (1992). Geochemistry and depositional environment of Mn oxide deposits in the Tokora Belt, Northeastern Hokkaido, Japan. *Economic Geology*, **87**:1265-1274.

Corathers, L.A. (2006). U.S. Geological survey (USGS) minerals year book: Manganese-2006. http://minerals.USGS.Gov. Date accessed: 02/02/2018.

Carniel, R., Jolis, E. M. and Jones, J. (2010). A geophysical multi-parametric analysis of hydrothermal activity at Dallol, Ethiopia. *J. Afr. Earth Sci*. **58**: 812-819.

Chorowicz, J. (2005). The East African rift system. *J. Afr. Earth Sci*. **43**: 379-410.

Chu, D. and Gordon, R. G. (1998). Current plate motions across the Red Sea. *Geophys. J. Int*., **135**: 315-328.

Chu, D., and Gordon, R.G. (1999). Evidence of motion between Nubia and Somalia along the southwest Indian ridge, *Nature*, **398**:64–67.

CNR-CNRS (Afar team) (1973). Geology of northern Afar (Ethiopia): Revue de Géographie Physique et de Géologie Dynamique, **15**:443–490.

Collet, B., Taud, H., Parrot, J. F., Bonavia, F. and Chorowicz, J. (2000). A new kinematic approach for the Danakil block using a Digital Elevation Model representation. *Tectonophysics*, **316**: 343-357.

Courtillot, V., Jaupart, C., Manighetti, I., Tapponnier, P. and Besse, J. (1999). On causal links between flood basalts and continental breakup, *Earth and Planetary Science Letters*, **166:**177–195.

Daoud, M., Maury, R., Barrat, J., Taylor, R. E., Bernard, L. G. (2010). A LREE-depleted component in the Afar plume: Further evidence from Quaternary Djibouti basalts, Lithos, *Elsevier*, **114 (3-4)**:327-336.

Darrah, T. H., Tedesco, D., Tassi, F., Vaselli, O., Cuoco, E and Poreda, R. J. (2013). Gas Chemistry of the Dallol Region of the Danakil Depression in the Afar region of the northern-most East African Rift. *Chem. Geol.* **339**:16-29.

Doubre, C., Manighetti, I., Dorbath, C. and Bertil, D. (2007). Crustal structure and Magmato tectonic processes in an active rift (Asal-Ghoubbet, Afar, East Africa): 2.Insights from the 23-year recording of seismicity since the last rifting event. *J. Geophys. Res.* **112**:B05406.

Eagles, G., Gloaguen, R. and Ebinger, C. (2002). Kinematics of the Danakil micro plate. *Earth Planet. Sci. Lett*., **203**: 607-620.

Ebinger, C. J., and Hayward, N. J. (1996). Soft plates and hot spots: Views from Afar. *Journal of Geophysical Research: Solid Earth*. **101**: 21859-21876.

Ebinger, C. J., Keir, D., AtalayAyele, Calais, E., Wright, T. j., Manahloh Belachew, Hammond, J. O. S., Campbell, E. and Buck, W. R. (2008). Capturing magma intrusion and faulting processes during continental rupture: seismicity of the Dabbahu (Afar) rift. *Geophys. J. Int.* **174**:1138–1152.

Elderfield, H. and Greaves, M. J. (1981). Negative cerium anomalies in the rare earth element patterns of oceanic ferromanganese nodules. *Earth Planetary Science Letters*, **55**:163-170.

Fan, D. and Yang, P. (1999). Introduction to and classification of manganese deposits in china, *Ore Geology Reviews*., **15:** 1:13.

Field, L., Blundy, J., Calvert, A., and Gezahegn Yirgu. (2013). Magmatic history of Dabbahu,a composite volcano in the Afar rift, Ethiopia, *Geol. Soc. Am. Bull*. **125**: 128-147.

Flohr, M. J. K. and Huebner, J. S. (1992). Mineralogy and geochemistry of two metamorphosed sedimentary manganese deposits, Sierra Nevada, California, USA, *Lithos*, **29**:57-85.

Force, E.R., and Cannon, W.F. (1988). Depositional model for shallow-marine manganese deposits around black-shale basins, *Economic Geology*, **83**:93-117.

Franzen H., Helgadóttir, H. M. and Óskarsson, F. (2015). Surface exploration and first conceptual model of the Dallol geothermal area, northern Afar, Ethiopia. In: Proceedings World Geothermal Congress, pp. 1-11. Melbourne, Australia.

Geology.com/usgs/manganese/ date accessed: 05.02.2018.

Geological survey of Ethiopia (2013). Opportunities for Manganese Recourse Development in Ethiopia. Unpublished Report, Addis Ababa, Ethiopia.

Getaneh, Assefa (1985). The mineral industry of Ethiopia: present conditions and future prospects, *J. Afr. Earth Sci*. **3 (3)**:331–345.

Glasby, G.P. (1988). Hydrothermal manganese deposits in island arcs and related and related to subduction processes: a possible model for genesis, *Ore Geology Review*, **4**:145–153.

Glasby, G.P., Stüben, D., Jeschke, G. and Garbe-Schönberg, C.D. (1997). A model for the formation of hydrothermal manganese crusts from the Pitcairn Island hotspot, Geochim. Cosmochim. Acta. **61**:4583–4597.

Guidarelli, M., Stuart, G., Hammond, J. O. S., Kendall, J. M., Atalay Ayele and Belache M. (2011). Surface wave tomography across Afar, Ethiopia: Crustal structure at a rift triple junction zone, *Geophysical Research letters*, **38**:L24313.

Gupta, A. and Scholz, C. H. (2000). Brittle strain regime transition in the Afar depression: Implications for fault growth and seafloor spreading. *Geology*, **28**:1087- 1090.

Hamling, I. J., Ayele, A., Bennati, L., Calais, E., Ebinger, C. J., Keir, D. and, GezahegnYirgu. (2009). Geodetic observations of the ongoing Dabbahu rifting episode: new dyke intrusions in 2006 and 2007. *Geophysical Journal International*, **178**: 989-1003.

Harben, p., Raleigh, C. and Harris, J. (1998). Manganese uses and markets, Industrial minerals information Ltd.

Hayward, N. J. and Ebinger, C. J. (1996). Variations in the along axis segmentation of the Afar Rift system, *Tectonics*, **15**: 244-257.

Heshmatbehzadi, K. and Shahabpour, K. (2010). Metallogeny of Manganese and Ferromanganese ores in Baft ophiolitic Melange, Kerman, Iran, *Australian Journal of Basic and Applied Sciences*, **4(2)**: 302-313.

Hodkinson, R., Stoffers, P., Scholten, P., Cronan, D. S., Jeschke, G. and Rogers, T. S. (1994).Geochemistry of hydrothermal manganese deposits from the Pitcairn Island hotspot, southeastern Pasifc, *Geochim Cosmochim Acta*. **58(22):**5011–5029.

Hofmann, C., Courtillot, V., Feráud, G., Rochette, P., GezahegnYirgu, Endale Ketefo and Pik,R. (1997). Timing of the Ethiopian flood basalt event and implications for plume birth and global change. *Nature*, **389**: 838-841.

Holwerda, J.G., and Hutchison, R.W. (1968). Potash bearing evaporites in the Danakil area, Ethiopia: *Economic Geology*, **63**:124–150.

https://www.accuweather.com/en/et/dalol/126842/january-weather/126842 assessed on 28.01.2018.

http://webmineral.com/assessed on 21.04.2018

Jeffrey, E. P. and Daniel, E. A. (1988). Chalcophanite, ZnMn3OT'3H2O: New crystal structure determinations, *American Mineralogist*, **73**:401-1404.

Jestin, F., Huchon, P., and Gaulier, J.M. (1994). The Somalia plate and the East African Rift System: Present-day kinematics, *Geophysical Journal International*, **116**:637–654.

Jiancheng, X., Xiaoyong, Y., Jianguo, D. and Wei, X. (2006). Geochemical Characteristics of Sedimentary Manganese Deposit of Guichi, Anhui Province, China, *Journal of Rare Earths*, ***24***:374 – 380.

Johnson, J.E., Webb, S. M., Chi, M. A. and Fischer, W.W. (2016).Manganese mineralogy and diagenesis in the sedimentary rock record, *Geochimica et Cosmochimica Acta*. **173**:210-231.

Joint Ore Reserves Committee of the Australasian Institute of Mining and Metallurgy, Australian Institute of Geoscientists and Minerals Council of Australia (JORC) (2012). Australasian Code for Reporting of Exploration Results, Mineral Resources and Ore Reserves.

Josso, P., Pelleter, E., Pourret, O., Fouquet, Y., Etoubleau, J., Cheron, S. and Bollinger, C. (2016). A New Discrimination Scheme for Oceanic Ferromanganese Deposits using High Field Strength and Rare Earth Elements, *Ore Geology Reviews*.

Kahrazehi, M., Lotf, M., Ghaderi, M., Mohajjel, M. and Jafari, M. (2015). First report of Geochemical Characteristics of the Sangan Manganese Occurrence, Northeast Khash, Iran, *Indian Journal of Science and Technology*, **8(S3):**85–93.

Kazmin, V. (1971). Precambrian of Ethiopia, *Nature*, **230**:176–177.

Keir, D., Manahloh Belachew, Ebinger, C.J., Kendall, J.-M., Hammond, J. O. S., Stuart, G. W., Atalay Ayele and Rowland, J. V. (2011). Mapping the evolving strain field during continental breakup from crustal anisotropy in the Afar Depression, *Macmillan Publishers Ltd.* 7pp.

Kogan, L., Fisseha, S., Bendick, R., Reilinger R., McClusky, S., King, R., and Solomon T. (2012). Lithospheric strength and strain localization in continental extension from observations of the East African Rift, *Journal of Geophysical Research*, **117**: B03402.

Kogel, J. E., Trivedi, N. C., Barker, J. M. and Krukowski, S. T. (2006).Industrial minerals and Rocks, Commodities, Market, and Uses, 7thed.,Society for Mining Metallurgy, Exploration Inc., Colorado, 683pp.

Krauskopf, k. b. (1957). Separation of Manganese from Iron in Sedimentary processes, Geochimica et Cosmochimica Acta, *Pergamon Press Ltd*., London, **12**: 61-84.

Kuleshov, V. and Maynard, J.B. (2017). Isotope Geochemistry: The origin and formation of manganese rocks and ores, Elsevier Inc., Amsterdam, 437pp.

Kuhn, T., Wegorzewski, A., Ruhlemann and Vink, A. (2017). Chapter 2: composition, formation and occurrence of polymetallic Nodules, Federal Institute of Geosciences and Natural resource, Hannover, Germany, 42p.

Lalou, C., Nguyen H. V., Faure, H., and Moreira, L. (1970). Datation par la methode U/Th des hauts niveaux decoreaux de la depression de l'Afar: *Rev. geographie physique geologie dynam*. **12**: 3-8.

Lange, G. J. D., van, O. B. and Poorter, R. (1992).Geochemical composition and inferred accretion rates ofsediments and manganese nodules from a submarine hill in the Madeira Abyssal Plain, Eastern North Atlantic, *Marine Geology*, **109:** 171-194.

Le Bas, M. J., Le Maitre, R., Streckeisen, A. and Zanettin, B. (1986). A chemical classification of volcanic rocks based on the total alkali-silica diagram. Journal of Petrology, 27(3):745-750 pp.

Liu, J., Zheng, H., Liu, B., Liu, H., Shi, K., Guo, R. and Zhang, X. (2017). Petrology and geochemical characteristics of dolomite in the Middle Permian Maoukou Formation, central Sichuan, *Petroleum Research*, **2**:366-377.

Maynard, J. B. (2010). The Chemistry of Manganese Ores through Time: A Signal of Increasing Diversity of Earth-Surface Environments, *Econ. Geol*. **105**: 535–552.

Makris, J., &Ginzburg, A. (1987). The Afar Depression: transition between continental rifting and sea-floor spreading. *Tectonophysics*, **141**: 199-214.

Mazzarini, F. (2007). Vent distribution and crustal thickness in stretched continental crust: The case of the Afar Depression (Ethiopia), Gosphere, **3(3)**:152-162.

McDonough, W. F. and Sun, S. S. (1995). The composition of the Earth. *Chemical Geology,* **120 (3):** 223-253 pp.

McKenzie, D.P., and Morgan, W.J. (1969). Evolution of triple junctions, *Nature*, **224**:125–133.

Mishra, P. P., Mohapatra B. K. and Singh, P. (2007). Contrasting REE signatures on manganese ores of in north Orissa India. *Journal of Rare Earths*, **25(6**): 749.

Mohr, P.A. (1975). Structural setting and evolution of Afar. In: Pilger, A., Rosler, A. (Eds.), Afar Depression of Ethiopia, Proceedings of an International Symposium on the Afar Region and Rift Related Problems, Bad Bergzabren, Germany, 1974, E. *Schweizerbart'sche Verlagsbuch hanlung*, Stuttgart, Germany, **1**:27–37.

Mohr, P. (1983b). Ethiopian flood basalt Province, *Nature*, 303:577-584.

Monnin, C, Wheat, C G., Dupre, B, Elderfield, H, Mottl, M J. (2001). Barium geochemistry in sediment pore waters and formation waters of the oceanic crust on the eastern flank of the Juan de Fuca Ridge (ODP Leg 168). *Geochem. Geophys. Geosyst*. 2**:**1008p.

Morten, L., Landini, F., Bocchi, G., Mottana, A. and Brunfelt, A.O. (1980). Fe--Mn crusts from the southern Tyrrhenian Sea, *Chem. Geol*. **28**: 261--278.

Nath, B. N., Pluger, W. L. and Roelandts, I. (1997).Geochemical constraints on the hydrothermal origin of ferromanganese encrustations from the Rodriguez Triple Junction, Indian Ocean, From Nicholson, K., Hein, J. R., Bfihn, B. & Dasgupta, S. (eds), 1997, Manganese Mineralization: Geochemistry and Mineralogy of Terrestrial and Marine Deposits, *Geological Society Special Publication*, **119**:199-211.

Nicholson, K. (1990). Stratiform manganese mineralisation near Inverness, Scotland: A Devonian sub-lacustrine hot-spring deposit? *Mineralium Deposita*, **25:**126-131.

Nicholson, K., Hein, J., Bühn, B., and Dasgupta, S. (1997). Manganese Mineralization: Geochemistry and Mineralogy of Terrestrial and Marine Deposits, Special Publication-*Geological Society of London*, 11**9**:5–27.

Nobile, A., Pagli, C., Keir, D., Wright, T. J., Atalay Ayele, Ruch, J. and Acocella, V. (2012). Dike-fault interaction during the 2004 Dallol intrusion at the northern edge of the Erta'Ale ridge (Afar, Ethiopia). Geophysical Resistivity Letter, **39**: L19305.

Oksuz, N. (2011). Geochemical characteristics of the Eymir (Sorgun-Yozgat) manganese deposit, Turkey, *Journal of Rare Earths*, **29**:282p.

Oksuz, N. and Okuyucu, N. (2014). Mineralogy, Geochemistry, and Origin of Buyukmahal Manganese Mineralization in the Artova Ophiolitic Complex, Yozgat, Turkey, Hindawi Publishing Corporation, *Journal of Chemistry*, Article ID 837972, 11p.

Ozturk, H. (1997). Manganese deposits in Turkey: Distribution, types and tectonicsetting, *Ore Geology reviews*, **12**: 187-203.

Papavassiliou, K., Voudouris, P., Kanellopoulos, C., Glasby, G., Alfieris, D. and Mitsis, I. (2017). New geochemical and mineralogical constraints on the genesis of the Vani hydrothermal manganese deposit at NW Milos island, Greece: Comparison with the Aspro Gialoudi deposit and implications for the formation of the Milos manganese mineralization, *Ore geology Reviews*, **80**:594-611.

Park, C. F. (1946). The spilite and manganese problems of the Olympic Peninsula, Washington, *American Journal of Science*, **244**:305-323.

Pedgley, D.E. 1967). Air Temperature at Dallol, Ethiopia, *Meteorological Magazine*, **96**:265-271.

Pierret, M.C., Clauer, N. and Bosch, D. (2010). Blanc G. Formation of Thetis Deep metal rich sediments in the absence of brines, Red Sea, *Journal of Geochemical Exploration **104**:12–26.*

Piper, D. Z. and Bau, M. (2013). Normalized Rare Earth Elements in Water, Sediments, and Wine: Identifying Sources and Environmental Redox Conditions, *American Journal of Analytical Chemistr*y**, 4:** 69-83.

Post, J. E. (1999). Manganese oxide minerals: Crystal structures and economic and environmental significance, *Proc. Natl. Acad. Sci*. **96**: 3447–3454.

Pracejus, B. (2008). The Ore Minerals Under the Microscope:An Optical Guide, Atlases in Geosciences, *Elsevier*, 895pp.

Redfield, T. F., Wheeler, W. H., and Often, M. (2003). A kinematic model for the development of the Afar Depression and its paleogeographic implications. *Earth and Planetary Science Letters*, **216**: 383-398

Roberson, A. H. F., and Varnavas, S. P. (1993). The origin of hydrothermal metalliferous sediments associated with the early Mesozoic Othris and Pindos ophiolites, mainland Greece, *Sedimentary Geology*, **83**: 87-113.

Rowland, J. V., Baker, E., Ebinger, C. J., Keir, D., Tesfaye Kidane, Biggs, J., Hayward, N. and Wright, T. J. (2007). Fault growth at a nascent slow-spreading ridge: 2005 Dabbahu rifting episode, Afar. *Geophys. J. Int*. **171**: 1226-1246.

Roy, S. (1992). Environments and processes of manganese deposition, *Econ. Geol.*, **87**:1218-1236.

Roy, S. (1997). Genetic diversity of manganese deposition in theterrestrial geological record, In: Nicholson, K., Hein, J., Bühn,B., Dasgupta, S. (Eds.), Manganese Mineralisation: Geochemistry and Mineralogy of Terrestrial and Marine Deposits. Special Publication-*Geological Society of London*, **119**:5–27.

Roy, S. (2006). Sedimentary manganese metallogenesis in response to the evolution of the Earth system, *Earth-Science Reviews*, **77**:273–305.

Rychert, C. A., Hammond, J. O. S., Harmon N, J. Kendall J. M., Keir, D., Ebinger, C., Bastow, I. D., Atalay Ayele, Manahloh Belachew, and Stuart, G. (2012). Volcanism in the Afar Rift sustained by decompression melting with minimal plume influence, published online, *Nature Geoscience*, 4pp.

Salem, I. A., El-Shibiny, N. H. and Monsef, M. A. (2016). Mineralogical and Geochemical Studies on Manganese Deposits at Abu Ghusun Area, South Eastern Desert, Egypt, *Journal of Geography and Earth Sciences*, **4(2)**:51-74.

Samson Tesfaye, Harding, D. J. and Kusky, T. M. (2003). Early continental breakup boundary and migration of the Afar triple junction, Ethiopia. *Geol. Soc. Am. Bull.* **115**:1053-1067.

Sasmaz, A, et al. (2013). Geology and geochemistry of Middle Eocene Maden complex ferromanganese deposits from the Elazig-Malatya region, eastern Turkey. *Ore Geol Rev*.

Shah, MT, Khan, A. (1999). Geochemistry and origin of Mn deposits in the Wazir is tanophiolite complex, north Waziristan,Pakistan, *Miner Deposita*, **34**:697–704

Shah, M. T. and Moon, C. J. (2007). Manganese and ferromanganese ores from different tectonic settings in the NW Himalayas, Pakistan, *Journal of Asian Earth Science*, **29**:455-465.

Solomon Tadesse, Milesi, J.P. and Deschamps, Y. (2003). Geology and mineral potential of Ethiopia: a note on geologyand mineral map of Ethiopia, *Journal of African Earth Sciences*, **36**: 273–313.

Stern, R. J. (1994). Arc Assembly and continental collision in the Neoproterozoic East African Orogen: Implications for the consolidation of Gondwanaland. *Annu. Rev. Eart Planet. Sci*. **22:**319-321.

Tazieff, H., Varet, J., Barberi, F., Giglia, G. (1971). Tectonic significance of the Afar (or Danakil) depression, *Nature*, **235**:144–147.

Tazieff, H., Varet, J., Barberi, F. and Giglia, G. (1972). Tectonic Significance of the Afar (or Danakil) Depression, *Nature*, **235 *(*5334)**:144-147.

Thurmond, A. K., Abdelsalam, M. G. and Thurmond, J. B. (2006). Optical-radar-DEM remote sensing data integration for geological mapping in the Afar Depression, Ethiopia. *J.Afr. Earth Sci*., **44**: 119-134.

Tilahun Mammo (2004). Mapping the crust-mantle boundary beneath Afar Depression, *Gondwana Research*, **3**: 855-861.

Tostevin, R., Shields, G. A., Tarbuck, G. M., H,e T., Clarkson, M. O. and Wood, R. A. (2016).Effective use of cerium anomalies as a redox proxy in carbonate-dominated marine settings, *Chemical geology*, **438**: 146-162.

Toth, J R. (1980). Deposition of submarine crusts rich in manganese and iron. *Geological Society of America Bulletin, **91***: 44-54.

Tribovillard, N., Algeo, T. J., Lyons, T. and Riboulleau, A. (2006). Trace metals as paleoredox and paleoproductivity Proxies, *chemical geology***, 232**: 12-32.

ULLAH, K., ARIF, M., SHAH, M. T. (2015). Petrography and geochemistry of the Kamlial Formation, southwestern Kohat plateau, Pakistan: implications for paleoclimate of the Western Himalayas, Turkish J Earth Sci. **24**:276-288.

Usui, A. and Someya, M. (1997). Distribution and composition of marine hydrogenetic and hydrothermal deposits in the northwest Pacific Nicholson, K., Hein, J. R., Biihn, B. & Dasgupta, S. (eds), 1997, Manganese Mineralization: Geochemistry and Mineralogy of Terrestrial and Marine Deposits, *Geological Society Special Publication*, **119**:177- 198.

Vail, J.R. (1985). Pan-African (late Precambrian) tectonic terranes and reconstruction of the Arabian–Nubian Shield, *Geology*, **13**:839–842.

Varet, J. and Gasse, F. (1978). Geology of central and southern Afar (Ethiopia and Djibouti Republic). *CNRS, Paris,* pp. 118.

Varet, J. (2006). The Afar triangle, a future "gulf region" for geothermal energy? In: Proceedings of the 1st African Rift Geothermal Conference, pp. 7-13. Addis Ababa, Ethiopia.

Varet, J. (2010). Contribution to favorable geothermal site selection in Afar triangle. In: Proceedings of the 3rd African Rift Geothermal Conference, pp. 139-155. Djibouti, Djibouti.

Varet, J., Tadiwos Chernet, Girma Weldetinsae and Arnason, K. (2012). Exploring for geothermal sites in northern and central Afar (Ethiopia). In: Proceedings of the 4th African Rift Geothermal Conference. Nairobi, Kenya.

Warren j. k. ., 2015. Danakil Potash, Ethiopia:Is the present geology the key Part 1 of 4 www.researchgate.net/publication/276248185.pdf on 26.01.2018.

Wolfenden, E., Ebinger, C., GezahegnYirgu, Deino, A. and DerejeAyalew. (2004) Evolution of the northern Main Ethiopian rift: birth of a triple junction. *Earth Planet. Sci. Lett.,* **244**:213–228.

Wolf, K. H. (1976). Handbook of strata-bound and stratiform ore deposits, II. Regional studies and specific deposits, Au, U, Fe, Mn, Hg, Sb, W and P deposits, Elsevier Scientific Publishing Company, Amsterdam. **7**: 649pp.

Worash Getaneh and Solomon Tadessse (2015). Textbook of Economic Geology, Addis *Ababa University Press*, 305P.

Wright, T. M., Ebinger, C., Biggs, J., AtalayAyele, GezahegnYirgu, Keir, D. and Stork, A. (2006). Magma-maintained rift segmentation at continental rupture in the 2005 Afar dyking episode. *Nature Lett*. **442**: 291-294.

Xionghan, F., Wenfeng, T., Fan L., Qiaoyun1, H. and Xiangwen, L. (2005). Pathways of birnessite formation in alkali medium, Science in China Ser. D Earth Sciences, **48 (9)**:1438—1451.

Yu, W., Algeo, T. J., Du Y., Maynard, B.,Guo, H., Zhou, Q., Peng, T., Wang, P. and Yuan, L. (2016). Genesis of Cryogenian Datangpo manganese deposit: Hydrothermal influence and episodic postglacial ventilation of Nanhua Basin, South China, Palaeogeography, Palaeoclimatology, Palaeoecology, 54p.

Zanettin, B. (1993). On the evolution of the Ethiopian volcanic province. In: Abbate, E., Sagri, M., Sassi, F.P. (Eds.), Geology and Mineral Resources of Somalia and Surrounding Regions, Istituto Agronomicoper L'Oltremare, Firenze, Relazioni e Monografie Agrarie Subtropicali e Tropicali Nuova Serie, **113**:279–310.

Zhang, W. and Cheng, C.Y. (2007). Manganese metallurgy review, Part I: Leaching of ores/ secondary materials and recovery of electrolytic /chemical manganese dioxide, *Hydrometallurgy, 89:137*-159.